



Received for publication, September, 06, 2023  
Accepted, September, 21, 2023

*Original article*

## **The role of lactate dehydrogenase of the pleural liquid in the cytopathological diagnosis**

**TURCU ELENA<sup>1, 2</sup>, ARDELEANU CARMEN<sup>2</sup>, MIHAESCU GRIGORE<sup>3,\*</sup>**

<sup>1</sup> Pathology Laboratory, Clinical Hospital “Prof. Dr. Th. Burghel”, Bucharest, Romania

<sup>2</sup> SC. OncoTeam Diagnostic SRL, Bucharest, Romania

<sup>3</sup> University of Bucharest, Faculty of Biology, Bucharest, Romania

### **Abstract**

Elevated serum or pleural fluid lactate dehydrogenase (LDH) enzyme levels can be associated with various conditions, including neoplasia, reticuloendothelial tumors, and leukemia. These conditions can lead to cell damage or death, causing LDH to be released into the bloodstream and pleural fluid. An increase in LDH levels may prompt further investigation into the underlying cause, which could include malignancies or other diseases. Elevated LDH levels in pleural fluid are often associated with certain conditions, and our study seeks to establish a quantitative assessment of LDH in conjunction with cytopathological examination for diagnostic purposes.

We show here that the presence of abnormal or malignant cells in pleural fluid, as indicated by positive cytopathological results, can be concerning and often necessitates further evaluation. Elevated LDH levels provide biochemical evidence that supports the cytopathological findings, strengthening the case for a potential underlying disease or condition.

### **Keywords**

LDH, cytology, pleural liquid

## Introduction

Cytology is a diagnosis method in malignant diseases and the most important method for early detection of neoplasms with different locations. Exfoliative cytology was the first method with practical application in the diagnosis of malignant tumours of the cervix. Due to the accuracy of this cytodiagnostic method, it has also been applied in the diagnosis of lung tumours.

Comparing the cytological results with the histological results, it was found that there was 80-90% concordance between the examinations. In order to obtain good quality cytological results, the cytologist needs to receive information on the patient's clinical and imaging datasets.

There are multiple major arguments supporting the importance of cytological diagnosis:

Cytology is a quick and inexpensive method compared to other diagnostic methods. The low psychological impact of cytology is important for the patient, as the waiting period for diagnosis is very short. Cytology helps in guiding therapy in inoperable patients. Cytology is the method that can identify the cell type in lung carcinoma, thus avoiding biopsy. In some cases, cytology is the only possible method of diagnosis. This method targets patients who refuse biopsy and cases where the puncture fragments are very small or cases where malignant intraepithelial lesions have no endoscopic expression.

The cytological examination is the procedure by which cells can be examined to identify their atypical features. Fine needle aspiration cytology (FNA) of serous membrane effusions can play an important role in the diagnostic analysis of both primary and metastatic disease. From this perspective, liquid-based cytology (LBC) represents a feasible and reliable method to empower the performance of ancillary techniques (i.e. immunocytochemistry and molecular testing) with high diagnostic accuracy [1].

The cell is plastic and sensitive to intracellular and extracellular changes. Through its components, it can adapt to variations, maintaining internal homeostasis, and if these variations exceed normal physiological values, cell abnormalities occur.

The cell membrane, the cytoplasm with its organelles and the nucleus and the coordinator of cellular activities play an active role in the cell's adaptation.

On smears, the cell membrane rarely appears as a structure different from the cytoplasm. In cytological examination it is particularly important to examine the cell boundaries as only morphologically intact cells will be interpreted. The sampling and smear methods play an important role in avoiding cellular artefacts. Cells with unclear membrane

boundaries can induce diagnostic confusion by overestimating the ratio of nucleus to cytoplasm.

The cytoplasm is made up of the cytosol, which includes the cell organelles. The cell nucleus consists of chromatin, nucleoli and nucleoplasm, surrounded by the two sheets of the nucleolus. The nucleus is in an interdependent relationship with the cytoplasm, the existence of one being strictly conditional on the existence of the other. The nucleus is the holder of the genetic code and consists of nucleic acids (DNA, RNA) and proteins.

The following main aspects are taken into account when formulating the cytological diagnosis: the location of the nucleus, the shape of the nuclear membrane, the nucleocytoplasmic ratio

, the type and distribution of chromatin (finely granular or in large blocks), the presence, number and size of nucleoli, the presence and type of mitoses.

## Normal exfoliative cytology of pleural fluids

The non-reactive mesothelial cell has variable shapes with large dimensions. The nucleus of the mesothelial cell may be single or multiple, being euchromatic with an obvious nucleolus or heterochromatic with an irregular outline. In most non-reactive mesothelial cells the cytoplasm is rich, so that the nucleus-to-cytoplasm ratio is subunitary as shown in Figure 1.

Other cell types found in pleural fluid are: erythrocytes, lymphocytes, polymorphonuclear, eosinophils, etc. and reactive mesothelial cells in pleural fluids. In pleural fluids, reactive mesothelial cells show discrete morphological changes compared to non-reactive mesothelial cells.

Increased RNA is reflected by more intense basophilia of the cytoplasm, as well as the presence of multiple large nucleoli and pleomorphism.

Reactive mesothelial cells show an increased nucleocytoplasmic ratio and adhere to each other in small clusters.

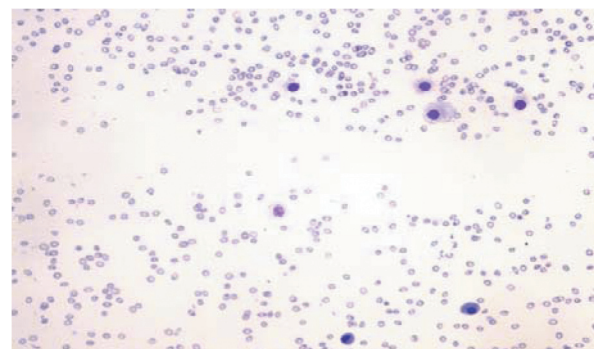


Figure 1. Mesothelial cells on a hematic background.

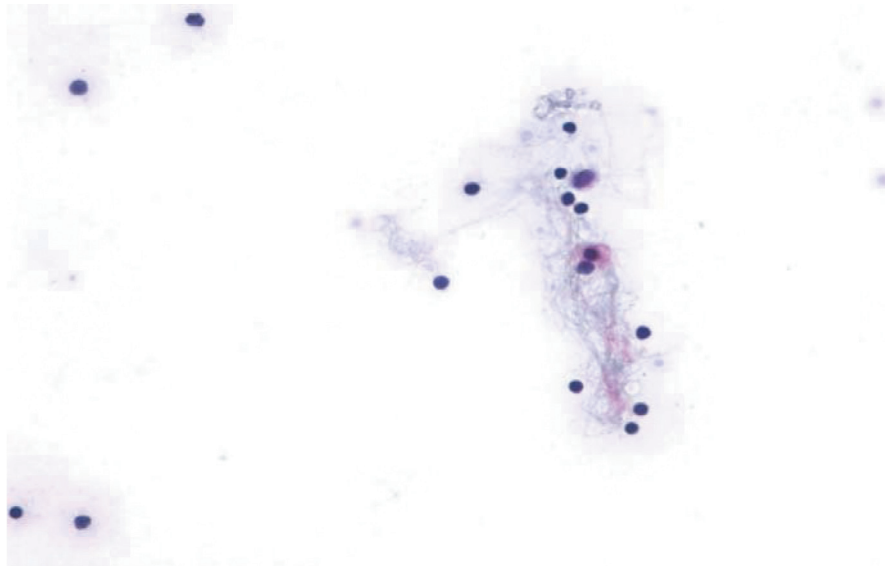


Figure 2. Reactive mesothelial cells. Papanicolaou stain X ob 40. Original

The nucleus may be eccentric, with coarse chromatin. Reactive mesothelial cells create difficulty in cytological diagnosis. It is important for cytopathological diagnosis to observe whether the atypical cells in the overgrowth are relatively uniform in size and shape, as seen in Figure 2.

### **Malignant mesothelial cells in pleural fluids**

In pleural effusion, differential diagnosis between proliferating mesothelial cells and malignant cells may be impossible [2]. For a good identification of malignant cells, the presence of enlarged nucleoli, abnormal mitoses, cellular elements that cannot be produced by mesothelial cells (melanin or mucus) or large cellular aggregates, papillary or glandular clusters are analysed. The absence of these landmarks, in medium-sized cells, can lead to diagnostic errors. Thus, clinical and imaging data are absolutely necessary.

Atypical cells, among mesothelial cells and other cells in the overgrowth, can be easily identified by examining the smear with the microscope's wide objective. The examination reveals the quality and intensity of the overall staining of the cells and their nuclei, as well as the number of different cell populations in the smear.

The presence of malignant cells in the smear together with other elements (haematocytes, lymphocytes, polymorphonuclear cells) allows the formulation of the cytodagnosis: positive cytology for malignancy. Fig.3.

The etiology of pleural effusions often remains unknown notwithstanding surgical pleural biopsy and further clinical observation [3]. Pleural effusions are classified as transudate or exudate effusions [4]. Certification of an effusion as transudate or exudate is given by a number of biochemical markers, including LDH enzyme, glucose, protein [5]. The LDH enzyme is an indicator of the differentiation of transudates from exudates [6].

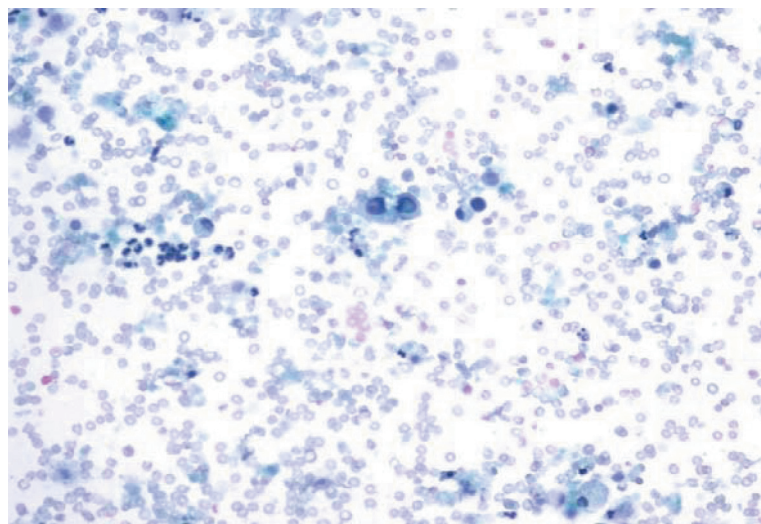


Figure 3. Papanicolaou stain Xob 40 - Malignant cells on a hematic background.

Elevated LDH levels are often associated with pleural fluid exudates and may indicate cellular damage or inflammation. Clinical practice associates elevated serum or pleural fluid LDH enzyme levels with a number of conditions, including: neoplasia, reticuloendothelial tumours, leukaemia, etc. This is because these conditions can cause cell damage or death, leading to the release of LDH into the blood and pleural fluid [6-8]. Thus, determination of LDH levels can help to assess the presence of these conditions in patients with pleural fluid above normal.

This research aims to demonstrate the relationship between pleural fluid LDH enzyme value and cytopathological outcome. The presence of lactate dehydrogenase (LDH) enzyme in pleural fluids from patients with different diseases was quantitatively assessed in conjunction with cytopathological examination.

### Materials and methods

Between 2016 and 2019, a prospective study was carried out on a group of 92 cytopathological samples analysed in the Pathological Anatomy Laboratory of the Clinical Hospital “Prof. Dr. Th. Burghel” and SC. OncoTeam Diagnostic, Bucharest, which could be correlated with the LDH enzyme values of pleural fluids from the first evacuation. The LDH enzyme values of pleural fluids from the first evacuation were collected from the Hypocrate computer system of the Clinical Hospital “Prof. Dr. Th. Burghel”.

Briefly, 100 pleural fluid samples were received in the laboratory, see Koss et al [2]. The pleural fluid samples were analysed macroscopically and then transferred to disposable tubes for centrifugation at 1000 rpm for 15 minutes using the Hettich EBA 20 centrifuge.

After removal of the supernatant from the obtained sediment (1ml) conventional smears were performed. In hypocellular samples the centrifugation and supernatant removal process was repeated 3-4 times.

Two smears were performed on each sample and fixed by direct drying. From purulent or serohaemor-

rhagic pleural fluids a smear was made directly from the homogenised product without centrifugation, then saline was added in 1:1 solution and centrifuged. After the smears were made, 5 ml of fixative liquid (aldehyde form, 10% dilution) was added to the remaining sample to obtain the cytoblock. The smears made from the pleural fluid samples, after fixation for not more than 12 hours, were stained by the Papanicolaou or May-Grunwald Giemsa methods. To obtain the cytoblock, the sample mixture with Formaldehyde was centrifuged at 1000 rpm for 15 minutes. The supernatant was removed and the new sediment obtained was transferred to filter paper. The contents wrapped in filter paper were placed in the special work box and processed on the Donatello processor. After embedding in paraffin, 2 µm sections were made using the microtometer. The sections transferred onto slides were subjected to the deparaffinization process. One slide was stained by the hematoxylin-eosin method.

In cases with suspected malignancy, additional tests were performed by the immunocytochemical method based on the binding of an antigen, which is a cellular component, to a specific labelled antibody.

### Results

Elevated LDH levels in pleural fluid can indicate cellular damage or inflammation in the pleural space. Elevated serum or pleural fluid LDH enzyme levels can be associated with various conditions, including neoplasia, reticuloendothelial tumors, and leukemia. These conditions can lead to cell damage or death, causing LDH to be released into the bloodstream and pleural fluid. An increase in LDH levels may prompt further investigation into the underlying cause, which could include malignancies or other diseases.

The results of the 92 cytopathological samples studied were the following: 18 positive, 22 suspect and 52 negative, shown in Fig.4. (N = Negative, P = Positive, S = Suspect).

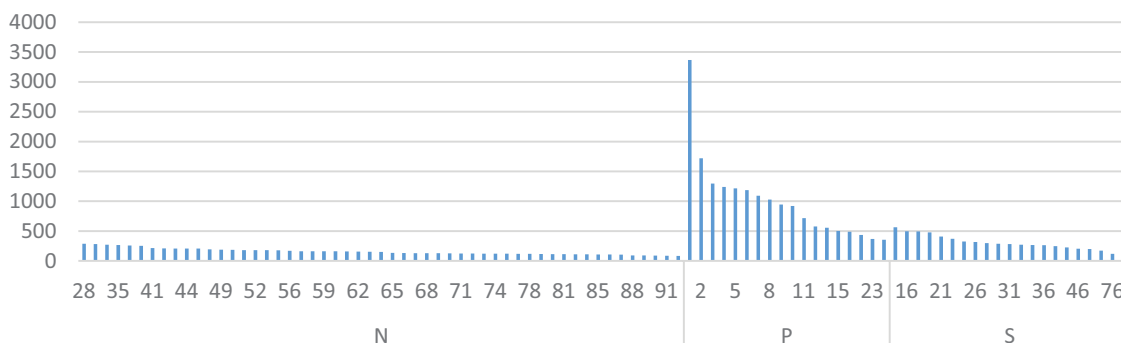
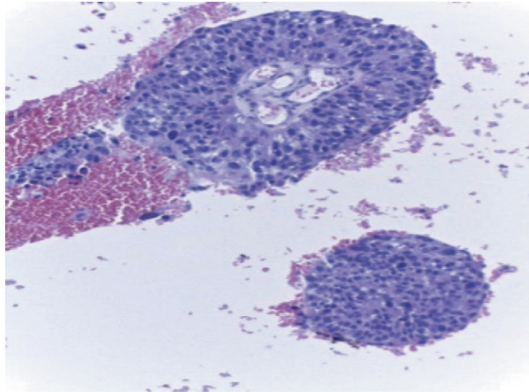


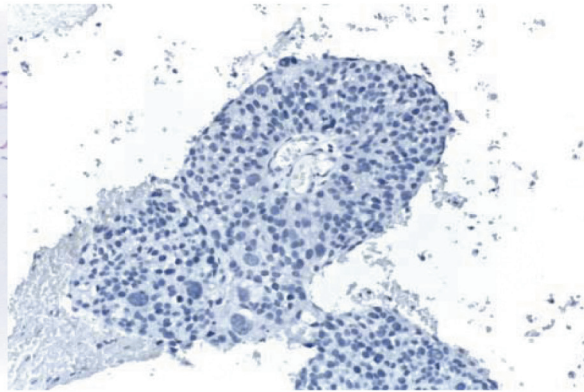
Figure 4. Correlation of LDH enzyme values with cytological result before immunocytochemical testing of suspect results.

LDH levels were correlated with cytopathological aspects. Six groups of LDH values were considered; For LDH levels above 350, 24 results were identified, of which: 18 positive, 6 suspect and 0 negative. All 18 positive cytologi-

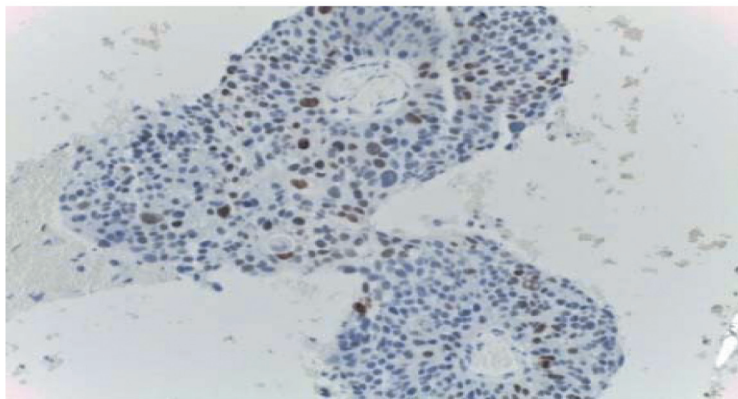
cal results had LDH values above 355. At the same time, the other 6 suspicious samples were analysed with tumour markers, resulting in each diagnosis of positive cytology for malignancy (e.g. the case below);



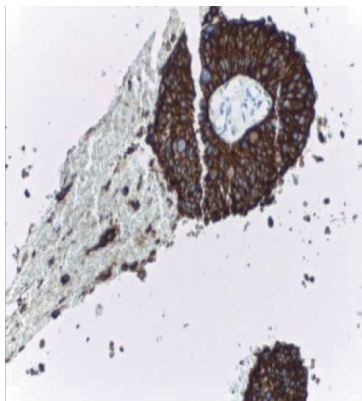
Cytoblock ob.20, Suspect



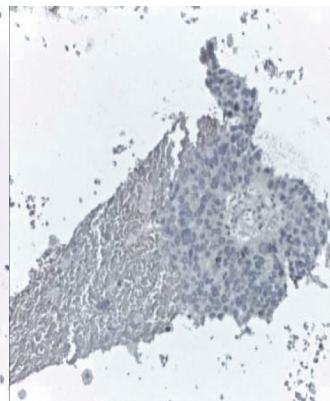
Calret ob.20, Negative



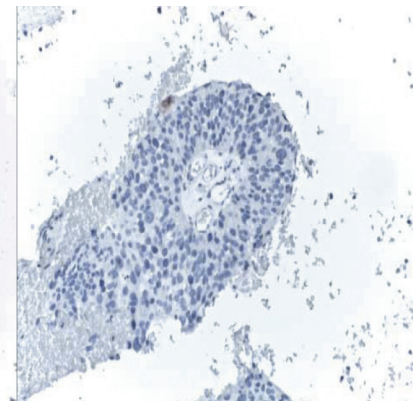
TTF1 ob.20, Positive



MCK ob.20, Positive



TRPS, ob.20, Negative



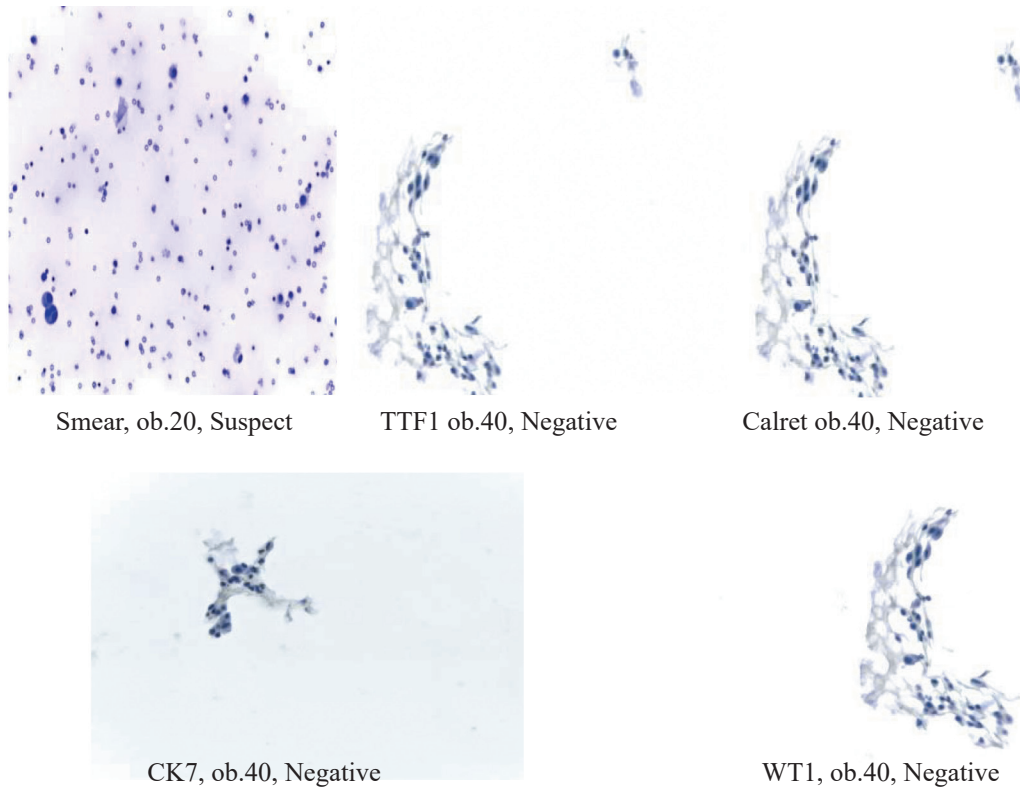
CK5-6, ob20, Negative

For LDH levels between 300-349, 3 results were identified, of which 0 positive, 3 suspect and 0 negative. The 3 suspect samples were analysed with tumour markers, resulting in:

- two with positive cytology diagnosis for malignancy;
- one cytologically negative for malignancy (e.g. the case on the next page);

For LDH levels between 270-299, 6 results were identified, of which 0 positive, 4 suspect and 2 negatives. The

4 suspect samples were analysed with tumour markers resulting in each diagnosis with negative cytology for malignancy; For LDH levels between 200-269, 14 results were identified, of which: 0 positive, 6 suspect and 8 negatives. The 6 suspect samples were analysed with tumour markers resulting in each diagnosis being cytology negative for malignancy; For LDH levels between 115-199, 35 results were identified, of which: 0 positive, 4 suspect and 31 negatives. The 4 suspect samples were analysed with



tumour markers resulting in negative cytology for malignancy at each diagnosis; For LDH levels between 50-114, 16 results were identified, of which: 0 positive, 0 suspect and 16 negatives.

**Conclusions**

LDH is an enzyme with an important role in the diagnosis and evaluation of pleural fluids. Its levels can provide useful information about the nature of the pleural fluid (transudate or exudate) and may suggest the presence of certain diseases.

Comparing the positive cytopathological results with the biochemical results of the pleural fluid from the first evacu-

ation, it was observed that there is a correlation between the positive cytopathological result and increased LDH values as shown in Figure.5.

Using the correlation of the positive cytological result, confirmed immunocytochemically for the suspected diagnostic samples, we found that these cytological results of the pleural fluid samples can be improved by the parallel determination of the LDH enzyme, thus the proportion of suspected cases becomes positive for malignancy in almost all cases with LDH values above 300. High LDH levels above 350 correlate 100% with positive cytopathological appearance for malignancy. This test can be recommended in clinical work for the detection of malignant cells in pleural effusion.

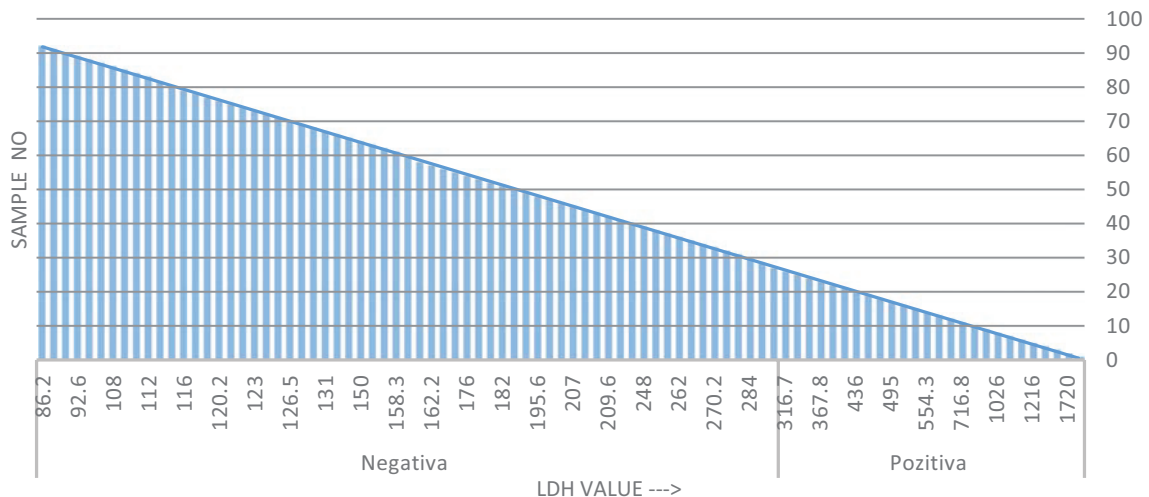


Figure 5. The correlation of LDH enzyme values with the cytological result after immunocytochemical testing of suspect results.

## References

1. Rossi ED, Bizzarro T, Schmitt F, Longatto-Filho A. - The role of liquid-based cytology and ancillary techniques in pleural and pericardic effusions: an institutional experience, *Am Cancer Society Journals*, 2015
2. Kos GL. Examination of effusion pleural, ascitic and pericardial fluids, *Compendium on diagnostic Cytology, the seventh Ed. Tutorials of Cytology*, Chicago, 1992.
3. Park, J. E., Do, Y. W., Lee, D. H., Lee, S. Y., Lim, J. K., Choi, S. H., Seo, H. W., Yoo, S. S., Lee, S. Y., Cha, S. I., Park, J. Y., Lee, J., & Kim, C. H. (2020). Idiopathic Pleural Effusions: Characteristics and Discrimination From Cytology-Negative Malignant Pleural Effusions. *The American journal of the medical sciences*, 360(3), 236–242. <https://doi.org/10.1016/j.amjms.2020.04.020>
4. Dabbs JD. *Diagnostic Immunohistochemistry Theranostic and Genomic Applications*, 5th Edition, 2019.
5. Syed Z, Ali Edmund S. *Cibas., Serous Cavity Fluid and Cerebrospinal Fluid Cytopathology*, 2012.
6. Koss GL, Melamed MR. *Koss' Diagnostic Cytology and Its Histopathologic Bases*, 5th Edition, 2006 Lippincott Williams & Wilkins.
7. Raica M. *Clinical Cytology*, Victor Babes University of Medicine and Pharmacy, Timisoara, 2001.
8. Serbescu A, Teleaga C, Toader C. *Cytological diagnosis in peripheral lung cancer - Bronchoalveolar lavage (BAL)*, National Conference of Bronhology Cluj 2013.



Received for publication, September, 20, 2023  
Accepted, October, 11, 2023

*Original article*

## **An-ecofriendly synthesis of silver nanoparticles using microalga *Desmodesmus protuberans* and evaluation of their antimicrobial activity**

**CLAUDIA - VERONICA UNGUREANU<sup>1\*</sup>, RODICA CHIHAI<sup>1</sup>,  
ALINA - FLORENTINA SARACU<sup>1</sup>, ALINA - MIHAELA CEOROMILA<sup>1</sup>**

<sup>1</sup> „Dunărea de Jos” University of Galați, Cross- Border Faculty, 47 Domnească Street, RO-800008, Galați, România

### **Abstract**

Due to the numerous uses for nanoparticles, nanoparticle production is currently a particularly fascinating topic of research. Since no harmful chemicals are employed during the biological process, it is thought to be the safest and cleanest method.

The strong ability of algae to absorb metals and decrease metal ions makes algal synthesis of Ag-NPs particularly intriguing.

The current work concentrated on the green synthesis of silver nanoparticles (AgNPs) using the microalgae *Desmodesmus protuberans*. The preparation of nanoparticles was confirmed by the observation of the color change of the mixture of silver nitrate, after the addition of the cell free algal extract, from bright green to reddish yellow. The biosynthesis of AgNPs was further confirmed by scanning electron microscopic and energy dispersive X-ray analysis. Furthermore, silver nanoparticles demonstrated a significant antimicrobial activity against the pathogenic microorganisms.

### **Keywords**

silver nanoparticles, microalgae, Green synthesis, *Desmodesmus protuberans*, antimicrobial activity

---

✉ \*Corresponding author: Claudia Ungureanu. e-mail: claudia.ungureanu@ugal.ro

## Introduction

The field of nanotechnology is either one of the foremost important and active areas of research in modern science.

Nanotechnology is an emerging field that includes synthesis, characterization, and development of various nanomaterials [1, 2] that have significant roles in daily life, providing valuable products that improve industrial production, agriculture, communication, and medicine) [3].

Nowadays, some metallic nanoparticles are crucial antibacterial agents. They are appropriate for additional applications such as carriers for medication administration, chemical sensing, cosmetics, antioxidants, and others due to their size, which fall within the range of 1-100nm [1, 2, 4, 5]. Synthesis of nanomaterials containing noble metal requires alternative strategies because of their high cost.

Though several physicochemical approaches (photo-induced reduction, electrochemical deposition, microwave-assisted, laser ablation, high-energy irradiation, pyrolysis) may be used to create AgNPs, they are both costly and possibly hazardous to the environment.

The use of biological species to synthesize nanomaterials is gaining popularity since biological approaches are less costly, nontoxic, environmental friendly aligned to “green chemistry” principles and presents simple approach [6, 7, 8]

A wide range of materials, including plants and plant products, algae, fungi, yeast, bacteria, and viruses, can be used in the biological production of NPs. The initial steps in the synthesis of NPs involve combining biomaterials and precursors of noble metal salts [9]. Proteins, alkaloids, flavonoids, reducing sugars, polyphenols, and other substances found in the biomaterials function as reducing and capping agents for the production of NPs from their metal salt predecessors [10].

Microalgae are microscopic organisms found in fresh or sea water, but also in nonaquatic habitats. Also, microalgae can potentially be used in a large number of biotechnological areas, including cosmetics, pharmaceuticals, nutrition, food additives, aquaculture, and pollution control such as wastewater treatment [11]. For this reason, algae are commonly chosen for green synthesis because their structures are a rich source of biologically active compounds like phycoyanin and phycoerythrin, containing varying concentrations of carbohydrates, proteins, minerals, vitamins, fatty acids, antioxidants, and pigments. Nanoparticle synthesis depends on the amount of algae and the type of algae used. Nanoparticle characteristics, as well as process variables like pH, temperature, precursor concentration, and reaction time, are known to be influenced by the specific biological com-

ponent used, such as the whole cell, extracted molecules, or the supernatant of the culture [12, 13, 14]. Common problems in nanoparticle synthesis include stabilization, crystal development, and particle aggregation. The ability to control the size and shape of metal nanoparticles obtained by green synthesis can only be possible by investigating the relevant biosynthesis mechanisms.

To date, several reports about the biosynthesis of silver nanoparticles through a diverse species of macro- and microalgae have been published [15,16]. Jayshree et al. [17] used the extract of economically important unicellular green alga *Chlorella vulgaris*, for the synthesis of silver nanoplates. During synthesis of Ag-NPs, chromatic changes in the reaction mixture act as a visual marker affirming the continuity of the process. Kannan et al. [18] observed an obvious change of brown to yellow colour after 48 h during reduction of AgNO<sub>3</sub> by the extract of *Codium capitatum* and a time-dependent increase in brown colour intensity at 422 nm. Other green algal species like *Chlorococcum humicola*, *Euglena gracilis*, *Caulerpa serrulata* etc. have been reported to synthesize Ag-NPs with variable shapes and applications [19, 20, 21]. Additionally, limited research has been done on utilizing *Desmodesmus sp.* (*Scenedesmeaceae*) to generate silver nanoparticles [22].

In most of the medicinal and industrial processes, silver has long been acknowledged as having inhibitory effects on microbes (Morones et al. 2005). Researchers who have successfully achieved green synthesis have simultaneously assessed the antibacterial and antifungal effects on a variety of microorganisms.

Present study developed an ideal, cost-effective and safe procedures for silver nanoparticles synthesis from fresh water green microalga *Desmodesmus protuberans*. The synthesized silver nanoparticles were characterized by UV-VIS spectroscopy and scanning electron microscopy (SEM) coupled with EDX (Energy Dispersive X-ray). Also, the antimicrobial effect on the human pathogen like, *Fusarium oxysporum*, *Aspergillus alterata*, *Staphylococcus aureus*, *Bacillus subtilis* and *Candida albicans* was investigated.

## Materials and methods

### Chemicals, Algae Culture and growth conditions

Silver nitrate (AgNO<sub>3</sub>, Cat. No. 209139) was obtained from Sigma-Aldrich Co, St. Louis, MO, USA. The freshwater microalgae used in our study, *Desmodesmus protuberans AICB 141* was procured from the Collection of Algae and Cyanobacteria of the Institute of Biological Research, Cluj, Romania. The culture was grown on Bold's Basal Medium which is composed of (mg L<sup>-1</sup>): NaNO<sub>3</sub>, 250; K<sub>2</sub>HPO<sub>4</sub>,

100;  $\text{KH}_2\text{PO}_4$ ; 150;  $\text{MgSO}_4 \cdot 7\text{H}_2\text{O}$ , 75;  $\text{CaCl}_2$ , 21.35; KOH, 31; 0.06; FE-EDTA, 0.05; 1mL; trace elements solution (g L<sup>-1</sup>):  $\text{H}_3\text{BO}_3$ , 2.86;  $\text{MnCl}_2 \cdot 4\text{H}_2\text{O}$ , 1.81;  $\text{ZnSO}_4 \cdot 7\text{H}_2\text{O}$ , 0.22;  $\text{CuSO}_4 \cdot 5\text{H}_2\text{O}$ , 0.08;  $\text{MnO}_3$ , 0.015, pH 7.0, at an ambient temperature of  $28 \pm 2$  °C. The microalgae were transferred to 250 mL Erlenmeyer flask and left to proliferate under sterile conditions.

Cultures were maintained under 3000 lx fluorescent light, 16:8 light–dark cycle, and 120 rpm for 15–20 days to be reproduced in suitable medium. When algae passed the log phase stage, cells were centrifuged at 1000 rpm and the biomass was obtained. All chemicals reagents were used as received, without any additional purification.

### Biosynthesis of silver nanoparticles

Cell free extract was prepared from *Desmodesmus protuberans* for nanoparticle synthesis. Healthy microalgal cultures were harvested in the logarithmic phase by centrifugation at 5.000 rpm for 10 min (Heltich Universal 320R) at 4°C and washed 3 times with sterile distilled water. Pellets were dried at 80° C (Drying Oven Sanyo, Japan) to constant weight.

About 1 grame of algal power was added with 30 ml of double distilled water in 100 mL conical flask and boiled at 100 °C for 20 minutes. After cooling, the crude extract was centrifuged at 5.000 rpm for 10 min (Heltich Universal 320R) and stored at 4°C for experimental use.

Biosynthesis of AgNP was done by adding 10 mL of cell free extract in 90 mL of 1mM aqueous  $\text{AgNO}_3$  (Sigma, St. Louis, MO) solution, pH 7 and incubated at room temperature for 24 hours under static condition. A color change of the solution was noted by visual inspection confirming the AgNP synthesis. As a control, fresh Bold's Basal Medium with addition of  $\text{AgNO}_3$  was used. Dark conditions were provided by wrapping the flasks with aluminum foil.

This experiment was repeated twice and the obtained data (presence of absorbance pick) were consistent for the tested strain. Stability of the synthesized AgNPS was checked by exposing the samples to ambient conditions for several months.

### Characterization of the Green-Synthesized AgNPs

#### UV–visible spectroscopy analysis

Biosynthesis of Ag-NPs was followed by the change of color of  $\text{AgNO}_3$  solution. The bioreduction of  $\text{AgNO}_3$  was confirmed by sampling the reaction mixture at regular intervals and the absorption maximum was scanned by UV–vis spectra, at the wavelength of 300–700 nm in Hanna HI839800 spectrophotometer.

For further characterization studies the nanoparticles solution was centrifuged at 10.000 rpm for 15 minutes and the resulting suspension was washed in sterile double-distilled water to get free of any biological molecule present in algal extract (i.e, proteins/enzymes), which are not able to capping the silver nanoparticles.

### SEM and EDX analysis

The size and exterior morphology of biosynthesized  $\text{AgNO}_3$  particles were deliberated by SEM (Scanning Electron Microscopy) coupled with EDX (Energy Dispersive X-ray) method. The imagistic evaluation of nanoparticles was carried out with a Quanta 200 type SEM equipment (FEI, Netherlands), under the low-vacuum conditions, at „Dunarea de Jos” University of Galati, Romania. Prior the insertion into the microscope chamber, the samples were fixed on the metallic stub surface by their attachment on a carbon adhesive tape. The analyses were performed with increasing the samples' conductivity. Thus, the  $\text{AgNO}_3$  nanoparticles were coated with a metallic layer of 7 nm as thickness by sputtering process, using a Sputter Coater system (SPI Supplies, USA). SEM micrographs were acquired at 2.000 and 5.000x100.000 magnifications, the most relevant images being analysed in this paper.

The microanalysis of biosynthesized  $\text{AgNO}_3$  particles was performed by EDX spectroscopy method, having a sapphire detector connected to the SEM equipment. The electron accelerating voltage of 25 kV was enough to detect a secondary electron signal due to the surface-beam interaction, and to stimulate the specific atoms from the samples. EDX data of chemical components were processed by dedicated software and quantified using the ZAF matrix correction, where Z is the atomic number, A is the absorption, and F is the fluorescence. SEM-EDX results indicate a local character of this analysis, taking into consideration the scanned micro-area of about 100mm<sup>2</sup> or μm<sup>2</sup>.

### Antimicrobial assay

The antimicrobial effects of synthesized AgNPs were examined against various types of microorganisms like: *Fusarium oxysporum*, *Aspergillus alterata*, *Staphylococcus aureus*, *Bacillus subtilis* and *Candida albicans*. The antimicrobial activity of biosynthesized AgNPs was performed by agar well diffusion method. About 20 mL of sterile Nutrition broth agar media was poured into the sterile Petri plates. The solid medium was gently punctured with cork borer to make a well. Positive control, Cell free algal extract, silver nitrate, and silver nanoparticles were added into each well on the nutrition broth agar media at various concentrations (50 μl, 75 μl, and 100 μl) and incubated for 24–48 h at 37 °C. After incubation, the zone of inhibition was measured



Figure 1. Color intensity after the addition of algal cell-free extract with 1 mM  $\text{AgNO}_3$ , indicates formation of silver nanoparticles. a) initial color change, (b) 15 minutes, (c) 24 hrs.

and expressed as millimeter (mm) in diameter. The statistical analysis of standard error was calculated using triplicates of experiments ( $n=3$ ).

## Results and discussion

### Visual examination and UV-Vis spectroscopy

The test organism *Desmodesmus protuberans* belonging to the class *Chlorophyceae* is a water alga with an oval or shuttle-shaped body. The colonies most often have two or four cells arranged linearly and are occasionally unicellular. In the present study, when algal extract was exposed to silver ions, the reaction started within 15 minutes and the colour of the algal extract changed from bright green to reddish yellow, indicating biotransformation of  $\text{Ag}^+$  ion to  $\text{Ag}^0$ , compared with the control. Also, the color is changed into deep brown color after 24 hrs incubation time (Figure 1). The color change resulted from excitation from SPR (surface plasmon resonance) in the metal of surface [23]. Intensity of brown colour increased in direct proportion to the incubation period. Surface plasmon resonance (SPR) is the manifestation of a resonance effect due to the interaction of conduction electrons of metal nanoparticles with incident photons.

Also, after 24 hrs time incubation, there is no significant color change, indicating the saturation of the reaction of silver nanoparticle formation.

UV-VIS spectroscopy is one of the important techniques to determine the formation and stability of metal nanoparticles in aqueous solution. The biosynthesized AgNPs were measured by UV-visible spectroscopy at different time intervals to study the change in light absorption and increase in intensity.

The absorption spectra of nanoparticles showed highly symmetric single band absorption with a definite peak at 453 nm at 15 minutes, and steadily increased in intensity at 24 hrs without any shift in the peak (Figure 2). Also, previous studies demonstrated that a usual silver nanoparticles SPR pattern is present in the range of 400-480 nm [23]. It was observed the band occurs at 420 nm and 450 nm for *Scenedesmus abudans* and *Spirulina sp.* [24].

### SEM and EDX analysis

Scanning electron microscopy was carried out to analyze the synthesized nanoparticles for the morphology and their size. SEM image revealed spherical nanoparticles with high agglomeration with an average size ranging from 58 nm to 107 nm (Figure 3).

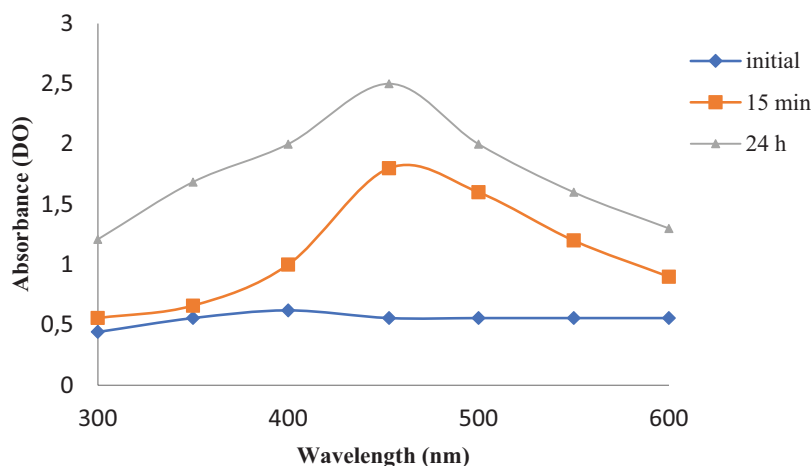


Figure 2. UV-Visible spectrum recorded the formation of nanoparticles in the reaction mixture of algal cell-free extract and  $\text{AgNO}_3$  at different time intervals.

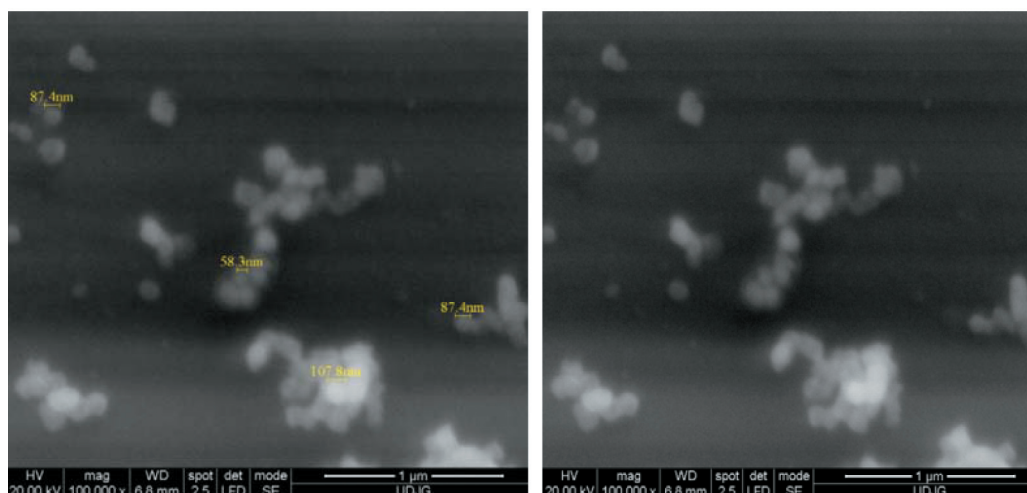


Figure 3. SEM image of silver nanoparticles synthesized from microalga *Desmodesmus protuberans*

The silver nanoparticles formed mostly spherical and cubical structure with high aggregation. Similarly, spherical, truncated and ellipsoidal nanoparticles biosynthesized by marine brown seaweed *Padina tetrastratica* was reported [25]. Jayashree et al. [26] reported spherical nanoparticles synthesized by microalga *Scenedesmus*.

Formation of elemental silver was confirmed through EDX analysis. The optical absorption band peaks were found in the range of 3-4 keV. It is the best evidence to identify that formation of pure silver (Figure 4).

EDX spectrum clearly confirms the purity of the silver nanoparticles with the weight percentage of 76.33% along with the signals of O, C, K and Cl as the mixed components in the reaction medium. Similar results were reported by Manivasagan et al. [27].

#### Antimicrobial studies

Based on the recent reports of the World Health Organization, infectious diseases pose one of the greatest health challenges. The resistance of human pathogens to the commercially available antimicrobial agents and antibiotics has prompted the researchers to explore new innovative strategies for developing new antimicrobials. Also, antimicrobial

activity of the silver ions, silver compounds has been thoroughly investigated, and surveys have revealed the remarkable antibacterial activity of SNPs. The antimicrobial activity of silver nanoparticles mainly depends on the size and shape of the nanoparticles.

The antimicrobial potential of the algal-synthesized silver nanoparticles showed the highest antimicrobial efficacy compared to pure cell algal extract against the various types of microorganisms, such as *Fusarium oxysporum*, *Aspergillus alterata*, *Staphylococcus aureus*, *Bacillus subtilis* and *Candida albicans* using agar well diffusion method. The inhibition zones formed against the pathogenic microorganisms at different concentrations are presented in Table 1.

The gram-positive bacteria *Bacillus subtilis* showed the highest clear zone of inhibition of 29.30 mm, at a concentration of 100 µg/ml, and then *Staphylococcus aureus* showed an inhibition zone of 28.00 mm. The maximum zone formation of silver nanoparticles against *Candida albicans* was 20.30 mm, followed by *Fusarium oxysporum* and *Aspergillus alterata* with 18.30 mm and 18.10 mm respectively.

Also, the biosynthesized AgNPs from algal aqueous cell-free extract were moderately susceptible to fungal pathogen

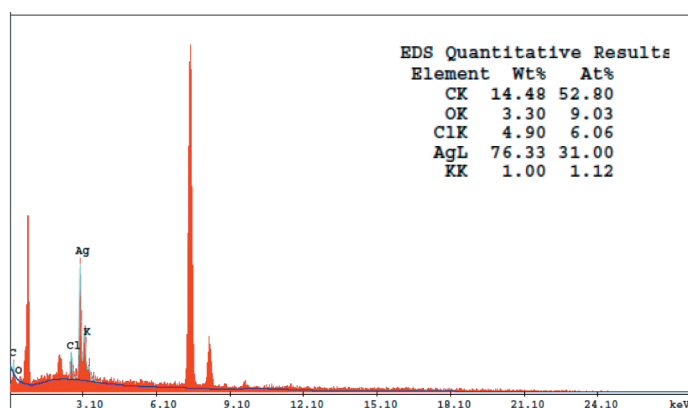


Figure 4. EDX spectra of silver nanoparticles synthesized from microalga *Desmodesmus protuberans*.

Table 1. The antimicrobial activities of biosynthesized AgNPS

Microorganisms strain	Inhibition zone (mm in diameter)			
	Concentrations	Silver nitrate	Cell free algal extract	AgNPS
<i>Fusarium oxysporum</i>	50µl	09.50	0	13.50
	75µl	11.30		16.00
	100µl	12.60		18.30
Cyclohexaminide (100µl)		17.10		
<i>Aspergillus alterata</i>	50µl	08.20	0	13.30
	75µl	11.10		15.20
	100µl	12.10		18.10
<i>Staphylococcus aureus</i>	50µl	12.50	0	20.20
	75µl	12.30		24.60
	100µl	14.00		28.00
Streptomycin (100µl)		27.60		
<i>Bacillus subtilis</i>	50µl	08.80	0	19.60
	75µl	10.50		25.60
	100µl	11.10		29.30
Streptomycin (100µl)		28.30		
<i>Candida albicans</i>	50µl	10.20	0	14.60
	75µl	11.00		18.00
	100µl	12.30		20.30

like, *Candida albicans*, suggesting that the increase in dose may tend to be efficiently toxic [28, 29]. However, the strains *Bacillus subtilis* and *Staphylococcus aureus* were found to be more susceptible bacteria against the synthesized AgNPs. A similar result was reported by Anita et al. [30], who observed a zone of inhibition in Ag nanoparticles generated using the aqueous algal extract of *Sargassum tenerrimum* in Gram-positive bacteria *Staphylococcus aureus* and *Bacillus subtilis*. Thus, one can explore the medicinal properties of AgNPs synthesized from the cell free algal extract.

## Conclusions

Nanoparticles have been employed because they are easy to process, environmentally benign, free of pollutants, nontoxic, low-cost, and have an excellent atom economy. Compared to other conventional procedures including physical and chemical methods, green synthesis methods offer a clean, non-toxic, and environmentally friendly approach to the synthesis of metal NPs. Similar to other biological species including fungi, yeast, and bacteria, microalgae significantly influence the creation of nanoparticles.

In this study, we have demonstrated a simple and reproducible way for the synthesis of silver nanoparticles using the fresh water microalga *Desmodesmus protuberans*.

Characterization of synthesized silver nanoparticles was carried out by UV-vis spectroscopy and SEM equipped with EDX. Silver nanoparticles exhibited a single absorbance band at 453 nm at 15 minutes and steadily increased in intensity at 24 hrs without any shift in the peak. SEM image of silver nanoparticles synthesized from *Desmodesmus* sp. showed highly agglomerated spherical nanoparticles at different magnifications. AgNPs shows an average size ranging from 58-107nm. EDX spectrum clearly confirms the

purity of the silver nanoparticles with the weight percentage of 76.33%.

The biogenic AgNPs showed significant antimicrobial effects against all studied species particularly, *Staphylococcus aureus* and *Bacillus subtilis*. Thus, biosynthesized AgNPs can find immense application in the field of biomedical and biotechnological applications.

Undoubtedly, it is necessary to conduct further research on the toxicity Of silver nanoparticles in relation to living organisms.

## Acknowledgements

This work was supported by an intern grant “Microbiological synthesis of metal nanoparticles”, project number. 14889/11.05.2022.

## Conflicts of Interest

The authors declare that there are no conflicts of interest.

## References

1. Khanna P, Kaur A, Goyal D. Algae-based metallic nanoparticles: Synthesis, characterization and applications. J Microbiol Methods. 2019 Aug;163:105656. doi: 10.1016/j.mimet.2019.105656. Epub 2019 Jun 17. PMID: 31220512.
2. Prasad SR, Teli SB, Ghosh J, Prasad N R, Shaikh, VS, Nazeruddin GM, Shaikh YI.. A review on bio-inspired synthesis of silver nanoparticles: their antimicrobial efficacy and toxicity. Engineered Science. 2021;16:90-128. doi: 10.30919/es8d479.
3. Ijaz I, Bukhari A, Gilani E, Nazir A, Zain H, Saeed R.. Green synthesis of silver nanoparticles using different

- plants parts and biological organisms, characterization and antibacterial activity. *Environmental Nanotechnology, Monitoring Management*. 2022;18:100704. doi: 10.1016/j.enmm.2022.100704
4. Malik M, Iqbal MA, Iqbal Y, Malik M, Bakhsh S, Irfan S, Pham PV. Biosynthesis of silver nanoparticles for biomedical applications: A mini review. *Inorganic Chemistry Communications*. 2022;109980. doi: 10.1016/j.inoche.2022.109980
  5. Merin DD, Prakash S, Bhimba BV. Antibacterial screening of silver nanoparticles synthesized by marine micro algae. *Asian Pacific journal of tropical Medicine*. 2010;3(10):797-799. doi: 10.1016/S1995-7645-(10)60191-5
  6. Navarro Gallón SM, Alpaslan E, Wang M, Larese-Casanova P, Londoño ME, Atehortúa L, Pavón JJ, Webster TJ. Characterization and study of the antibacterial mechanisms of silver nanoparticles prepared with microalgal exopolysaccharides. *Mater Sci Eng C Mater Biol Appl*. 2019 Jun;99:685-695. doi: 10.1016/j.msec.2019.01.134. Epub 2019 Feb 1. PMID: 30889742.
  7. Mora-Godínez S, Contreras-Torres FF, Pacheco A. Characterization of Silver Nanoparticle Systems from Microalgae Acclimated to Different CO<sub>2</sub> Atmospheres. *ACS Omega*. 2023 Jun 5;8(24):21969-21982. doi: 10.1021/acsomega.3c01914. PMID: 37360473; PMCID: PMC10286254.
  8. Koçer AT, Özçimen D. Eco-friendly synthesis of silver nanoparticles from macroalgae: optimization, characterization and antimicrobial activity. *Biomass Conversion and Biorefinery*. 2022;1-12. <https://doi.org/10.1007/s13399-022-02506-0>.
  9. Sriramulu M, Shanmugam S, Ponnusamy VK. Agaricus bisporus mediated biosynthesis of copper nanoparticles and its biological effects: An in-vitro study. *Colloid and Interface Science Communications*. 2020;35:100254. doi:10.1016/j.colcom.2020.100254.
  10. Kuppusamy, P, Yusoff, M. M, Maniam, G. P, Govindan, N. (2016). Biosynthesis of metallic nanoparticles using plant derivatives and their new avenues in pharmacological applications—An updated report. *Saudi Pharmaceutical Journal*, 24(4), 473-484. doi:10.1016/j.jsps.2014.11.013
  11. Chugh D, Viswamalya VS, Das B. Green synthesis of silver nanoparticles with algae and the importance of capping agents in the process. *Journal of Genetic Engineering and Biotechnology*, 2021;19(1), 1-21. doi:10.1186/2Fs43141-021-00228-w
  12. Kashyap M, Samadhiya K, Ghosh A, Anand V, Shirage PM, Bala K. Screening of microalgae for biosynthesis and optimization of Ag/AgCl nano hybrids having antibacterial effect. *RSC advances*. 2019;9(44):25583-25591 doi: 10.1039/c9ra04451e.
  13. Priyadarshini SS, Sethi S, Rout S, Mishra PM, Pradhan N. Green synthesis of microalgal biomass-silver nanoparticle composite showing antimicrobial activity and heterogenous catalysis of nitrophenol reduction. *Biomass Conversion and Biorefinery*. 2023;13(9):7783-7795. doi: 10.21203/rs.3.rs-398850/v1
  14. Verma AK, Kumar P. On recent developments in biosynthesis and application of Au and Ag nanoparticles from biological systems. *Journal of Nanotechnology*. 2022:1-19. doi: 10.1155/2022/5560244
  15. Merin DD, Prakash S, Bhimba BV. Antibacterial screening of silver nanoparticles synthesized by marine micro algae. *Asian Pacific journal of tropical Medicine*. 2010;3(10):797-799. doi: 10.1016/S1995-7645-(10)60191-5
  16. Jayashree J, Nilotpala P, Rati RN, Bishnu PD, Lala BS, Prasanna KP, Barada KM. Microalga *Scenedesmus* sp.: a potential low-cost green machine for silver nanoparticle synthesis. *Journal of Microbiology and Biotechnology*. 2014;24(4):522-533. doi: 10.4014/jmb.1306.06014.
  17. Kannan RRR, Stirk WA, Van Staden J. Synthesis of silver nanoparticles using the seaweed *Codium capitatum* PC Silva (Chlorophyceae). *South African Journal of Botany*. 2013;86:1-4. doi: 10.1016/j.sajb.2013.01.003
  18. Jena J, Pradhan N, Dash BP, Sukla LB, Panda PK. Biosynthesis and characterization of silver nanoparticles using microalga *Chlorococcum humicola* and its antibacterial activity. *Int J Nanomater Biostruct*. 2013;3(1):1-8. ISSN 2277-3851.
  19. Li X, Schirmer K, Bernard L, Sigg L, Pillai S, Behra R. Silver nanoparticle toxicity and association with the alga *Euglena gracilis*. *Environmental Science: Nano*. 2015;2(6):594-602. doi: 10.1039/C5EN00093A
  20. Aboelfetoh EF, El-Shenody RA, Ghobara MM. Eco-friendly synthesis of silver nanoparticles using green algae (*Caulerpa serrulata*): reaction optimization, catalytic and antibacterial activities. *Environmental Monitoring and Assessment*. 2017;189:1-15. doi: 10.1007/s10661-017-6033-0.
  21. Dağlıoğlu Y, Yılmaz Öztürk B.. A novel intracellular synthesis of silver nanoparticles using *Desmodesmus* sp.(Scenedesmaceae): different methods of pigment change. *Rendiconti Lincei. Scienze Fisiche e Naturali*. 2019;30:611-621. doi: 10.1007/s12210-019-00822-8
  22. Morones JR, Elechiguerra JL, Camacho A, Holt K, Kouri JB, Ramírez JT, Yacaman MJ. The bacteri-

- cidal effect of silver nanoparticles. *Nanotechnology*. 2005;16(10):2346. doi: 10.1088/0957-4484/16/10/059.
23. Mulvaney P. Surface plasmon spectroscopy of nano-sized metal particles. *Langmuir*. 1996;12(3):788-800. doi: 10.1021/la9502711
24. Haghghi Pak Z, Abbaspour H, Karimi N, Fattahi A. Eco-friendly synthesis and antimicrobial activity of silver nanoparticles using *Dracocephalum moldavica* seed extract. *Applied sciences*. 2016;6(3):69. doi: 10.3390/app6030069.
25. Muthusamy G, Thangasamy S, Raja M, Chinnappan S, Kandasamy S. Biosynthesis of silver nanoparticles from *Spirulina* microalgae and its antibacterial activity. *Environmental Science and Pollution Research*. 2017;24(23):19459-19464. doi: 10.1007/s11356-017-9772-0.
26. Rajeshkumar S, Malarkodi C, Kumar V. Synthesis and characterization of silver nanoparticles from marine brown seaweed and its antifungal efficiency against clinical fungal pathogens. *Asian Journal of Pharmaceutical and Clinical Research*, 2017;190-193. doi: 10.22159/ajpcr.2017.v10i2.15127.
27. Annamalai J, Nallamuthu T. Green synthesis of silver nanoparticles: characterization and determination of antibacterial potency. *Applied nanoscience*. 2016;6:259-265. doi: 10.1007/s13204-015-0426-6.
28. Kim KJ, Sung WS, Moon SK, Choi JS, Kim JG, Lee DG. Antifungal effect of silver nanoparticles on dermatophytes. *Journal of microbiology and biotechnology*. 2008;18(8):1482-1484. PMID: 18756112.
29. Kim KJ, Sung WS, Suh BK, Moon SK, Choi JS, Kim JG, Lee DG. Antifungal activity and mode of action of silver nano-particles on *Candida albicans*. *Biometals*. 2009;22:235-242. doi: 10.1007/s10534-008-9159-2. PMID: 18769871.
30. Solanki AD, Patel IC. *Sargassum tenerrimum*-mediated green synthesis of silver nanoparticles along with antimicrobial activity. *Applied Nanoscience*. 2023;13(6):4415-4425. doi: 10.1007/s13204-022-02709-x.



Received for publication, October 01, 2023  
Accepted, October, 09, 2023

## Review

# Relationship between dentifrices based on hydroxyapatites and human enamel remineralization

ALEXANDRA AVRAM<sup>1</sup>, AURORA MOCANU<sup>1</sup>,  
SORIN RIGA<sup>1,2</sup>, MARIA TOMOAI A-COTISEL<sup>1,2,\*</sup>

<sup>1</sup> Babes-Bolyai University of Cluj-Napoca, Faculty of Chemistry and Chemical Engineering, Research Centre of Physical Chemistry, 11 Arany Janos Str., RO-400028, Cluj-Napoca, Romania

<sup>2</sup> Academy of Romanian Scientists, 3 Ilfov Street, RO-050044, Bucharest, Romania

## Abstract

Enamel demineralization is an intricate process that holds significant clinical consequences, being a central part of the emergence and progression of various dental problems, most notably dental caries. This demineralization of tooth enamel is linked to a variety of factors, including the composition of oral microbiota and that of saliva, the prevalence of sugar consumption or acidic soft drinks, and, of course, oral hygiene practices. The oral microbiome plays a role in generating organic acids that foster an environment conducive to enamel breakdown. Additionally, a decrease in saliva production can lower the oral environment's ability to neutralize acids and support the remineralization process, thereby intensifying demineralization. Dentifrices enriched with biomimetic hydroxyapatites are important in preventing demineralization as they not only help with oral hygiene but also provide key ions that help strengthen enamel. Considering their similarity to the natural component in enamel, synthetic hydroxyapatites have recently emerged as potent remineralizing agents. Hence, this work aims to illustrate in a simple and concise manner, some of the aspects involved in enamel demineralization and its subsequent remineralization, namely in the relationship between enriched toothpastes containing biomimetic hydroxyapatites and their remineralization efficacy.

## Keywords

demineralization, remineralization, tooth enamel, hydroxyapatite, biomimetic hydroxyapatites, tooth-paste

## Introduction

Tooth enamel is arguably the strongest tissue within the human body, a necessary attribute considering the endless masticatory cycles throughout a human lifespan. The process by which enamel is formed is called amelogenesis, which involves extracellular mineralization. While the intricacies of this process may appear convoluted and complex, for the purpose of this paper, it remains necessary to convey certain aspects in a more concise manner. Hence, remineralization is comprised of two primary stages – the secretory stage and that of maturation [1]. The extracellular matrix is secreted by ameloblasts, specialized cells that secrete unique matrix proteins (that have little in common with other known proteins) [2] and proteinases (matrix metalloproteinase-20 and kallikrein-related peptidase-4) at the dentin surface [3]. The main component in the development of enamel is amelogenin, a protein highly hydrophobic in nature, and possessing a hydrophilic C-terminus region [4]. For further clarification, one work [5] employed NMR spectroscopy to reveal four primary amelogenin structural elements, namely a N-terminus grouping of four  $\alpha$ -helical fragments (S9-V19, T21-P33, Y39-W45, V53-Q56), an elongated random coil section interrupted by two 310 helices (P60-Q117), an extended proline-rich PPII-helical region (P118-L165), and a charged hydrophilic C-terminus (L165-D180). C-terminus is reported to be a determining factor for the parallel alignment of hydroxyapatite crystals [4]. The adsorption of amelogenin onto calcium phosphate, which encourages the alignment of amorphous calcium phosphate particles into ribbons, is critical for enamel formation [6]. The other two major structural proteins are enamelin and ameloblastin. The second most abundant protein next to amelogenin is ameloblastin and it is located between enamel rods [7]. Ameloblastin is reported to be integral in maintaining the differentiation state of ameloblasts, a crucial part of enamel formation [8]. It is also involved in cell-matrix adhesion as well as in mineral formation [9]. While the largest, enamelin is also the least abundant (around 1-5%) of all matrix proteins and its domains are mostly found near the surface of the enamel [10]. It is suggested that the presence of enamelin is necessary to control crystal growth, achieve prism structural organization, and attain the ideal thickness of enamel [11]. All these primary matrix proteins are hydrolyzed by matrix metalloproteinase 20 (MMP20). During tooth development, the majority of the organic enamel matrix, which is made up of amelogenins and enamelins, is resorbed away, leaving behind a calcified tissue that is primarily made up of minerals and a sparse organic matrix. Enamel prisms or rods, which are keyhole-shaped structures with a diameter of roughly 5

$\mu\text{m}$ , are created by the structural arrangement of the material [12]. Therefore, enamel is capable of withstanding daily damage from countless masticatory cycles within the oral environment and remain intact for decades without issues. This is due to the high content of calcified tissue which bestows a high level of hardness and great resistance to wear [12]. However, while very durable, mature enamel lacks cells, thus is unable to regenerate itself. Any damage caused is irrevocable because there is no biological process capable of restoration. Classically, several processes that lead to the wear of enamel have been classified: abrasion (mechanical process involving external matter); demastication (food-teeth mechanical interplay); attrition (tooth-tooth interaction); abfraction (Pathological tooth material loss brought on by biomechanical loading pressures); erosion (chemical etching followed by dissolution); resorption (degradation of biological origin) [13].

Tooth decay, alternatively referred to as dental caries or cavities, represents a prevalent concern within oral health. This condition is characterized by the gradual deterioration and demineralization of the tough structures of teeth. The primary instigator is the interaction between specific bacteria residing in the oral cavity and sugars and starches derived from dietary sources. There are a large number of species within the oral cavity that can be associated with carries. Among them, *Streptococcus mutans* (*S. mutans*) is considered the specific pathogen, followed by lactobacilli, members of the *Bifidobacterium*, *Propionibacterium*, and *Scardovia* genera [14, 15]. This interaction initiates the creation of acid. Conjoined with the bacteria and food particles, this acid culminates in the formation of a sticky layer known as dental plaque, adhering to the tooth surface [16]. As time progresses, the acid generated by these bacteria starts to erode the enamel resulting in its gradual weakening and eventual formation of cavities. Furthermore, it is imperative to acknowledge that enamel demineralization isn't solely confined to the acids generated by the oral microbiota. A paramount contributing factor to this phenomenon is external acidity, principally attributed to the overconsumption of acidic soft drinks. These beverages are laden with corrosive agents, exemplified by citric and phosphoric acid that wield the power to instantly and substantially plummet the pH levels within the oral environment. To better understand this aspect, a clinical review [17] presents the case of a 25 year old man with poor oral hygiene and a 7 year cola-drinking history. Advanced decay affected the incisors and canines, whereas the premolars and molars exhibited milder lesions. Another relevant example would be a cross-sectional study with 400 middle-income adults (age 18-25) in Chennai, India [18]. Overall, a weekly consumption of carbonated

drinks was linked to less erosion when compared to daily consumption. A higher consumption was associated with a higher Erosion Index. Carbonated soft drinks showed higher erosion than non-carbonated regardless of the gender of participants.

Dental caries represents a disease continuum that commences with the depletion of ions from apatite crystals during its initial phase, ultimately resulting in the formation of cavities within lesions [19]. Here, the primary objective should be to halt or reverse the progression of demineralized lesions at an early stage in order to avert the potential for cavity formation and the consequent necessity for invasive interventions. Demineralization is the removal of mineral ions from crystals of hydroxyapatite that make up hard tissues like enamel, which, if unregulated, may culminate in dental cavities [20]. This demineralization of enamel leads to nanoscale level changes in topography, disintegration and reduced mechanical properties, and, if not properly managed, leads to hypersensitivity in the dentin and pain [21, 22]. The imperative to develop more effective tooth enamel remineralization aids is paramount in addressing the escalating challenges posed by enamel erosion and demineralization. Traditional approaches to oral care often fall short in reversing the damage caused by acidic attacks and bacterial activity. The easiest way to prevent such problems is the use of daily oral care products that are enriched with different compounds with remineralizing and antibacterial properties.

Various agents that aid in remineralization have been researched over time, with fluoride emerging as the favored option due to its ability to hinder inherent demineralization by promoting the creation of fluorapatite, a less soluble compound when compared to regular hydroxyapatite (HAP) [23]. A few decades ago, scientists started to observe a correlation: individuals residing in regions where fluoride occurred naturally in water sources exhibited fewer cavities and more resilient teeth. This finding prompted a keen interest in comprehending the potential advantages of fluoride for promoting dental well-being. Later (1930-1940) researchers carried out investigations to examine the impact of fluoride on tooth enamel [24]. Their findings revealed that fluoride played a role in fortifying enamel by facilitating the creation of fluorapatite. This compound, compared to the hydroxyapatite constituting enamel, exhibited increased resilience and decreased solubility. During the 1940-1950 period, extensive research endeavors were undertaken to investigate the concept of water fluoridation on a grand scale. These studies provided conclusive evidence that the deliberate addition of carefully regulated quantities of fluoride to communal water sources led to a noteworthy decrease in the occurrence of

cavities, all while avoiding any detrimental health impacts [25]. This pivotal discovery heralded the commencement of community water fluoridation initiatives—an enduring public health strategy that persists in numerous countries up to the present day. In the 1950s, scientists initiated efforts to integrate fluoride into formulations for toothpaste, this endeavor culminating in the introduction of fluoride-infused toothpaste. As such, Crest toothpaste, the first cavity-prevention dentifrice recognized by the American Dental Association, debuted in 1956 [26]. This innovation significantly facilitated the access of individuals to the enamel-strengthening properties of fluoride on a daily basis. Dental researchers have honed their comprehension of fluoride's mechanisms in thwarting cavities and facilitating enamel remineralization. Furthermore, they have devised a range of fluoride-infused products like mouth rinses and dental gels, tailored to accommodate diverse preferences and requirements.

According to scientific literature [27, 28], fluoride primarily operates via two key pathways: stimulating remineralization and impeding demineralization. Upon fluoride exposure, teeth assimilate it into the enamel structure, fostering the creation of fluorapatite crystals. These crystals exhibit heightened resistance to acid assaults from bacteria, thereby aiding in the prevention of cavity development. Additionally, fluoride can disrupt the metabolic processes of acid-producing oral bacteria, thereby further diminishing the likelihood of enamel erosion.

However, toothpaste formulations contain different other ingredients, among which abrasives have been shown to negatively impact the added fluorine compounds. When utilizing abrasives containing aluminum and calcium, the depletion of supplemented fluorides from sodium fluoride (NaF) tends to range from 60% to 90% following one week of storage under ambient conditions. Substances such as sodium bicarbonate and sodium metaphosphate are comparatively milder in their impact, yet they still result in the deactivation of approximately 20% to 25% of the introduced fluoride content within a span of nine months of storage [29]. Also, given the narrow margin between toxic and therapeutic concentrations of fluoride, the scientific community searched for alternatives that even in higher doses would not be harmful.

## **The use of synthetic hydroxyapatite for enamel remineralization**

Innovative remineralization aids hold the potential to replenish essential minerals like calcium and phosphate, fortifying the enamel's structural integrity and resilience. These aids could encompass advanced formulations incorporating hydroxyapatite or other enamel-strengthening compounds, tailored to facilitate efficient remineralization.

Hydroxyapatite has garnered significant research interest for its diverse potential in biomedical applications due to its unique properties and biocompatibility [30-49]. Owing to its similarity to the hydroxyapatite component in enamel, its synthetic counterpart has also been the subject of many studies regarding the demineralization-remineralization process. This is of no surprise considering that roughly at a concentration of 10%, nanoHAP has been noted to contribute to the remineralization of the enamel surface [50]. Additionally, a crucial aspect of maintaining optimal oral health involves the tooth-desensitizing attributes of hydroxyapatite [51-53]. Furthermore, smaller nanoparticles exhibit an enhanced capacity to permeate beneath the enamel surface, enhancing their efficacy in this regard [54]. The levels of calcium and phosphate present in saliva and plaque, serving as primary constituents of hydroxyapatite (HA) crystals, exert a significant influence on the process of tooth demineralization and formation. A calcium-to-phosphate ratio of 1.6 is deemed optimal for facilitating enamel remineralization when considering similar levels of supersaturation. Notably, the calcium-to-phosphate ratio in plaque fluid measures around 0.3 [55]. Consequently, an increased availability of calcium may prove beneficial in promoting enamel remineralization. Furthermore, existing literature indicates a proportional relationship between HAP concentration and both the whitening effect and adherence to enamel [56, 57]. Scientific literature outlines various pathways through which hydroxyapatite functions within the oral environment [58]:

- **Physical Enamel Revitalization:** This involves the attachment of nanoparticles to the enamel’s surface, leading to its physical restoration.
- **Chemical Impact:** Hydroxyapatite releases calcium and phosphate ions in the acidic oral environment. This establishes a connection between tooth enamel and HAP nanoparticles by forming an interface.
- **Biological Interactions:** Hydroxyapatite nanoparticles interact with microorganisms, demonstrating a biological influence.

In theory, HAP found in oral care products can affix itself to demineralized outer layers of tooth tissues and directly aid in the remineralization processes. By adhering to enamel, HAP nanoparticles create a protective layer that has demonstrated resilience against multiple acid challenges. Consistent application of HAP through oral care products consequently results in the reinforcement and renewal of this adhered layer, thereby augmenting its protective attribute [59].

In view of these benefits, several commercial toothpaste compositions containing hydroxyapatite have been developed. One of the first studies concerning a hydroxyapatite-based toothpaste reported its results on Japanese schoolchildren in the 1980s [60]. Evidently the results are in favor of HAP addition when compared to placebo, though it was more successful in girls, with a higher reduction in tooth decay occurrence as opposed to boys (35.86% among boys and 55.93% among girls). In Europe the first dentifrice containing nano-hydroxyapatite was introduced in 2006 [61]. Some of these commercial dentifrices have been subjected to testing and comparison by various scientific papers. Some studies involving toothpaste containing different types of hydroxyapatite, as found by the authors, are presented in Table 1.

The use of hydroxyapatite that is enriched with different ions is understandable as these ions are known to generally improve upon the properties of HAP. Most of the commercial toothpaste available employ HAP with Zn, an ion with antibacterial properties that functions by inhibiting glycolytic enzymes thereby slowing down bacterial metabolism and diminishing their capacity to thrive [68]. Literature also reports that zinc contributes to addressing dental calculus formation, although it necessitates a substantial concentration for effectiveness [69]. Some of these formulations also rely on strontium and magnesium. Sr is noted for its capacity to reduce enamel demineralization and mitigate the loss of surface hardness, particu-

**Table 1.** Studies involving toothpastes containing hydroxyapatite and substituted hydroxyapatite and their effect on tooth enamel

Type of HAP	Toothpaste name and composition	Effect	Ref.
Zn-carbonate substituted n-HAP	<b>Biorepair Total Protection Plus / Coswell Funo (BO) Italy</b> Purified water, zinc carbonate hydroxyapatite, glycerin, sorbitol, hydrated silica, silica, aroma, cellulose gum, tetrapotassium pyrophosphate, sodium myristoyl sarcosinate, sodium methyl cocoyl taurate, sodium saccharin, citric acid, phenoxyethanol, benzyl alcohol, sodium benzoate.	No differences in early colonization (EC, 12 h) and biofilm formation (BF, 24 h) when compared to control	[51]
Fluoride HAP Mg, Sr-carbonate substituted n-HAP	<b>Biosmalto Caries Abrasion and Erosion / Curasept A.p.A. Saronno (VA) Italy</b> Purified water, glycerin, hydrated silica, fluoride hydroxyapatite, Mg-Sr-carbonate hydroxyapatite conjugated with chitosan, cellulose gum, xylitol, cocamidopropyl betaine, xantham gum, aroma, acesulfame K, ethylhexylglycerin, phenoxyethanol, sodium benzoate, citric acid.	Lower in early colonization (EC, 12 h) and biofilm formation (BF, 24 h) compared to the control. The association of fluoride and strontium may be more effective in reducing EC and BF than zinc alone at the tested concentrations	[51]

NaF/1% nHAP	<b>Apacare / Cumdente GmbH</b> Aqua, Hydrated Silica, Sorbitol, Propylene Glycol, Glycerin, Sodium C14-16 Olefin Sulfonate, Hydroxyapatite, Aroma, Cellulose Gum, CI 77891, Sodium Fluoride, Allantoin, Sodium Saccharin, Tetrapotassium yrophosphate, Limonene	Apacare exhibited a higher effect than Biorepair. This difference in effectiveness could be attributed to the distinct levels of abrasiveness between the two products and the presence of fluoride in Apacare toothpaste.	[53]
ZnCO <sub>3</sub> -HAP	<b>BioRepair / Dr. Kurt Wolff Forschung</b> Aqua, Zinc Carbonate Hydroxylapatite, Hydrated Silica, Glycerin, Sorbitol, Silica, Aroma, Cellulose Gum, Sodium Myristoyl Sarcosinate, Sodium Methyl Cocoyl Taurate, Tetrapotassium Pyrophosphate, Zinc PCA, Cetraria Islandica Extract, Sodium Saccharin, Citric Acid, Phenoxyethanol, Benzyl Alcohol, Methylparaben, Propylparaben	Biorepair demonstrated the least effectiveness in the current experiment, as well as in a separate in vitro study evaluating the impact of toothpastes with specialized formulations on enamel erosion.	[53]
HAP	<b>Mirasensitive / Hager Werken</b> Aqua, Hydroxyapatite, Xylitol, Sorbitol, Propylene Glycol, Potassium Citrate, Tetrapotassium Pyrophosphate, Sodium C 14–16 Olefin Sulfonate, Disodium Pyrophosphate, Cellulose Gum, Aroma, Sodium Fluoride, Cocamidopropyl Betaine, Sodium Saccharin, Limonene, CI77891	Mirasensitive fell in between Apacare and Biorepair when it comes to dentine loss. Evidence suggests that HAP nanoparticles could penetrate dentine.	[53]
HAP	<b>Karex / Dr. Kurt Wolff GmbH &amp; Co. KG, Bielefeld, Germany</b> 10% hydroxyapatite, aqua, hydrated silica, glycerin, xylitol, hydrogenated starch hydrolysate, silica, cellulose gum, sodium methyl cocoyl taurate, sodium sulfate, menthol, eucalyptol, 1,2-hexanediol, caprylyl glycol, sodium cocoyl glycinate, tetrapotassium pyrophosphate, phosphoric acid, zinc chloride, cetylpyridinium chloride	The HAP-containing toothpaste Karex had a highly significant lower remineralization potential compared to the fluoride-containing toothpaste Elmex This may be attributed to pH values	[62]
HAP	<b>Garda Silk toothpaste</b> Water, Hydrated Silica, Glycerin, Hydrogenated Starch Hydrolysate, Hydroxyapatite, Sodium Methyl Cocoyl Taurate, Xanthan Gum, Aroma, Echinacea Purpurea Extract, Polyol Germanium Complex (PGC) with the Amino Acid Threonine, Menthol, Sodium Saccharin, O-Cymen-5-Ol, Hydroxyacetophenone.	Tooth sensitivity was significantly reduced after 14 days of treatment	[63]
Zn-HAP	<b>Microrepair® Biorepair / Coswell S.P.A., 40050 Funo, Italy</b> Zn-HAP toothpaste without fluoride	The extent of damage observed on enamel surfaces subsequent to treatment with Zn-HAP dentifrice underscored the preservation of rod integrity. This preservation resembled a less progressed state of demineralization when contrasted with samples treated with toothpastes containing fluoride and those without fluoride	[64]
Zn-HAP	<b>Microrepair® Biorepair / Coswell S.P.A., 40050 Funo, Italy</b> Zn-HAP toothpaste without fluoride	Enamel hardness after four cycles of erosive challenge and toothpaste treatment was higher for Microrepair® Biorepair when compared to a non-fluoride one and one containing fluoride.	[65]
ZnHAP	<b>Microrepair® Biorepair Plus / Coswell S.P.A., 40050 Funo, Italy</b> Zn-HAP toothpaste without fluoride and zinc pyrrolidone carboxylic acetate (Zn-PCA) without fluoride	Enamel hardness after four cycles of erosive challenge and toothpaste treatment was higher for Microrepair® Biorepair Plus when compared to a non-fluoride one and one containing fluoride.	[65]
Nanohydroxyapatite (nHAP)	<b>Curapox</b> Aqua, Sorbitol, Hydrated Silica, Glycerin, Hydroxyapatite, Cellulose Gum, Sodium Myristoyl Sarcosinate, Sodium Methyl Cocoyl Taurate, Aroma, Xanthan Gum, Stevia Rebaudiana Extract, Anethole, Tetrasodium Glutamate Diacetate, Tocopheryl Acetate, Eucalyptol, o-Cymen-5-ol, Citric Acid, Vitis Vinifera (Grape) Seed Extract, Tannase, Thymol, Limonene	A notable reduction in tooth sensitivity was observed after a 2-week period among both the nHAP followed by a reduction after 4 weeks.	[66]

<p>Nnano-Zn-Mg-hydroxyapatite (nZnMgHAP)</p>	<p><b>Curaprox</b> Aqua, Sorbitol, Hydrated Silica, Glycerin, Zn-Mg-hydroxyapatite, Cellulose Gum, Sodium Myristoyl Sarcosinate, Sodium Methyl Cocoyl Taurate, Aroma, Xanthan Gum, Stevia Rebaudiana Extract, Anethole, Tetrasodium Glutamate Diacetate, Tocopheryl Acetate, Eucalyptol, o-Cymen-5-ol, Citric Acid, Vitis Vinifera (Grape) Seed Extract, Tannase, Thymol, Limonene</p>	<p>A notable reduction in tooth sensitivity was observed after a 2-week period among both the nZnMgHAP followed by a reduction after 4 weeks.</p>	<p>[66]</p>
<p>Nnano-fluoroapatite (nFAP)</p>	<p><b>Curaprox</b> Aqua, Sorbitol, Hydrated Silica, Glycerin, Fluorapatite, Cellulose Gum, Sodium Myristoyl Sarcosinate, Sodium Methyl Cocoyl Taurate, Aroma, Xanthan Gum, Stevia Rebaudiana Extract, Anethole, Tetrasodium Glutamate Diacetate, Tocopheryl Acetate, Eucalyptol, o-Cymen-5-ol, Citric Acid, Vitis Vinifera (Grape) Seed Extract, Tannase, Thymol, Limonene</p>	<p>The toothpaste containing nZnMgHAP exhibited notably superior effectiveness compared to the toothpaste with nFAP after the 2-week assessment and demonstrated greater efficacy compared to other tested toothpaste variants after the 4-week evaluation.</p>	<p>[66]</p>
<p>Fluoro-hydroxyapatite magnesium-strontium-carbonate hydroxyapatite conjugated with chitosan</p>	<p><b>Biosmalto Caries Abrasion and Erosion / Curasept S.p.A., Saronno (VA), Italy</b> Purified water, glycerin, hydrated silica, fluorohydroxyapatite, magnesium-strontium-carbonate hydroxyapatite conjugated with chitosan, cellulose gum, xylitol, cocamidopropyl betaine, xanthan gum, aroma, sodium monofluorophosphate, potassium acesulfame, ethylhexylglycerin, phenoxyethanol, sodium benzoate, citric acid.</p>	<p>The toothpaste resulted in the formation of a mineral deposit on the specimen's surface, which led to the closure of dentinal tubules and the filling of spaces between enamel prisms.  This process effectively replenished the mineral content that had been diminished due to acid etching.</p>	<p>[67]</p>

larly in more acidic environments [70, 71]. The incorporation of magnesium is also pertinent as it can actively enhance dental well-being by mitigating oral inflammation and leveraging its antimicrobial properties [72]. It also holds a role in facilitating proper calcium integration within tooth structure with insufficient Mg levels resulting in weakened enamel, irrespective of calcium levels [73]. A more recent study [74] evaluated 2 experimental toothpaste formulations, one containing simple HAP and one a substituted HAP with Mg, Zn and Si. While both toothpastes exhibited an improvement when compare to the artificially demineralized enamel, the substituted HAP toothpaste demonstrated a superior performance, resulting in consistent improvements in the morphology of the dental enamel surface.

Over the course of ten treatment days, investigations through Atomic force Microscopy (AFM) revealed complete remineralization of demineralized enamel lesions, as evidenced by changes in structural morphology and surface roughness. While synthetic HAP seems like an ideal choice for remineralization purposes there are certain aspects one needs to consider. Firstly, the dimensions of the HAP particles have to be smaller than 100 nm, as it is reported that nanohydroxyapatite is much more effective towards promoting enamel remineralization [75]. For instance, Li et al. [76] revealed that 20 nm nano-hydroxyapatite particles form a better bond with enamel than

larger particles of more conventional hydroxyapatites or calcium phosphates. Here, the enamel surface, which is coated with a layer of hydroxyapatite (HAP) measuring approximately 40–50 nm in thickness, exhibits a hardness of  $4.6 \pm 0.4$  GPa and an elastic modulus of  $95.6 \pm 8.4$  GPa. These values are similar to the ones exhibited by natural enamel (hardness:  $4.2 \pm 0.2$ ; elastic modulus:  $94.1 \pm 5.4$  GPa) [77]. The nanoscale dimensions of HAP enable it to easily infiltrate enamel pores or micro cracks, potentially leading to remineralization. Moreover, nanoHAP can be utilized as a filler for minor cavities and contribute to the enhancement of tooth whiteness [78]. This underscores its role in supporting saliva's restorative functions, ensuring suitable mineral density on enamel surfaces, and addressing plaque-related issues.

The composition and physico-chemical parameters of dentifrice formulations also play a role in the effectiveness of the remineralizing agent. To put things into perspective one can discuss the addition of both HAP and fluoride within toothpaste. For instance, a study involving school children conducted a comparison between regular fluorinated toothpaste and toothpaste containing hydroxyapatite with fluoride substitution [79]. The results indicated that the hydroxyapatite with fluoride substitution demonstrated superior effectiveness in preserving and rejuvenating dental health compared to the conventional addition of sodium fluoride. Interestingly, another study [62] revealed that a commercial

toothpaste with fluoride (olaflur - 1.400 ppm; Elmex CP GABA GmbH, Hamburg, German) had significantly higher remineralization when compared to a commercial toothpaste containing hydroxyapatite (10% hydroxyapatite; Karex Dr. Kurt Wolff GmbH & Co. KG, Bielefeld, Germany). This discrepancy is explained by the authors to the fact that acidic pH (Elmex) leads to better remineralization results from neutral pH (Karex).

The remineralization and desensitizing improvements in enamel by using hydroxyapatite dentifrices are indeed promising. This can be noticed through the increasing number of commercial toothpastes present on the market, with newer compositions containing different types of substituted HAPs.

## Remineralization and dentifrices efficacy

### Reduction in dental caries coupled with antimicrobial and antioxidant effect

Clearly hydroxyapatite is the “new fluorine” in toothpastes. The results are exceptional in terms of remineralization and HAP can be used in higher amounts without raising any of the concerns fluorine does, especially regarding children. However, as previously mentioned, one of the aspects regarding enamel deterioration involves bacteria. This includes microorganisms like *Streptococcus mutans* and *Streptococcus sobrinus*, the primary culprits behind dental caries; *Pseudomonas aeruginosa* and *Enterococcus faecalis*, associated with periodontal diseases; *Candida albicans*, implicated in conditions like candidiasis and various superficial or systemic infections, including dental caries [80].

While a strong remineralizing agent, HAP does not possess any intrinsic antibacterial properties. It could be said that by lattice substitution with different ions (i.e. Si, Mg) HAP could gain such properties. While this is true, the brushing time (contact of HAP with enamel) has to be taken into account. While the general consensus is that brushing time has to be 2-3 minutes, the general population only brushes for 45 seconds [81], thus limiting the contact time of active ingredients with enamel.

Therefore, there is a need to further enhance dentifrices with other antibacterial compounds that would act faster than the ions in HAP. Silver is a well-known antibacterial agent [82-91]. There are quite a few dental hygiene products containing silver in various forms and concentrations. Silver in toothpaste has been proven to be quite effective against *S. mutans* the major bacterial strain in the oral microbiota. For example, one study [92] compared an experimental toothpaste containing nano-silver fluoride with one

containing sodium fluoride. While both toothpastes proved efficient in remineralization (with the addition of fluoride), the one containing nano-silver led to a lower MIC and provided better results regarding bacterial adhesion and pH decreases. While there are some concerns within the general public regarding potential silver toxicity the concentrations are not that high and toothpaste is generally not ingested. However, to address this, other compounds of more natural origin could also be employed as antibacterial ingredients. Different plant extracts such as carotenoids [93-111] would probably be more palatable to the general public. For example, curcumin was shown to present an inhibitory effect on the biofilm viability of clinical strains of *S. mutans* [112]. Notably, the study suggested that the prolonged exposure to curcumin yields a more potent inhibitory effect compared to short-term exposure. This biofilm reduction could be explained through an inhibition in the activity of sortase A, the enzyme responsible for the covalent attachment of Pac proteins to the cell wall in *S. mutans* [113]. Conversely, a nanoemulsion of astaxanthin has also been shown to exhibit an in vitro effect on *S. mutans* with a minimum inhibitory concentration (MIC) of 0.5-2 µg/mL and a minimum bactericidal concentration (MBC) of 2-8 µg/mL [114]. The difference in concentration arises from variations in the preparation of nanoemulsions.

It can be firmly asserted that the integration of natural plant extracts and highly potent bioactive compounds, recognized for their exceptional antibacterial properties, into toothpaste formulations signifies a paramount stride towards fostering a comprehensive and ecologically responsible method for enhancing oral health.

## Conclusions

Hydroxyapatite-based toothpaste formulations have surged in significance due to their remarkable potential in bolstering enamel remineralization and overall dental health. Research findings unequivocally support their efficacy in combating tooth decay, particularly when fortified with essential ions like zinc, strontium, and magnesium. Notably, the utilization of nano-sized hydroxyapatite particles exhibits superior capability in infiltrating enamel and enhancing mineral density. The composition of toothpaste emerges as a pivotal factor, with formulations encompassing both hydroxyapatite and fluoride substitution yielding notably superior outcomes. Nevertheless, it's imperative to acknowledge that these toothpastes inherently lack antibacterial properties, necessitating the integration of antibacterial agents such as silver or natural extracts to effectively counter bacterial concerns. Hence, the quest for alternative antibacterial compounds becomes

imperative to effectively combat bacterial challenges. Silver, a long-established and potent antibacterial agent, has proven its mettle within toothpaste formulations by effectively tackling notorious oral troublemakers like *S. mutans*. Furthermore, the exploration of natural antibacterial elements, exemplified by plant extracts such as curcumin and astaxanthin, presents an enticing and potentially efficacious path towards elevating oral health. In essence, the amalgamation of these antibacterial warriors into toothpaste formulations signifies a substantial leap towards embracing a more comprehensive and eco-conscious approach to oral hygiene.

## Acknowledgment

The authors acknowledge their sincere thanks to the Ministry of Research, Innovation and Digitization, CNCS/CCCDI-UEFISCDI, for funding through project number 186, within PNCDI III.

## Conflict of Interest

No competing interest was found during this work.

## Funding/Support

This work was supported by grants from the Ministry of Research, Innovation and Digitization, CNCS/CCCDI-UEFISCDI, project number 186, within PNCDI III.

## References

1. Prajapati S, Tao J, Ruan Q, De Yoreo JJ, Moradian-Oldak J. Matrix metalloproteinase-20 mediates dental enamel biomineralization by preventing protein occlusion inside apatite crystals. *Biomaterials*. 2016; 75: 260-270. doi: 10.1016/j.biomaterials.2015.10.031
2. Habelitz S, Bai Y. Mechanisms of enamel mineralization guided by Amelogenin Nanoribbons. *J Dent Res*. 2021; 100: 1434–14443. doi: 10.1177/00220345211012925
3. Neel EAA, Aljabo A, Strange A, Ibrahim S, Coathup M, Young AM, Bozec L, Mudera V. Demineralization–remineralization dynamics in teeth and bone. *Int J Nanomed*. 2016; 11: 4743-4763. doi: 10.2147/IJN.S107624
4. Beniash E, Simmer JP, Margolis HC. The effect of recombinant mouse amelogenins on the formation and organization of hydroxyapatite crystals in vitro. *J Struct Biol*. 2005; 149: 182-190. doi: 10.1016/j.jsb.2004.11.001
5. Zhang X, Ramirez BE, Liao S, Diekwisch TGH. Amelogenin supramolecular assembly in nanospheres defined by a complex helix-coil-PPII helix 3D-structure. *Plos One*. 2011; 6(10): e24952. doi: 10.1371/journal.pone.0024952
6. Tao J, Hanson E, Dohnalkova AC, Buchko GW, Jin B, Shaw WJ, Tarasevich BJ. Changes in the C-terminal, N-terminal, and histidine regions of amelogenin reveal the role of oligomer quaternary structure on adsorption and hydroxyapatite mineralization. *Front Physiol*. 2022; 13: 1034662. doi: 10.3389/fphys.2022.1034662
7. Bartlett JD. Dental enamel development: proteinases and their enamel matrix substrates. *ISRN Dent*. 2013; 2013: 684607. doi: 10.1155/2013/684607
8. Fukumoto S, Yamada A, Nokana K, Yamada Y. Essential roles of ameloblastin in maintaining ameloblast differentiation and enamel formation. *Cells Tissues Organs*. 2005; 181(3-4): 189–195. doi: 10.1159/000091380
9. Kegulian NC, Langen R, Moradian-Oldak J. The dynamic interactions of a multitargeting domain in ameloblastin protein with amelogenin and membrane. *Int J Molec Sci*. 2023; 24: 3484. doi: 10.3390/ijms24043484
10. Masuya H, Shimizu K, Sezuku H, Sakuraba Y, Nagano J, Shimizu A, Fujimoto N, Kawai A, Miura I, Kaneda H, Kobayashi K, Ishijima J, Maeda T, Gondo Y, Noda T, Wakana S, Shiroishi T. Enamelin (Enam) is essential for amelogenesis: ENU-induced mouse mutants as models for different clinical subtypes of human amelogenesis imperfecta (AI). *Hum Mol Genet*. 2005; 14(5): 575-583. doi: 10.1093/hmg/ddi054
11. Hu JCC, Hu Y, Lu Y, Smith CE, Lertlam R, Wright JT, Suggs C, MacKee MD, Beniah E, Kabir ME, Simmer JP. Enamelin is critical for ameloblast integrity and enamel ultrastructure formation. *Plos One*. 2014; 9(3): e89303. doi: 10.1371/journal.pone.0089303
12. Sakaguchi RL, Powers JM, Eds. Chapter 2 - The oral environment, Craig's Restorative Dental Materials, 13th Edition, 2012; pag 5-23. doi: 10.1016/B978-0-323-08108-5.10002-7
13. Infeld T. Dental erosion. Definition, classification and links. *Eur J Oral Sci*. 1996; 104(2(2)): 151-155. doi: 10.1111/j.1600-0722.1996.tb00063.x
14. Wade WG. The oral microbiome in health and disease. *Pharm Res*. 2013; 69: 137-143. doi: 10.1016/j.phrs.2012.11.006
15. Dewhirst FE, Chen T, Izard J, Paster BJ, Tanner ACR, YU W-H, Lakshmanan A, Wade WG. The human oral microbiome. *J Bacteriol*. 2010; 192(19): 5002-5017. doi:10.1128/JB.00542-10
16. Boisen G, Davies JR, Neilands J. Acid tolerance in early colonizers of oral biofilm. *BMC Microbiol*. 2021; 21: 45. doi: 10.1186/s12866-021-020892

17. Cheng R, Yang H, Shao M-Y, Hu T, Zhou X-D. Dental erosion and severe tooth decay related to soft drinks: a case report and literature review. *J Zhejiang Univ Sci B*. 2009; 10(5): 395-399.
18. Kannan A, Ahmed MAA, Duraisamy P, Manipal S, Adusumillil P. Dental hard tissue erosion rates and soft drinks – A gender based analysis in Chennai city, India. *Saudi J Oral Dent*. 2014; 5: 21-27. doi: 10.1016/j.ksujds.2013.08.003
19. Hamba H, Nakamura K, Nikaido T, Tagami J, Muramatsu T. Remineralization of enamel subsurface lesions using toothpaste containing tricalcium phosphate and fluoride: an in vitro  $\mu$ CT analysis. *BMC Oral Health*. 2020; 20(1): 292. doi: 10.1186/s12903-020-01286-1
20. Anil A, Ibraheem WI, Meshni AA, Preethanath R, Anil S. Demineralization and Remineralization Dynamics and Dental Caries, In *Dental Caries - The Selection of Restoration Methods and Restorative Materials*, Rusu LC, Ardelean LC Eds., IntechOpen 2022. doi: 10.5772/intechopen.105847
21. Hayashi O, Chiba T, Shimoda S, Momoi Y. Demineralization and remineralization phenomena of human enamel in acid erosion model. *J Hard Tissue Biol*. 2016; 25(1): 27-34. doi: 10.2485/jhtb.25.27
22. Inchingolo AM, Malcangi G, Ferrante L, Del Vecchio G, Viapiano F, Mancini A, Inchingolo F, Inchingolo AD, Di Venere D, Dipalma G, Patano A. Damage from carbonated soft drinks on enamel: a systematic review. *Nutrients*. 2023; 15:1785. doi: 10.3390/nu15071785
23. Arifa MK, Ephraim R, Rajamani T. Recent advances in dental hard tissue remineralization: a review of literature. *Int J Clin Pediatr Dent*. 2019; 12(2): 139–144. doi: 10.5005%2Fjpp-journals-10005-1603
24. Carstairs C. Debating Water fluoridation before Dr. Strangelove. *Am J Public Health*. 2015; 105(8):1559–1569. doi:10.2105/ajph.2015.302660
25. Unde MP, Patil RU, Dastoor PP. The untold story of fluoridation: revisiting the changing perspectives. *Indian J Occup Environ Med*. 2018; 22: 121-127. doi: 10.4103/ijoem.ijoem\_124\_18
26. Miskell P. Cavity protection or cosmetic perfection? Innovation and marketing of toothpaste brands in the United States and Western Europe, 1955–1985. *Bus Hist Rev*. 2004; 78(1): 29–60. doi: 10.2307/25096828
27. Nassar Y, Brizuela M. The Role of Fluoride on Caries Prevention. In: *StatPearls* [Internet]. Treasure Island (FL): StatPearls Publishing; 2023 Jan. Available from: <https://www.ncbi.nlm.nih.gov/books/NBK587342/>
28. Featherstone JD. Prevention and reversal of dental caries: role of low level fluoride. *Community Dent Oral Epidemiol*. 1999; 27(1): 31-40. doi: 10.1111/j.1600-0528.1999.tb01989.x
29. Gleisner, H, Einax JW, Moes S, Welz, B, Carasek, E. A fast and accurate method for the determination of total and soluble fluorine in toothpaste using high-resolution graphite furnace molecular absorption spectrometry and its comparison with established techniques. *J Pharm Biomed Anal*. 2011; 54(5): 1040-1046. doi: 10.1016/j.jpba.2010.12.013
30. Tomoaia G, Tomoaia-Cotisel M, Pop LB, Pop A, Horovitz O, Mocanu A, Jumate N, Bobos LD. Synthesis and characterization of some composites based on nanostructured phosphates, collagen and chitosan. *Rev Roum. Chim*. 2011; 56(10-11): 1039-1046.
31. Prejmerean C, Tomoaia-Cotisel M, Vasile E, Furtos G, Pop LB, Moldovan M, Sarosi C, Petean I. Characterisation of surface organisation and morphology of some new experimental dental resin-based composites. *Int J Nano Biomater*. 2011; 3(4):344-359. doi: 10.1504/IJNB.2011.045886
32. Tomoaia G, Soritau O, Tomoaia-Cotisel M, Pop LB, Pop A, Mocanu A, Horovitz O, Bobos LD. Scaffolds made of nanostructured phosphates, collagen and chitosan for cell culture. *Powder. Technol*. 2013; 238: 99-107. doi: 10.1016/j.powtec.2012.05.023
33. Furtos G, Tomoaia-Cotisel M, Garbo C, Senila M, Jumate N, Vida-Simiti I, Prejmerean C. New composite bone cement based on hydroxyapatite and nanosilver. *Particul Sci Technol*. 2013; 31(4): 392-398. doi: 10.1080/02726351.2013.767293
34. Forizs E, Goga F, Avram A, Mocanu A, Petean I, Horovitz O, Tomoaia-Cotisel M. Thermal analysis of pure and multisubstituted hydroxyapatite pastes. *Stud UBB Chem*. 2017; 62(4(1)): 173-180. doi: 10.24193/subbchem.2017.4.14
35. Tomoaia G, Mocanu A, Vida-Simiti I, Jumate N, Bobos LD, Soritau O, Tomoaia-Cotisel M. Silicon effect on the composition and structure of the composition and structure of nanocalcium phosphates in vitro biocompatibility to human osteoblasts. *Mater Sci Eng C*. 2014; 37: 37-47. doi: 10.1016/j.msec.2013.12.027
36. Mocanu A, Furtos G, Rapuntean S, Horovitz O, Flore C, Garbo C, Danisteanu A, Rapuntean G, Prejmerean C, Tomoaia-Cotisel M. Synthesis characterization and antimicrobial effects of composites based on multisubstituted hydroxyapatite and silver nanoparticles. *Appl Surf Sci*. 2014; 298: 225-235. doi: 10.1016/j.apsusc.2014.01.166
37. Frangopol PT, Mocanu A, Almasan V, Garb C, Balint R, Borodi G, Bratu I, Horovitz O, Tomoaia-Cotisel M.

- Synthesis and structural characterization of strontium substituted hydroxyapatites. *Rev Roum Chim.* 2016; 61(4-5): 337-344.
38. Mocanu A, Balint R, Garbo C, Timis L, Petean I, Horovitz O, Tomoaia-Cotisel M. Low crystallinity nano-hydroxyapatite prepared at room temperature. *Stud UBB Chem.* 2017; 62(2), 95-103. doi: 10.24193/subbchem.2017.2.07
39. Goga F, Forizs E, Rotaru A, Lucian A, Petean I, Mocanu A, Tomoaia-Cotisel N. Synthesis and thermal treatment of hydroxyapatite doped with magnesium, zinc and silicon. *Rev Chim.* 2017; 68(6): 1193-1200. doi: 10.37358/RC.17.6.5640
40. Garbo C, Sindilaru M, Carlea A, Tomoaia G, Almasan V, Petean I, Mocanu A, Horovitz O, Tomoaia-Cotisel M. Synthesis and structural characterization of novel porous zinc substituted nanohydroxyapatite powders. *Particul Sci Technol.* 2017; 35(1): 29-37. doi: 10.1080/02726351.2015.1121180
41. Avram A, Gorea M, Balint R, Timis L, Jitaru S, Mocanu A, Tomoaia-Cotisel M. Portland cement enriched with hydroxyapatite for endodontic applications. *Stud UBB Chem.* 2017; 62(4): 81-92. doi: 10.24193/subbchem.2017.4.07
42. Goga F, Forizs E, Borodi G, Tomoaia G, Avram A, Balint R, Mocanu A, Horovitz O, Tomoaia-Cotisel M. Behavior of doped hydroxyapatites during the heat treatment. *Rev. Chim.* 2017; 68(12), 2907-2913. doi: 10.37358/RC.17.12.6004
43. Rapuntean S, Frangopol PT, Hodisan I, Tomoaia G, Oltean-Dan D, Mocanu A, Prejmerean C, Soritau O, Racz LZ, Tomoaia-Cotisel M. In vitro response of human osteoblasts cultured on strontium substituted hydroxyapatites. *Rev. Chim. (Bucharest).* 2018; 69(12): 3537-3544. doi: 10.37358/RC.18.12.6787
44. Oltean-Dan D, Dogaru GB, Tomoaia-Cotisel M, Apostu D, Mester A, Benea HRC, Paiusan MG, Jianu EM, Mocanu A, Balint R, Popa CO, Berce C, Bodizs GI, Toader AM, Tomoaia G. Enhancement of bone consolidation using high-frequency pulsed electromagnetic short-waves and titanium implants coated with biomimetic composite embedded into PLA matrix: in vivo evaluation. *Int. J. Nanomed.* 2019; 14: 5799-5816. doi: 10.2147/IJN.S205880
45. Garbo C, Locs J, D'Este M, Demazeau G, Mocanu A, Roman C, Horovitz O, Tomoaia-Cotisel M. Si multi-substituted hydroxyapatites for bone regeneration. *Int J Nanomed.* 2020; 15: 1037-1058. doi: 10.2147/IJN.S226630
46. Balint R., Petean I, Frangopol PT, Mocanu A, Arghir G, Riga S, Tomoaia G, Horovitz O, Tomoaia-Cotisel M. Biomimetic nanocomposite structures designed for coating of orthopedic implants: AFM investigation. *Stud UBB Chem.* 2021; 66(3): 141-160. doi: 10.24193/subbchem.2021.3.08
47. Oltean-Dan D, Dogaru GB, Jianu EM, Riga S, Tomoaia-Cotisel M, Mocanu A, Barbu-Tudoran L, Tomoaia G. Biomimetic composite coatings for activation of titanium implant surfaces: methodological approach and in vivo enhanced osseointegration. *Micromachines.* 2021; 12(11): 1325. doi: 10.3390/mi12111352
48. Mocanu A, Frangopol PT, Balint R, Cadar O, Vancea IM, Mantiu R, Horovitz O, Tomoaia-Cotisel M. Higuchi model applied to ions release from hydroxyapatites. *Stud UBB Chem.* 2021; 66(3): 195-207. doi: 10.24193/subbchem.2021.3.12
49. Mocanu A, Cadar O, Frangopol PT, Petean I, Tomoaia G, Paltinean GA, Racz CP, Horovitz O, Tomoaia-Cotisel M. Ion release from hydroxyapatite and substituted hydroxyapatites in different immersion liquids: in vitro experiments and theoretical modelling study. *R Soc Open Sci.* 2021; 8(1): 201785. doi: 10.1098/rsos.201785
50. Juntavee N, Juntavee A, Plongniras P. Remineralization potential of nano-hydroxyapatite on enamel and cementum surrounding margin of computer-aided design and computer-aided manufacturing ceramic restoration. *Int J Nanomed.* 2018; 13: 2755-2765. doi: 10.2147/IJN.S165080
51. Ionescu AC, Cazzaniga G, Ottobelli M, Garcia-Godoy F, Brambilla E. Substituted Nano-hydroxyapatite toothpastes reduce biofilm formation on enamel and resin-based composite surfaces. *J Funct Biomater.* 2020; 11(2):36. doi: 10.3390/jfb11020036
52. de Melo Alencar C, Freitas de Paula BL, Guanipa Ortiz MI, Barauna Magno N, Martins Silva C, Cople Maia L. Clinical efficacy of nano-hydroxyapatite in dentin hypersensitivity: A systematic review and meta-analysis. *J Dent.* 2019; 82: 11-21. doi: 10.1016/j.jdent.2018.12.014
53. Aykut-Yetkiner A, Attin T, Wiegard A. Prevention of dentine erosion by brushing with anti-erosive toothpastes. *J Dent.* 2014; 42: 856-861. doi: 10.1016/j.jdent.2014.03.011
54. Chen L, AL-Bayatree S, Khurshid Z, Shavandi A, Brunton P., Ratnayake J. Hydroxyapatite in oral care products—a review. *Materials.* 2021; 14:4865. doi: 10.3390/ma14174865
55. Li X, Wang J, Joiner A, Chang J. The remineralisation of enamel: a review of the literature. *J Dent.* 2014;

- 42(Suppl. 1): S12–S20. doi: 10.1016/s0300-5712-(14)50003-6
56. Fabritius-Vilpoux K, Enax J, Herbig M, Raabe D, Fabritius HO. Quantitative affinity parameters of synthetic hydroxyapatite and enamel surfaces in vitro. *Bioinspired, Biomim Nanobiomaterials*. 2019; 8(2): 141–153. doi: 10.1680/jbibn.18.00035
  57. Niwa M, Sato T, Li W, Aoki H, Aoki H, Daisaku T. Polishing and whitening properties of toothpaste containing hydroxyapatite. *J Mater Sci Mater Med*. 2001; 12: 277–281. doi: 10.1023/a:1008927502523
  58. Enax J, Epple M. Synthetic hydroxyapatite as a biomimetic oral care agent. *Oral Health Prev Dent*. 2018; 16(1): 7–19. doi: 0.3290/j.ohpd.a39690
  59. Meyer F, Enax J, Amaechi BT, Limeback H, Fabritius H-O, Ganss B, Pawinska M, Paszynska E. Hydroxyapatite as remineralization agent for children’s dental care. *Front Dent Med*. 2022; 3: 859560. doi: 10.3389/fdmed.2022.859560
  60. Kani T, Kani M, Isozaki A, Shintani H, Ohashi T, Tokumoto T. Effect to apatite-containing dentifrices on dental caries in school children. *J Dental Health*. 1989; 39:104–109.
  61. Pepla E, Besharat LK, Palaia G, Tenore G, Migliau G. Nano-hydroxyapatite and its applications in preventive, restorative and regenerative dentistry: A review of literature. *Ann. Stomatol*. 2014; 5: 108. doi: 10.11138/ads/2014.5.3.108
  62. Guntermann L, Rohrbach A, Scafer E, Dammaschke T. Remineralization and protection from demineralization: effects of a hydroxyapatite-containing, a fluoride-containing and a fluoride and hydroxyapatite-free toothpaste on human enamel in vitro. *Head & Face Med*. 2022; 18: 26. doi: 10.1186/s13005-022-00330-5
  63. Vlasova N, Samusenko V, Novikova I, Nikolenko D, Nikolashvili N, Gor I, Danilina A. Clinical efficacy of hydroxyapatite toothpaste containing Polyol Germanium Complex (PGC) with threonine in the treatment of dentine hypersensitivity. *Saudi Denl J*. 2022; 34: 310–314. doi: 10.1016/j.sdentj.2022.03.001
  64. Colombo M, Mirando M, Rattalino D, Beltrami R, Chiesa M, Poggio C. Remineralizing effect of a zinc-hydroxyapatite toothpaste on enamel erosion caused by soft drinks: Ultrastructural analysis. *J Clin Exp Dent*. 2017; 9(7): e861–e868. doi: 10.4317/jced.53790
  65. Poggio C, Mirando M, Rattalino D, Viola M, Colombo M, Beltrami R. Protective effect of zinc-hydroxyapatite toothpastes on enamel erosion: An in vitro study. *J Clin Exp Dent*. 2017; 9(1): e118–e122. doi: 10.4317/jced.53068
  66. Polyakova M, Sokhova I, Doroshina V, Arakelyan M, Novozhilova N, Babina K. The effect of toothpastes containing hydroxyapatite, fluoroapatite, and Zn-Mg-hydroxyapatite nanocrystals on dentin hypersensitivity: a randomized clinical trial. *J Int Soc Prev Community Dent*. 2022; 12: 252–259. doi: 10.4103/jispcd.jispcd\_333\_21
  67. Degli Esposti L, Ionescu AC, Brambilla E, Tampieri A, Iafisco M. Characterization of a toothpaste containing bioactive hydroxyapatites and in vitro evaluation of its efficacy to remineralize enamel and to occlude dentinal tubules. *Materials*. 2020; 13(13): 2928. doi: 10.3390/ma13132928
  68. Enax J, Amaechi BT, Schulze zur Wiesche E, Meyer F. Overview on adjunct ingredients used in hydroxyapatite-based oral care products. *Biomimetics*. 2022; 7:250. doi: 10.3390/biomimetics7040250
  69. Lynch RJM. Zinc in the mouth, its interactions with dental enamel and possible effects on caries; a review of the literature. *Int Dent J*. 2011; 61(Suppl. 3): 46–54. doi: 10.1111/j.1875-595X.2011.00049.x
  70. Wang YL, Chang HH, Chiang YC, Lin CH, Lin CP. Strontium ion can significantly decrease enamel demineralization and prevent the enamel surface hardness loss in acidic environment. *J Formos Med Assoc*. 2019; 118(1(1)): 39–49. doi: 10.1016/j.jfma.2018.01.001
  71. Dai LL, Mei ML, Chu CH, Zhao IS, Lo ECM. Effect of Strontium-doped bioactive glass on preventing formation of demineralized lesion. *Materials*. 2021; 14(16): 4645 doi: 10.3390/ma14164645
  72. Jawed M, Al Abdulmonem W, Alkhamiss A, Alghsham R, Alsaeed T, Alhumaydhi FA, Hershan AA, Shahid SM. Role of serum magnesium in dental caries. *Bahrain Medical Bull*. 2021; 43(1): 327–330.
  73. Uwitonze AM, Rahman S, Ojeh N, Grant WB, Kaur H, Haq A, Razzaque MS. Oral manifestations of magnesium and vitamin D inadequacy. *J Steroid Biochem Molec Biol*. 2020; 200: 105636. doi: 10.1016/j.jsbmb.2020.105636
  74. Florea DA, Mocanu A, Pop LC, Tomoaia G, Dobrota C-T, Varhely Jr C, Tomoaia-Cotisel M. Remineralization of tooth enamel with hydroxyapatite nanoparticles: an in vitro study. *Stud UBB Chem*. 2023; 68(2): 99–113. doi:10.24193/subbchem.2023.2.07
  75. Du M, Chen J, Liu K, Xing H, Song C. Recent advances in biomedical engineering of nano-hydroxyapatite including dentistry, cancer treatment and bone repair. *Compos B*. 2021; 215: 108790. doi: 10.1016/j.compositesb.2021.108790
  76. Li L, H Pan, J Tao, X Xu, C Mao, X Gu, R Tang. Repair of enamel by using hydroxyapatite nanoparticles as the building blocks. *J Mater Chem*. 2008; 18: 4079–4084.

77. He LH, Swain MV. Enamel—A “metallic-like” deformable biocomposite. *J Dent.* 2007; 35: 431-437. doi: 10.1016/j.jdent.2006.12.002
78. Babayevska N, Woźniak-Budych M, Litowczenko J, Peplińska B, Jarek M, Florczak P, Bartkowiak G, Czarnecka B, Jurga S. Novel nanosystems to enhance biological activity of hydroxyapatite against dental caries. *Mater Sci Eng C Mater Biol Appl.* 2021; 124: 112062. doi: 10.1016/j.msec.2021.112062
79. Cagetti MG, Cocco F, Wierichs RJ, Wolf TG, Salerno C, Arghittu A, Campus G. Efficacy of HAF toothpastes in primary and permanent dentitions. A 2-years triple-blind RCT. *J Dent.* 2022; 121: 104049. doi: 10.1016/j.jdent.2022.104049
80. de Rossi A, Cunha Araujo Ferrira D, Assed Bezerra da Silva R, Mussolino de Queiroz A, Assed Bezerra da Silva L, Nelso-Filho P. Antimicrobial activity of toothpastes containing natural extracts, chlorhexidine or triclosan. *Braz Dent J.* 2014; 25(3): 186-190. doi: 10.1590/0103-6440201300027
81. Gallagher A, Sowinski J, Bowman J, Barrett K, Lowe S, Bosma ML, Creeth JE. The effect of brushing time and dentifrice on dental plaque removal in vivo. *J Dent Hyg.* 2009; 83(3): 111-116.
82. Danistean A, Gorea M, Avram A, Rapuntean S, Tomoaia G, Mocanu A, Garbo C, Horovitz O, Tomoaia-Cotisel M. Antimicrobial activity of ceramic disks loaded with silver ions and nitroxoline. *Stud UBB Chem.* 2016; 61(3(1)): 275-283.
83. Horovitz O, Tomoaia-Cotisel M, Racz C, Tomoaia G, Boboș LD, Mocanu A. The interaction of silver nanoparticles with lipoic acid. *Stud UBB Chem.* 2009; 54(3):89-96.
84. Horovitz O, Tomoaia-Cotisel M, Tomoaia G, Bobos LD, Cozar O, Barbu-Tudoran L, Mocanu A. Investigation on the self-assembled arrangement of silver nanoparticles in the presence of protein and amino acids. *J Optoelectron Adv. Mater-Symposia.* 2010; 2(1): 39-43.
85. Mocanu A, Pasca RD, Tomoaia G, Garbo C, Frangopol PT, Horovitz O, Tomoaia-Cotisel M. New procedure to synthesize silver nanoparticles and their interaction with local anesthetics. *Int J Nanomed.* 2013; 8: 3867-3874.
86. Mocanu A, Horovitz O, Racz CP, Tomoaia-Cotisel M. Green synthesis and characterization of gold and silver nanoparticles. *Rev Roum Chim.* 2015; 60(7-8): 721-726.
87. Rapuntean S, Balint R, Paltinean GA, Tomoaia G, Mocanu A, Racz CP, Horovitz O, Tomoaia-Cotisel M. Antibacterial activity of silver nanoparticles obtained by co-reduction with sodium citrate and tannic acid. *Stud UBB Chem.* 2018; 63(3): 73-85.
88. Balint R, Paltinean GA, Mocanu A, Horovitz O, Tomoaia-Cotisel M. Interaction of silver nanoparticles with vancomycin: An Uv-Vis study. *Stud UBB Chem.* 2019; 64(2(2)): 335-343.
89. Avram A, Gorea M, Rapuntean S, Mocanu A, Paltinean GA, Varhelyi Jr C, Petean I, Horovitz O, Tomoaia-Cotisel M. In-vitro antibacterial activity of novel nanostructured composites based on forsterite and silver nanoparticles. *Rev Chim (Bucharest).* 2020; 71(1):13-21.
90. Ujica MA, Paltinean GA, Mocanu A, Tomoaia-Cotisel M. Silver and gold nanoparticles: Challenges and perspectives. *Annals - Series on Biological Sciences, of the Academy of Romanian Scientists.* 2020; 9(1): 97-139.
91. Avram A, Mocanu A, Horovitz O, Tomoaia G, Tomoaia-Cotisel M. Antibacterial effect of hydroxyapatite and silver. *Academy of Romanian Scientists Annals Series on Physics and Chemistry.* 2022; 7(2): 7-33 doi: 10.56082/annalsarsciphyschem.2022.2.7
92. Araujo Teixeira J, Vieira Costa e Silva A, dos Santos Junior VE, Correia de Melo Junior P, Arnaud M, Goretti Lima M, Pelagio Flores MA, Montenegro Stamford TC, Dias Pereira JR, Gadelha Ribeiro Targino A, Galembeck A, Rosenblatt A. Effects of a new nano-silver fluoride-containing dentifrice on demineralization of enamel and streptococcus mutans adhesion and acidogenicity. *Int J Dent.* 2018; 2018:1351925. doi: 10.1155/2018/1351925
93. Zsako J, Chifu E, Tomoaia-Cotisel M. Rotating rigid-plate model of carotenoid molecules and the behaviour of their monolayers at the air/water interface. *Gazz Chim Ital.* 1979; 109(11-12): 663-668.
94. Chifu E, Tomoaia-Cotisel M, Andrei Z. Mixed monolayers of canthaxanthin with lipids. *Stud UBB Chem.* 1979; 24(2): 63-67.
95. Chifu E, Tomoaia-Cotisel M. Insoluble monolayers of lecithin and carotenoid pigments. *Rev Roum Chim.* 1979; 24(7): 979-986.
96. Chifu E, Tomoaia M, Ioanette A. Behaviour of canthaxanthin at the benzene/water and air/water interfaces. *Gazz Chim Ital.* 1975; 105(11-12): 1225-1232.
97. Chifu E, Tomoaia M, Nicoară E, Olteanu A. Isozeaxanthin films at the oil/water and air/water interfaces. *Rev Roum Chim.* 1978; 23(8): 1163-1169.
98. Chifu E, Tomoaia-Cotisel M, Andrei Z, Bonciu E.  $\beta$ -apo-8-carotenoic acid ethyl ester films at fluid interfaces. *Gazz Chim Ital.* 1979; 109(6-7): 365-369.

99. Chifu E, Tomoaia-Cotisel M, Ioanette A. Mixed insoluble monolayers of cholesterol and  $\beta$ -apo-8-carotenol. *Gazz Chim Ital.* 1979; 109(6-7): 397-398.
100. Chifu E, Zsako J, Tomoaia-Cotisel M. Xanthophyll films. I. Single-component monolayers at the air/water interface. *J Colloid Interface Sci.* 1983; 95(2): 346-354.
101. Tomoaia-Cotisel M, Chifu E. Carotenoid pigment films at fluid interface. *Rev Chim (Bucharest).* 1981; 32(11): 1063-1069.
102. Tomoaia-Cotisel M, Chifu E. Mixed insoluble monolayers with  $\beta$ -apo-8-carotenol acid ethyl ester. *Gazz Chim Ital.* 1979; 109(6-7): 371-375.
103. Tomoaia-Cotisel M, Chifu E, Zsako J. Mixed monolayers of egg lecithin and carotenoids. *Colloids Surf.* 1985; 14: 239-246.
104. Tomoaia-Cotisel M, Zsako J, Chifu E. Ejection curves and miscibility of egg lecithin with some carotenoid derivatives. *Rev Roum Chim.* 1987; 32(7): 663-670.
105. Tomoaia-Cotisel M, Albu I, Chifu E. Adsorption of carotene and albumin at the oil/water interface. *Stud UBB Chem.* 1979; 24(2): 68-73.
106. Tomoaia-Cotisel M, Zsako J, Sălăjan M, Chifu E. Interaction of unimolecular films of some carotenoids with electrolytes at the air/water interface, in *Water and Ions in Biological Systems* (A. Pullman, V. Vasilescu, and L. Packer Eds.), Union of Societies for Medical Sciences, Bucharest, Romania, 1985; pp. 371-381.
107. Tomoaia-Cotisel M, Chifu E. Xanthophyll films. II. Two-component monolayers of some xanthophylls and egg lecithin at the air/water interface. *J Colloid Interface Sci.* 1983; 95(2): 355-361.
108. Rácz LZ, Paltinean GA, Petean I, Tomoaia G, Pop LC, Arghir G, Levei E, Mocanu A, Rácz CP, Tomoaia-Cotisel M. Curcumin and whey protein binding and structural characteristics of their complex evidenced by atomic force microscopy. *Stud UBB Chem.* 2022; 67(3): 61-74. doi: 10.24193/subbchem.2022.3.05.
109. Rácz LZ, Rácz CP, Horovitz O, Tomoaia G, Mocanu A, Kacso I, Sárközi M, Dan M, Porav S, Borodi G, Tomoaia-Cotisel M. Complexation of Curcumin using Whey Proteins to Enhance Aqueous Solubility, Stability and Antioxidant Property. *Stud UBB Chem.* 2022; 67(3): 75-99 doi: 10.24193/subbchem.2022.3.06.
110. Rácz LZ, Rácz CP, Pop LC, Tomoaia G, Mocanu A, Barbu I, Sárközi M, Roman I, Avram A, Tomoaia-Cotisel M, Toma VA. Strategies for improving bioavailability, bioactivity, and physical-chemical behavior of the curcumin. *Molecules.* 2022; 27: 6854. doi: 10.3390/molecules27206854
111. Rácz CP, Rácz LZ, Floare CG, Tomoaia G, Horovitz O, Riga S, Kacso I, Borodi G, Sarkozi M, Mocanu A, Roman C, Tomoaia-Cotisel M. Curcumin and whey protein concentrate binding: Thermodynamic and structural approach. *Food Hydrocoll.* 2023; 139: 1088547. doi: 10.1016/j.foodhyd.2023.108547
112. Li B, Pan T, Lin H, Zhao Y. The enhancing antibiofilm activity of curcumin on *Streptococcus mutans* strains from severe early childhood caries, *BMC Microbiol.* 2020; 20: 286. doi: 10.1186/s12866-020-01975-5
113. Hu P, P Huang, MW Chen. Curcumin reduces *Streptococcus mutans* biofilm formation by inhibiting sortase A activity. *Arch Oral Biol.* 2013; 58: 1343-1348. doi: 10.1016/j.archoralbio.2013.05.004
114. Shanmugapriya K, Kim H, Saravana PS, Chun BS, Kang HW. Astaxanthin-alpha tocopherol nanoemulsion formulation by emulsification methods: investigation on anticancer, wound healing, and antibacterial effects. *Colloids Surf. B Biointerfaces.* 2018; 172: 170-179. doi: 10.1016/j.colsurfb.2018.08.042



Received for publication, September, 06, 2023  
Accepted, October, 01, 2023

*Original article*

## Use of formaldehyde to increase result quality in urinary cytology

**TURCU ELENA<sup>1, 2</sup>, ARDELEANU CARMEN<sup>2</sup>, MIHAESCU GRIGORE<sup>3,\*</sup>**

<sup>1</sup> Pathology Laboratory, Clinical Hospital “Prof. Dr. Th. Burghel”, Bucharest, Romania

<sup>2</sup> SC. OncoTeam Diagnostic SRL, Bucharest, Romania

<sup>3</sup> University of Bucharest, Faculty of Biology, Bucharest, Romania

### Abstract

Cytology is often used in screening programs for individuals at high risk of certain diseases, such as urothelial (bladder) tumors and prostate cancer. High-risk individuals may include those with a family history of cancer or other risk factors. While cytology is less commonly used for prostate cancer screening compared to other methods like prostate-specific antigen (PSA) testing, it can still be employed in certain cases to detect abnormal prostate cells. Specimen collection, often through urine or brushing of specific surfaces, doesn't typically require special preparation or invasive procedures, reducing the need for prolonged hospitalization.

Our study aimed to optimize the long-term preservation of urine samples for cytopathological diagnosis by using 10% formaldehyde, ensuring high-quality smear preparation, and assessing the effectiveness of Papanicolaou staining. These objectives are essential for advancing the field of cytopathology and improving the accuracy of diagnostic procedures.

### Keywords

Papanicolaou staining, formaldehyde, cytology

---

✉ \*Corresponding author: Prof. Grigore Mihaescu. e-mail: grigore.mihaescu@bio.unibuc.ro

## Introduction

Cytology is an ideal method for screening in people at high risk. There are specific programs for screening for urothelial tumours, prostate cancer, etc. Cytology prevents or eliminates prolonged hospitalization of the patient because specimen collection does not always require special preparation. Exfoliative cytology is used to detect lesions of the urothelium as a method of surveillance of the patient. For patients with malignant tumours of the urinary tract, urinary cytopathological examination may contribute to early diagnosis. Urine sampling was done by bladder lavage, spontaneous urine, urethro-pyelo-calyceal lavage, urethral lavage and urinary catheter sampling. The amount of spontaneous urine collected was a minimum of 160 ml.

Processing of urine samples, is done within 2 hours of collection. This duration is recommended to avoid cell cytolysis. The first cells affected by the cytolytic process are malignant cells and thus the incidence of false-negative results increases.

The majority of false-negative results are caused by improper collection or paucity of samples.

False-negative results are those in which cytology does not identify atypical cells, while endoscopic and histopathological examination confirms the presence of tumour. The goal for the atypical urothelial cells (AUC) category is to capture those cases worrisome for high-grade urothelial carcinoma (HGUC) but that fall short of the suspicious for HGUC (SHGUC) category [1].

The causes of false-negative results are diverse, including limited or intermittent exfoliation of atypical cells, abundant exfoliation of cells of no diagnostic significance masking atypical cells and delaying examination of samples. To make a correct diagnosis in these two situations, the immunocytochemical method may be required.

In patients who have recently undergone resection for bladder tumours, false-positive results may occur due to the presence of post-TUR reactive cells, characterised by hyperchromatic nuclei and granular basophilic cytoplasm.

An important role in obtaining quality urine sample results is played by the fixation step, done as soon as possible after collection [2]. Fixation preserves the shape, structure and relationships between cellular constituents in a state very close to the time of collection. The fixation agent commonly used in the preparation of urine samples is 50% alcohol. Alcohol has a rapid denaturing action on proteins and is used especially in smears, allowing good nuclear detail to be obtained.

Another fixative used in fixation is formaldehyde (10% standard solution). This has a slow fixing action by polym-

erizing proteins. Formaldehyde provides good penetration power, does not alter the structure of proteins and is recommended in immunological techniques. Formaldehyde is a strong preservative and can influence the chemical and staining processes of urine samples.

Cytodiagnosis has become one of the most important and effective methods for the early detection of malignant tumours [1]. Accuracy of results is essential for the clinical utility of cytodiagnostics. The processing of the material is complex and involves many steps, from collection to sample processing and interpretation. The most accurate interpretation is performed by the immunocytochemical method.

In the case of smears obtained from urine samples, repeated cytological examinations may detect atypical cells, even if endoscopically or by random biopsy the presence of a tumour is not revealed [1, 3, 4]. However, the result can only be considered false-positive after excluding the possibility of a tumour in the upper urinary tract, prostatic urethra or neighbouring organs. This category of results is very important as it may lead to urological investigations that may be unnecessary or, in their absence, to neglect of an early stage malignancy.

Normal urine contains few cells, most of which are urothelial cells. These cells rarely exfoliate, especially in situations such as physical exertion or endoscopic manoeuvres. They may occur singly or in small groups and have frequent cytolytic forms. Urothelial cells often have single, centrally located nuclei with basophilic cytoplasm.

Renal tubular cells are rare in normal urine but common in patients with chronic renal failure or inflammatory renal disease. These cells have central, hyperchromatic nuclei and the cytoplasm may have a cyanophilic or chromophobic appearance.

Calyceal cells are rare in normal spontaneous urine, but are found in pyelo-calyceal lavages. They are variable in size, with basophilic or chromophobic cytoplasm and may have 2-3 nuclei.

Pavement cells are common in normal urine and originate from the trigonal bladder in females or the anterior urethra in males. They are large cells with small nuclei and rich cytoplasm.

Columnar cells are rarer and come from different areas such as the bladder cap, membranous urethra or prostate. They may have poorly orthorhombic or chromophobe cytoplasm and contain small vacuoles.

Prostate cells are cubic, triangular or round and are rare in urine. They are more commonly found in benign prostatic lesions and have centralised nuclei. Seminal cells are rare and have a different appearance from prostatic cells. Other cell types, such as macrophages, binucleated cells, multinu-

cleated cells, erythrocytes, leukocytes, bacteria and crystals, may be found in the urine depending on the urological condition or operation.

Urinary cytodiagnosis involves examination of smears obtained from samples taken from the urinary tract. In this process, a small lens is used to avoid areas of cell clumping or overlap. To establish a diagnosis, at least 3 major criteria of malignancy are looked for in single cells or in plaques.

In the urinary environment, exfoliated cells tend to have spherical or oval shapes, so their shape is not a major criterion for detecting malignancy [5]. Cytolysis is common and only cells with all well-defined structural elements are considered for interpretation. Sometimes urinary tract infections can complicate cytological diagnosis, as smears may contain numerous urothelial cells that originate from deep layers or regenerating areas following benign lesions such as surgery, bladder lithiasis or chronic cystitis.

Malignant tumors of the urinary tract are mostly transitional cell carcinomas. Exfoliation of atypical cells in spontaneous urine is influenced by the degree of differentiation of the tumor and is more evident in grade 2 (G2) and grade 3 (G3) cases.

Cytodiagnosis has a detection rate of malignant cells in spontaneous urine samples of more than 90% of cases when performed on sequential samples [2].

One of the biggest challenges in urine cytodiagnosis is grade 1 (G1) transitional cell carcinomas. Particularly troublesome is the low sensitivity in detecting low-grade non-invasive lesions [1]. The majority of urothelial tumours are well differentiated and the literature indicates true-positive results in these on average above 38% [3].

In the urinary tract lavage method, better detection results of malignant cells are found than in spontaneous urine. The presence and morphology of atypical cells in urinalysis is not correlated with the histopathological form of the tumour or the degree of invasion. Urinary cytology is indicated for prostate carcinoma and transitional cell carcinoma.

Our research aimed to: test the use of 10% formaldehyde in the long-term preservation of the cellularity of the urine sample in order to perform the smear and/or cytoblot under optimal conditions for cytopathological diagnosis, ii) perform smears by the method of placing sediment on glass slide using a seeding loop; iii) investigate the quality of Papanicolaou staining obtained after using 10% formaldehyde.

Preserving cellularity is crucial for maintaining the quality of the sample and ensuring that a sufficient number of cells are available for cytopathological analysis. The first objective of this study was to investigate whether 10% formaldehyde is effective for preserving the cellularity of urine samples over

an extended period. The second objective involves performing smears using the sediment from urine samples. This likely includes collecting the sediment and applying it to glass slides using a seeding loop or similar technique.

Finally, the third objective is to evaluate the quality and accurate diagnostic information of Papanicolaou staining achieved after using 10% formaldehyde for preservation.

## **Material and methods**

During 2016 - 2019, a study was conducted on a group of 30 urine samples analyzed in the Pathological Anatomy Laboratory of the Clinical Hospital "Prof. Dr. Th. Burghele" and SC. OncoTeam Diagnostic, Bucharest, which were preserved with formaldehyde.

Thirty freshly collected urine samples were received in the laboratory.

The samples received were divided into 7 batches, resulting in 210 samples, as follows:

- Batch 1 with 30 freshly collected samples, which were immediately processed;
- Batch 2 with 30 freshly collected samples in which 1 ml of formaldehyde was added to 20 ml of urine sample and left to stand at room temperature above 22° Celsius;
- Batch 3 with 30 freshly collected samples to which 3 ml of formaldehyde was added to 20 ml of urine sample and allowed to stand at room temperature above 22° Celsius;
- Batch 4 with 30 freshly collected samples to which 5 ml of formaldehyde was added to 20 ml of urine sample and allowed to stand at room temperature above 22° Celsius;
- Batch 5 with 30 freshly collected samples to which 7 ml of formaldehyde was added to 20 ml of urine sample and allowed to stand at room temperature above 22° Celsius;
- Batch 6 with 30 freshly collected samples to which 9 ml of formaldehyde was added to 20 ml of urine sample and allowed to stand at room temperature above 22° Celsius;
- Batch 7 with 30 freshly collected samples to which 11 ml formaldehyde was added to 20 ml urine sample and left to stand at room temperature above 22° Celsius.

Macroscopic analysis of the urine samples was conducted, after which they were transferred to disposable tubes for centrifugation at 1000 rpm for 15 minutes using the Hettich EBA 20 centrifuge.

In hypocellular samples, the centrifugation and supernatant removal process was repeated 3-4 times.

After removal of the supernatant from the obtained sediment (1 ml), conventional smears were performed.

In order to decrease cases of unsatisfactory paucicellularity, the smear was performed by placing the sediment on glass slide with disposable seeding loop used in microbiology technique.

Two smears were taken from each sample and fixed by direct drying.

A total of 420 smears were made in 7 batches as follows:

- Batch 1 with 60 smears from the sample received and processed immediately;
- Batch 2 with 60 smears made from the sample preserved by adding 1 ml of formaldehyde to 20 ml of urine sample and processed (after 4, 24 and 48 hours);
- Batch 3 with 60 smears made from the preserved sample by adding 3 ml of formaldehyde to 20 ml of urine sample and processed (after 4, 24 and 48 hours);
- Batch 4 with 60 smears made from the preserved sample by adding 5 ml of formaldehyde to 20 ml of urine sample and processed (after 4, 24 and 48 hours);
- Batch 5 with 60 smears made from the preserved sample by adding 7 ml of formaldehyde to 20 ml of urine sample and processed (after 4, 24 and 48 hours);
- Batch 6 with 60 smears made from the preserved sample by adding 9 ml of formaldehyde to 20 ml of urine sample and processed (after 4, 24 and 48 hours);
- Batch 7 with 60 smears made from the preserved sample by adding 11 ml of formaldehyde to 20 ml of urine sample and processed (after 4, 24 and 48 hours).

From the processed smears (after 4, 24 and 48 hours) one specimen (smear) was taken and kept for fixation by direct drying in the sample receiving room under the influence of formaldehyde vapour, while the other 210 smears were kept for fixation in another room without exposure to formaldehyde vapour.

After direct fixation (drying in formaldehyde vapour-free medium) for up to 12 hours, all 420 smears were stained by the Papanicolaou method.

Upon final examination of the 210 smears exposed in the formaldehyde vapour chamber, the following results were found:

- All 30 of lot 1 had qualitative deficiencies in staining and were unsatisfactory for examination;
- The other 180 smears from lots 2-7, stained and were partially suitable for examination. The staining result was unsatisfactory;
- Batch 4 was the least affected by the action of formaldehyde vapour.

On final examination of the 210 smears stored in the formaldehyde vapour-protected space, the following results were found:

- All 210 smears, had Papanicolaou staining satisfactory for examination;

- The smears in lot 2 had partially lysed cells. Less lysed cells were present on smears processed 4 hours after preservation, and more affected cells were present on smears processed 48 hours after preservation;
- The smears from batch 3, had less lysed cells than those from batch 2. The least lysed cells were on smears processed 4 hours after preservation and the most affected cells were on smears processed 48 hours after preservation;
- The smears from lot 4, showed the most satisfactory staining, with rich, clear and well differentiated cellularity;
- The smears from lots 5-7 had lower cellularity with no lysed cells. The lowest cellularity was present on smears processed 48 hours after preservation.

To preserve the sample until the result was prepared, 10% formaldehyde was added. After examination of the smears, if necessary, since the cells were already fixed, the processing of the material to obtain the cytoblot was proceeded directly. Thus, the cytoblock could be obtained 24 hours earlier than when using alcohol.

## Results

In smears obtained by placing the sediment with the seeding loop on the glass slide, a richer cellularity was observed compared to those obtained by smearing the sediment on the glass slide using another slide (Fig 1-2).

All samples in batch 1 and all formaldehyde-preserved samples resulted in smears satisfactory for examination if

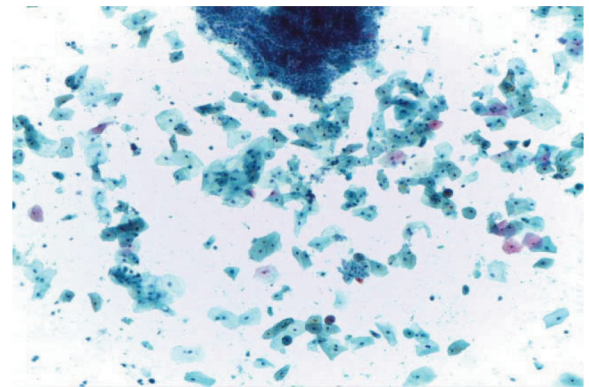


Figure 1. Smear spread with seeding loop

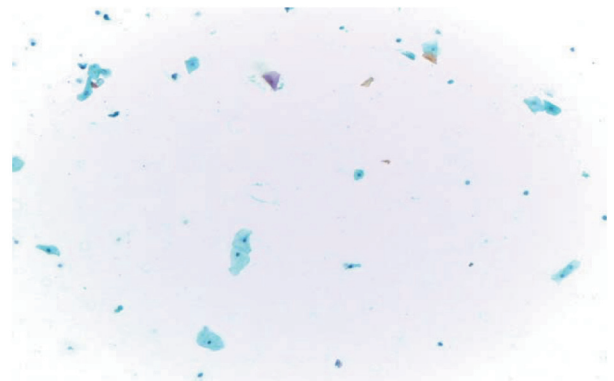


Figure 2. Smear spread with 45-degree angle blade

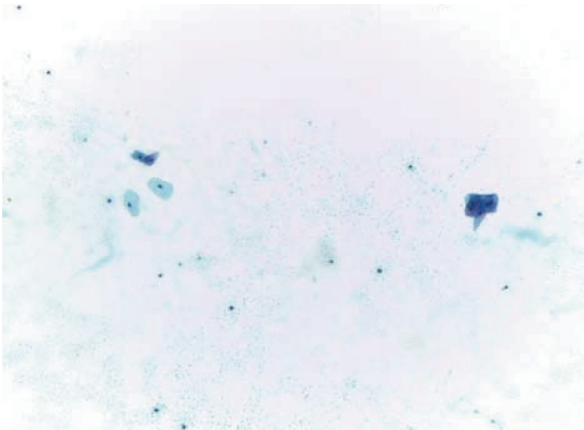


Figure 3. Smear, 1ml formaldehyde to 20 ml urine

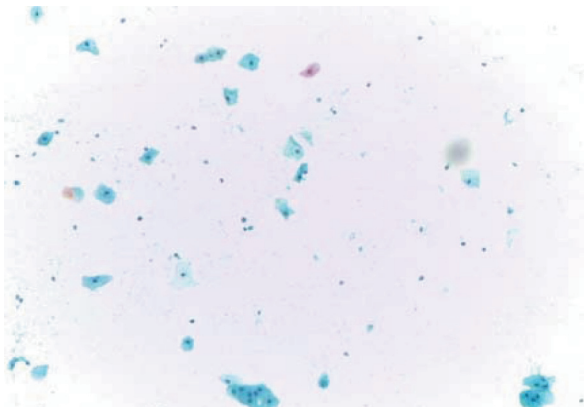


Figure 4. Smear, 3ml formaldehyde to 20 ml urine

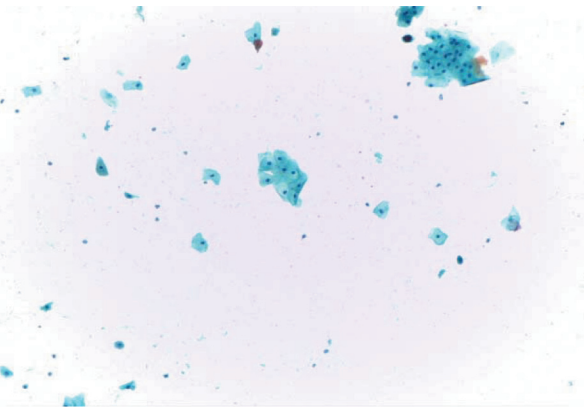


Figure 5. Smear, 5ml formaldehyde to 20 ml urine

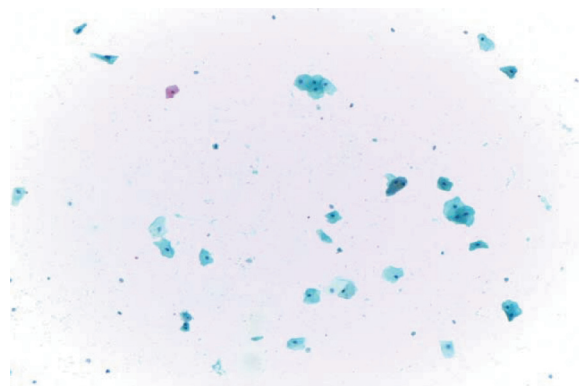


Figure 6. Smear, over 7ml formaldehyde to 20 ml



Figure 7. Smear affected by formaldehyde vapour

protected from formaldehyde vapour. The method of preserving the freshly collected urine sample by adding 5 ml of formaldehyde to 20 ml of urine sample gave the best results.

Similar Papanicolaou staining quality standards were found for both smears from samples preserved at receipt and processed after 48 hours and smears from freshly collected samples processed immediately.

Smears obtained from samples preserved with the addition of 1 ml formaldehyde to 20 ml freshly collected urine sample had cells partially lysed for examination (Fig 3). Smears obtained from samples preserved with the addition of 3 ml formaldehyde to 20 ml freshly collected urine sample had less lysed cells compared to smears from batch 2 (Fig 4). Smears obtained from samples preserved with the addition of 5 ml formaldehyde to 20 ml freshly collected urine sample had cells suitable for examination (Fig 5).

Smears obtained from samples preserved with the addition of 7-11 ml formaldehyde to 20ml freshly collected urine sample had lower cellularity compared to those preserved with 5 ml formaldehyde (Fig 6).

It was found practically that the presence of formaldehyde vapour negatively influenced Papanicolaou staining in all smears (Fig 7).

## Conclusions

The use of the glass slide sediment placement method using a disposable seeding loop, inspired by the technique used in biochemical analysis, improved the cellularity of smears, decreased the incidence of paucicellular cases and thus the number of false-negative results.

The addition of 5 ml formaldehyde to 20 ml of freshly collected urine allowed good preservation of the urine sample for a period of at least 48 hours from collection to the start of sample processing, without affecting the quality of Papanicolaou staining of the smears obtained.

After the use of formaldehyde, it was possible to obtain Papanicolaou stained smears, qualitatively similar for examination to those obtained using alcohols.

The presence of formaldehyde vapours affects the smears exposed to their action and prevents Papanicolaou staining. This may lead to difficulties in cytopathological diagnosis.

The use of formaldehyde allowed the cytoblock to be obtained more quickly, reducing the immunocytological diagnostic time by one day, compared to the method using alcohol. The use of formaldehyde, which can be purchased at half the price of alcohol, reduced the cost of sample analysis. It is important to follow proper procedures to protect smears from contact with formaldehyde vapour.

In summary, our research aimed to optimize the long-term preservation of urine samples for cytopathological diagnosis by using 10% formaldehyde, ensuring high-quality smear preparation, and assessing the effectiveness of Papanicolaou staining. The results shown in this paper are essential for advancing the field of cytopathology and improving the accuracy of diagnostic procedures.

## References

1. Barkan GA, Wojcik EM, Nayar R, Savic-Prince S, Quek ML, Kurtycz DF, Rosenthal DL. The Paris System for Reporting Urinary Cytology: The Quest to Develop a Standardized Terminology. *Adv Anat Pathol.* 2016 Jul;23(4):193-201. doi: 10.1097/PAP.000000000000118. PMID: 27233050.
2. Raica M and col., *Clinical Cytology*, Victor Babes University of Medicine and Pharmacy, Timisoara, 2001.
3. Nikas IP, Seide S, Proctor T, Kleinaki Z, Kleinaki M, Reynolds JP. The Paris System for Reporting Urinary Cytology: A Meta-Analysis. *J Pers Med.* 2022 Jan 27;12(2):170. doi: 10.3390/jpm12020170. PMID: 35207658; PMCID: PMC8874476.
4. David J. Dabbs – *Diagnostic Immunohistochemistry Theranostic and Genomic Applications*, 5th Edition, 2019.
5. Koss GL, Melamed Myron R. *Koss' Diagnostic Cytology and Its Histopathologic Bases*, 5th Edition, 2006 Lippincott Williams &Wilkins.



Received for publication, September, 03, 2023  
Accepted, October, 26, 2023

*Original article*

## Investigating the association between the CRISPR-Cas system and antibiotic resistance genes in *Neisseria* spp.

SANTHIYA K<sup>1</sup>, ANANTHASUBRAMANIAN M<sup>1\*</sup>

<sup>1</sup> Department of Biotechnology, PSG College of Technology, Coimbatore – 641004, Tamilnadu, India

### Abstract

The study aims to examine the CRISPR Cas-systems in the *Neisseria* species, with a specific focus on its potential role in antibiotic resistance (AR). A total of 360 *Neisseria* strains belonging to different species were retrieved from the NCBI database. The CRISPR Cas arrays were found among 89 *Neisseria* genomes with 140 distinct direct repeats and 1661 spacer regions. While, 69% were determined to have the type II-C system and 28% had the I-C system. The CRISPR type II-C was found to have efflux pump AR (71%) majorly. It was found that species with several CRISPR arrays often had either no or just one AR genes in their genomes. The study highlights multiple CRISPR array in *Neisseria* spp. might have played a prominent role in the prevention of horizontal gene transfer of AR genes.

### Keywords

Antibiotics, CRISPR Cas, Direct repeats, *Neisseria*, Spacer

---

✉ \*Corresponding author: Prof. Ananthasubramanian M, Department of Biotechnology, PSG College of Technology, Coimbatore – 641004, Tamilnadu, India. e-mail: mas.bio@psgtech.ac.in. Ph. No: 9994610422  
Santhiya K. e-mail: 221rbfn01@psgtech.ac.in

## Introduction

The *Neisseria* genus encompasses a group of closely related Gram-negative bacterial species, with some appearing as coccoid shapes (such as *N. gonorrhoeae*, *N. lactamica*, *N. meningitidis*, and *N. subflava*) and others as rod-shaped (*N. bacilliformis* and *N. elongata*). While most of these species are typically harmless and coexist on mucosal surfaces, but two of them, *Neisseria meningitidis* and *Neisseria gonorrhoeae*, have the potential to cause diseases in humans [1]. In 2015, there were approximately 395,200 reported cases of multidrug resistant gonorrhea, which represented a notable 27% increase compared to 2012. This increase is likely even more pronounced in the aftermath of the COVID-19 pandemic, as limitations in both sensitive diagnostic capabilities and accessible testing centers in resource-constrained regions may have led to an underreporting of cases [2]. The rise of antibiotic resistance (AR) in *Neisseria* is a significant global public health concern. Horizontal gene transfer (HGT) is a fundamental process driving the development of AR in bacteria. In nature, this phenomenon occurs through mechanisms like transformation, transduction, and conjugation, enabling the transfer of mobile genetic elements (MGEs), including transposons, integrons, and gene cassettes, between different bacterial species [3]. Nevertheless, efforts to detect and diagnosis the presence of AR genes in *Neisseria spp.* face challenges due to the lack of rapid diagnosis and high costs associated with traditional methods.

The genome editing technique, CRISPR (Clustered Regularly Interspaced Short Palindromic Repeats) Cas is a highly specific and effective gene knockout approach. It has been investigated as a potential strategy for targeting bacteria and AR genes in a sequence-specific manner. A typical CRISPR-Cas system has a CRISPR array which are made up of unique spacer sequences interspaced by repeat sequences, and CRISPR-associated (Cas) proteins [4]. This technique has recently been designed to facilitate genome editing and expression analysis in a wide variety of organisms, notably human cells. The genome editing studies have also been reported in bacterial species, like *Pseudomonas aeruginosa*, *Mycobacterium tuberculosis*, and *Escherichia coli* etc [5]. Recent studies indicate that the CRISPR-Cas systems may have a role in influencing AR in bacteria. For example, in *Streptococcus pneumoniae*, it was observed that the native state of the CRISPR-Cas system prevented plasmid transformation. However, some statistical models have not shown evidence that the CRISPR-Cas system can effectively prevent horizontal gene transfer (HGT) over extended periods of bacterial evolution. Previous studies have demonstrated that the impact of CRISPR-Cas systems on AR differ among

various bacteria. In *Klebsiella pneumoniae*, certain types of CRISPR-Cas systems may limit the acquisition of AR, while in *Francisella* bacteria, it facilitate AR [6]. Further investigations into the functions of the CRISPR-Cas systems, its interactions with HGT mechanisms, and its relationship with AR could provide valuable insights into bacterial defense mechanisms against antibiotics and aid in the development of effective approaches to tackle AR infections.

In this study, the prevalence of CRISPR Cas systems in *Neisseria spp.* was analyzed by retrieving the genome sequence from the NCBI dataset. By examining the genetic structure and functionality of CRISPR array and their relationship with AR, we sought to shed light on the defense mechanisms of *Neisseria* against genetic invaders and explore the possible link between CRISPR-Cas systems and AR genes.

## Methodology

### Identification of CRISPR-Cas system

Genomic data of *Neisseria* genome sequences from NCBI RefSeq (<https://ftp.ncbi.nlm.nih.gov/genomes/refseq/bacteria/Neisseria>) were consider for the study. Complete genomes were only considered for the analysis. The CRISPR miner (<http://www.microbiome-bigdata.com/CRISPRminer2/index/>) and CRISPR Cas finder (<https://CRISPRCas.i2bc.paris-saclay.fr/>) were used to detect the existence of the CRISPR locus region. CRISPR Cas Finder uses Shannon's entropy and entropy-based conservation to provide evidence levels to putative CRISPR array. CRISPR Cas Finder version 2.0 was used to find the Cas types in genomes with anticipated CRISPR array [7]. CRISPR miner is a web-based programme that offers a collection of CRISPR Cas array, similar to CRISPR Cas Finder, but additionally includes information on self-targeting, anti-CRISPR regions, and host phage interaction [8].

### Detection of AR genes

The presence of AR genes was found using Comprehensive Antibiotic Resistance Database (CARD) (<https://card.mcmaster.ca>) and Resfinder (<https://cge.cbs.dtu.dk/services/ResFinder/>) tool [9, 10]. The *Neisseria* genome which shows presence of CRISPR Cas system was only considered for the further analysis. In both the tools, fasta format of the genome sequence was given as an input. The major criteria for finding resistance genes were high-quality sequence coverage and the exclusion of incomplete gene predictions.

### Structural stability of direct repeats

The structure of direct repeats was analyzed using the RNA fold web server (<http://rna.tbi.univie.ac.at/cgi-bin/>)

RNAWebSuite/RNAfold.cgi). It's part of the Vienna RNA package, and it was created to estimate the minimal free energy (MFE) for each RNA secondary structure using the dynamic programming technique outlined by Zuker and Stiegler [11, 12].

### Evaluation of spacer region

In this analysis, spacer sequences were initially extracted from predicted CRISPR arrays. To link these spacers with potential phage and plasmid associations, it was compared to a database containing plasmid and phage sequences using the BLASTN algorithm. Spacer sequences were considered associated if it exhibited characteristics such as greater than 90% sequence identity, query coverage greater than 85%, and an e-value < 0.001 in their BLAST hits. Spacer sequences that met these criteria were retained for further analysis. Subsequently, spacer targeting phage regions were grouped into distinct categories, including lytic, temperate, and non-lytic, to provide insights into the types of phages being targeted by the CRISPR system. This approach helps to characterize the host's defense mechanisms against plasmids and phages based on the specific interactions observed in the spacer sequences.

### Statistical analysis

The statistical analysis was performed to examine the correlation of two variables: the presence of a CRISPR-Cas system and the existence of AR genes in *Neisseria* spp. For each species under investigation, the total number of *Neisseria* genomes (denoted as N) and the subset of genomes that exhibited both a CRISPR-Cas system and AR genes (denoted as O) was calculated. To determine whether this co-occurrence was statistically significant or merely a chance outcome, the estimation was done by calculating the expected number of genomes (E) where the presence of both the CRISPR array and the AR genes would occur purely by

random chance. This estimation was derived using the formula  $E = N \times Pb(\text{CRISPR}) \times Pb(\text{AR genes})$ , where Pb signifies the probability associated with each event occurring.

## Results

### Identification and analysis of CRISPR Cas array

A total of 360 complete genome sequences of *Neisseria* spp. were evaluated for the presence of the CRISPR Cas system using the CRISPR miner and CRISPR Cas finder tools, with 89 genomes (24%) containing the CRISPR locus. Most of the genomes (82) were reported as known species: *animalis*(2), *animaloris* (1), *arctica* (1), *brasiliensis* (1), *canis* (1), *chenwenguii* (1), *cinerea* (2), *dentiae* (1), *dumasiana* (1), *elongata* (4), *flavescens* (1), *lactamica* (2), *macacae* (1), *meningitidis* (44), *mucosa* (2), *musculi*(1), *shayegani* (1), *sicca* (2), *subflava* (8), *wadsworthii* (1), *weaveri* (2), *weixii* (1), and *zoodegmatis* (1). The remaining seven genomes were from unnamed species and will be referred as *Neisseria* from here on. The CRISPR-Cas positive isolates were from the United States of America (USA; n = 31), United Kingdom (UK; n=16), Sweden (n = 11), Canada (n = 8), China (n = 8), Singapore (n = 6), Australia (n = 2), Germany (n = 2), Korea (n = 2), France (n = 2), and Japan (n = 1). The source of isolation of these genomes were from *Homo sapiens* (79), Marmot (2), Plateau pika (2), *Anser albifrons* (1), Bovine (1), *Felis catus*(1), Guinea pig (1), *Mus musculus*(1) and Rhesus monkey (1) (Table 1). The number of CRISPR array discovered in *Neisseria* spp. varies from each other. The data revealed that 71 *Neisseria* spp. had just one identified CRISPR locus, 16 *Neisseria* spp. had two verified CRISPR arrays, and only two spp. had three CRISPR arrays.

### CRISPR types and Cas genes in *Neisseria* spp.

In this study, the presence of the CRISPR type and Cas gene cluster was investigated in 89 different *Neisseria* spp.

Table 1. Information of *Neisseria* spp. utilized in this study

S. No	Acc. No	Species	NCBI		Country	Source	Strain
			Submission Date	Size (bp)			
1	CP000381.1	<i>Neisseria meningitidis</i>	31-Jan-14	2153416 bp	China	<i>Homo sapiens</i>	053442
2	CP016672.1	<i>Neisseria meningitidis</i>	02-Aug-16	2172926 bp	USA	<i>Homo sapiens</i>	M22828
3	FR774048.1	<i>Neisseria meningitidis</i>	27-Feb-15	2227255 bp	Germany	<i>Homo sapiens</i>	WUE2594
4	CP002422.1	<i>Neisseria meningitidis</i>	31-Jan-14	2287777 bp	USA	<i>Homo sapiens</i>	M01-240355
5	FM999788.1	<i>Neisseria meningitidis</i>	27-Feb-15	2277550 bp	UK	<i>Homo sapiens</i>	8013
6	CP016671.1	<i>Neisseria meningitidis</i>	02-Aug-16	2180570 bp	USA	<i>Homo sapiens</i>	M22783
7	CP016654.1	<i>Neisseria meningitidis</i>	02-Aug-16	2185698 bp	USA	<i>Homo sapiens</i>	M22811
8	CP016647.1	<i>Neisseria meningitidis</i>	02-Aug-16	2182171 bp	USA	<i>Homo sapiens</i>	M22809
9	AL157959.1	<i>Neisseria meningitidis</i>	06-Feb-15	2184406 bp	UK	<i>Homo sapiens</i>	Z2491
10	CP016646.1	<i>Neisseria meningitidis</i>	02-Aug-16	2173686 bp	USA	<i>Homo sapiens</i>	M22819
11	CP016660.1	<i>Neisseria meningitidis</i>	02-Aug-16	2174791 bp	USA	<i>Homo sapiens</i>	M22804
12	CP007524.1	<i>Neisseria meningitidis</i>	21-May-14	2188020 bp	China	<i>Homo sapiens</i>	510612
13	CP007726.1	<i>Neisseria elongata</i>	22-Jul-15	2256647 bp	Canada	<i>Homo sapiens</i>	ATCC 29315
14	FN995097.1	<i>Neisseria lactamica</i>	03-Nov-16	2220606 bp	UK	<i>Homo sapiens</i>	020-06
15	CP012392.1	<i>Neisseria meningitidis</i>	02-Aug-16	2170619 bp	Germany	<i>Homo sapiens</i>	DE10444
16	CP031332.1	<i>Neisseria meningitidis</i>	05-Aug-18	2190201 bp	USA	<i>Homo sapiens</i>	M22814

S. No	Acc. No	Species	NCBI		Country	Source	Strain
			Submission Date	Size (bp)			
17	CP020401.2	<i>Neisseria meningitidis</i>	02-Oct-19	2397461 bp	USA	<i>Homo sapiens</i>	FDAARGOS 214
18	CP021723.1	<i>Neisseria meningitidis</i>	09-Sep-19	2170095 bp	Sweden	<i>Homo sapiens</i>	13-600
19	CP020420.2	<i>Neisseria meningitidis</i>	30-Sep-19	2181232 bp	USA	<i>Homo sapiens</i>	FDAARGOS 209
20	CP021518.1	<i>Neisseria meningitidis</i>	09-Sep-19	2168615 bp	Sweden	<i>Homo sapiens</i>	12-176
21	CP021523.1	<i>Neisseria meningitidis</i>	09-Sep-19	2167995 bp	Sweden	<i>Homo sapiens</i>	98-182
22	CP039887.1	<i>Neisseria subflava</i>	07-May-19	2195659 bp	UK	<i>Homo sapiens</i>	ATCC 49275
23	CP021516.1	<i>Neisseria meningitidis</i>	09-Sep-19	2166707 bp	Sweden	<i>Homo sapiens</i>	14-563
24	CP021725.1	<i>Neisseria meningitidis</i>	09-Sep-19	2165984 bp	Sweden	<i>Homo sapiens</i>	95-134
25	CP023429.1	<i>Neisseria weixii</i>	21-Sep-17	2511904 bp	China	<i>Plateau pika</i>	10022
26	CP021521.1	<i>Neisseria meningitidis</i>	09-Sep-19	2198497 bp	Sweden	<i>Homo sapiens</i>	09-292
27	CP031255.1	<i>Neisseria elongata</i>	01-Aug-18	2534634 bp	USA	<i>Homo sapiens</i>	M15910
28	CP021522.1	<i>Neisseria meningitidis</i>	09-Sep-19	2167920 bp	Sweden	<i>Homo sapiens</i>	06-178
29	CP045960.1	<i>Neisseria meningitidis</i>	17-Nov-19	2166248 bp	Australia	<i>Homo sapiens</i>	AUSMDU00005726
30	CP020402.2	<i>Neisseria meningitidis</i>	02-Oct-19	2305818 bp	USA	<i>Homo sapiens</i>	FDAARGOS 215
31	CP021520.1	<i>Neisseria meningitidis</i>	09-Sep-19	2157444 bp	Sweden	<i>Homo sapiens</i>	strain 11-7
32	CP039886.1	<i>Neisseria flavescens</i>	07-May-19	2231882 bp	USA	<i>Homo sapiens</i>	ATCC 13120
33	CP040504.1	<i>Neisseria</i>	29-May-19	2502158 bp	Australia	<i>Homo sapiens</i>	F0314
34	CP031699.1	<i>Neisseria animalis</i>	03-Oct-19	2236930 bp	USA	<i>Guinea pig</i>	ATCC 49930
35	CP021724.1	<i>Neisseria meningitidis</i>	09-Sep-19	2169717 bp	Sweden	<i>Homo sapiens</i>	12-330
36	CP031334.1	<i>Neisseria meningitidis</i>	05-Aug-18	2314390 bp	USA	<i>Homo sapiens</i>	M22293
37	CP012694.1	<i>Neisseria meningitidis</i>	03-Oct-16	2191116 bp	China	<i>Homo sapiens</i>	331401
38	CP031253.1	<i>Neisseria lactamica</i>	01-Aug-18	2200224 bp	USA	<i>Homo sapiens</i>	M17106
39	CP016883.1	<i>Neisseria meningitidis</i>	11-Aug-16	2168169 bp	USA	<i>Homo sapiens</i>	M22790
40	CP031324.1	<i>Neisseria meningitidis</i>	05-Aug-18	2291778 bp	USA	<i>Homo sapiens</i>	M23347
41	CP046027.1	<i>Neisseria brasiliensis</i>	19-Nov-19	2617510 bp	USA	<i>Homo sapiens</i>	N.177.16
42	CP022527.1	<i>Neisseria</i>	31-Jul-17	2371912 bp	Korea	<i>Homo sapiens</i>	KEM232
43	CP021517.1	<i>Neisseria meningitidis</i>	09-Sep-19	2167947 bp	Sweden	<i>Homo sapiens</i>	12-221
44	CP022278.1	<i>Neisseria chenwenguii</i>	10-Jul-17	2496444 bp	China	<i>Plateau pika</i>	10023
45	CP031251.1	<i>Neisseria subflava</i>	01-Aug-18	2321871 bp	USA	<i>Homo sapiens</i>	M18660
46	CP016682.1	<i>Neisseria meningitidis</i>	02-Aug-16	2175832 bp	USA	<i>Homo sapiens</i>	M24705
47	CP016680.1	<i>Neisseria meningitidis</i>	02-Aug-16	2173901 bp	USA	<i>Homo sapiens</i>	M22822
48	CP021519.1	<i>Neisseria meningitidis</i>	09-Sep-19	2156539 bp	Sweden	<i>Homo sapiens</i>	11_14
49	CP031252.1	<i>Neisseria elongata</i>	01-Aug-18	2397276 bp	USA	<i>Homo sapiens</i>	M15911
50	CP020422.2	<i>Neisseria meningitidis</i>	30-Sep-19	2305805 bp	USA	<i>Homo sapiens</i>	FDAARGOS 211
51	CP031328.1	<i>Neisseria meningitidis</i>	05-Aug-18	2223855 bp	USA	<i>Homo sapiens</i>	M18755
52	CP020452.2	<i>Neisseria mucosa</i>	27-Sep-19	2783943 bp	USA	<i>Homo sapiens</i>	FDAARGOS 260
53	CP065653.1	<i>Neisseria meningitidis</i>	14-Dec-20	2181321 bp	USA	<i>Homo sapiens</i>	FDAARGOS 914
54	CP073116.1	<i>Neisseria subflava</i>	11-Jul-22	2409157 bp	Singapore	<i>Homo sapiens</i>	TT0073
55	CP053939.1	<i>Neisseria mucosa</i>	04-Jun-20	2224757 bp	USA	<i>Homo sapiens</i>	FDAARGOS 758
56	CP065726.1	<i>Neisseria cinerea</i>	14-Dec-20	1832901 bp	USA	<i>Homo sapiens</i>	FDAARGOS 871
57	CP059570.1	<i>Neisseria dentiae</i>	04-Aug-20	2755930 bp	Canada	<i>Cattle</i>	DSM 19151
58	CP073119.1	<i>Neisseria subflava</i>	11-Jul-22	2277784 bp	Singapore	<i>Homo sapiens</i>	HP0069
59	CP091522.1	<i>Neisseria</i>	11-Apr-22	2749212 bp	Canada	<i>Felis catus</i>	Dent CA1/247
60	CP073115.1	<i>Neisseria subflava</i>	11-Jul-22	2479061 bp	Singapore	<i>Homo sapiens</i>	TT0077
61	CP091509.1	<i>Neisseria dumasiana</i>	11-Apr-22	2679563 bp	Canada	<i>Homo sapiens</i>	LMG 30012
62	CP059566.1	<i>Neisseria sicca</i>	04-Aug-20	2864419 bp	Canada	<i>Homo sapiens</i>	DSM 17713
63	CP060414.1	<i>Neisseria muscoli</i>	28-May-21	2928421 bp	USA	<i>Musmus culus</i>	NW831
64	CP059567.1	<i>Neisseria shayeganii</i>	04-Aug-20	2419744 bp	Canada	<i>Homo sapiens</i>	DSM 22244
65	CP091510.1	<i>Neisseria arctica</i>	11-Apr-22	2378219 bp	Canada	<i>Anser albifrons</i>	KH1503
66	CP073114.1	<i>Neisseria subflava</i>	11-Jul-22	2243952 bp	Singapore	<i>Homo sapiens</i>	HP0048
67	CP059565.1	<i>Neisseria wadsworthii</i>	04-Aug-20	2501534 bp	Canada	<i>Homo sapiens</i>	DSM 22245
68	CP094241.1	<i>Neisseria macacae</i>	29-Mar-22	2801968 bp	Korea	<i>Rhesus monkey</i>	ATCC 33926
69	CP064367.1	<i>Neisseria meningitidis</i>	11-Apr-22	2181327 bp	USA	<i>Homo sapiens</i>	PartJ-N meningitidis-RM8376
70	CP073118.1	<i>Neisseria subflava</i>	11-Jul-22	2332965 bp	Singapore	<i>Homo sapiens</i>	CG0073
71	CP072524.1	<i>Neisseria sicca</i>	05-Apr-21	2566407 bp	China	<i>Homo sapiens</i>	NS20201025
72	CP062976.1	<i>Neisseria</i>	20-Oct-20	2645607 bp	China	<i>Marmot</i>	ZJ785
73	AP024489.1	<i>Neisseria meningitidis</i>	27-Feb-21	2158475 bp	Japan	<i>Homo sapiens</i>	NIID777
74	CP073117.1	<i>Neisseria subflava</i>	11-Jul-22	2213981 bp	Singapore	<i>Homo sapiens</i>	HP0015
75	CP116766.1	<i>Neisseria</i>	05-Feb-23	2065000 bp	China	<i>Marmot</i>	ZJ106
76	LT906434.1	<i>Neisseria zoodegmatis</i>	15-Aug-17	2552522 bp	UK	<i>Homo sapiens</i>	NCTC12230
77	LR134287.1	<i>Neisseria animalis</i>	19-Dec-18	2240945 bp	UK	<i>Homo sapiens</i>	NCTC10212
78	OW969598.1	<i>Neisseria</i>	22-May-22	2024518 bp	France	<i>Homo sapiens</i>	Marseille-Q6792
79	LR134533.1	<i>Neisseria weaveri</i>	19-Dec-18	2238481 bp	UK	<i>Homo sapiens</i>	NCTC12742
80	LS483369.1	<i>Neisseria cinerea</i>	17-Jun-18	1832904 bp	UK	<i>Homo sapiens</i>	NCTC10294
81	OX336253.1	<i>Neisseria</i>	21-Sep-22	2354813 bp	France	<i>Homo sapiens</i>	Marseille-Q5346
82	LR134516.1	<i>Neisseria animaloris</i>	19-Dec-18	2283939 bp	UK	<i>Homo sapiens</i>	NCTC12227
83	LT571436.1	<i>Neisseria weaveri</i>	17-May-16	2188497 bp	UK	<i>Homo sapiens</i>	NCTC13585
84	LS483435.1	<i>Neisseria elongata</i>	17-Jun-18	2249415 bp	UK	<i>Homo sapiens</i>	NCTC11050
85	LR134313.1	<i>Neisseria canis</i>	19-Dec-18	2569389 bp	UK	<i>Homo sapiens</i>	NCTC10296
86	LR134525.1	<i>Neisseria meningitidis</i>	19-Dec-18	2186098 bp	UK	<i>Homo sapiens</i>	NCTC10025
87	LR134522.1	<i>Neisseria meningitidis</i>	19-Dec-18	2182188 bp	UK	<i>Homo sapiens</i>	NCTC3372
88	LR134526.1	<i>Neisseria meningitidis</i>	19-Dec-18	2305833 bp	UK	<i>Homo sapiens</i>	NCTC10026
89	LR134528.1	<i>Neisseria meningitidis</i>	19-Dec-18	2228346 bp	UK	<i>Homo sapiens</i>	NCTC12163

The CRISPR-Cas system was classified into six types: I-A, I-C, I-F, II-C, III-A, and III-B. Among the tested *spp.*, 69% (16 out of 89) were found to have type II-C CRISPR system, while 28% (31 out of 89) had type I-C system. Sixteen *spp.* of *Neisseria* were identified to possess two CRISPR Cas array in their genome. Among this *spp.* a majority (69%) had both type II-C and I-C systems. Especially, two *spp.* *Neisseria subflava* and *Neisseria dumasiana*, were discovered to have three CRISPR Cas array in their genomes. The study examined 44 CRISPR positive *spp.* of *Neisseria meningitidis* and found that it possessed the II-C CRISPR system alone exclusively (Table 2). However, in contrast, no CRISPR arrays were detected in the *Neisseria gonorrhoeae* strains indicating the absence of the typical CRISPR-Cas system in this species. But observed the presence of an orphan CRISPR, which means that a CRISPR locus was identified without the associated Cas genes that are typically part of the CRISPR-Cas system. This suggests that although *Neisseria gonorrhoeae* lacks the complete CRISPR-Cas system, it still retains some remnants of the CRISPR machinery, possibly reflecting evolutionary changes or previous interactions with foreign genetic elements.

In all the CRISPR-positive *spp.* investigated in this study, the essential components of the active CRISPR system, namely the *cas1* and *cas2* genes, were identified. These two genes are essential for the CRISPR system's ability to acquire and incorporate additional viral or foreign DNA sequences into the bacterial CRISPR array. The Type II-C CRISPR system depends on a single effector protein that can target and cleave both single-stranded and double-stranded DNA utilising a dual RNA-guided mechanism, in contrast to the Type I-C CRISPR system, which uses a multi-subunit complex (Csy) to target and cleave single-stranded DNA [13]. The signature protein for type I-C is Cas8c whereas for II-C

is Cas9. CRISPR Cas I-F system utilizes a multi-subunit effector complex known as the Csy-F (Cascade-F complex). The Cascade- complex includes various Cas proteins such as Cas8f, Cas7f, Cas6f, Csy2 and Cas3 in the *Neisseria* spp. The CRISPR Cas Type III-A and III-B were detected in two and five *spp.* of *Neisseria*, respectively. In which type III-B and type I-C co-occurred in four out of five *spp.* of *Neisseria*. The presence of unique genes for small subunits of respective effector complexes, specifically *csm2* for III-A and *cmr5* for III-B, distinguishes these subtypes. In subtype III-A, *cas1*, *cas2*, and *cas6* genes are often present. Additionally, III-A systems have been shown to target DNA, providing them with DNA-targeting capabilities.

### Analysis of spacer sequences in CRISPR arrays

There were 3093 CRISPR spacer sequences in 89 species of the *Neisseria* altogether. After eliminating the duplicate sequences, 1661 unique spacer sequences were screened manually. The direct repeats found were of 26 – 37 bp in length and spacer sequences of 30 – 48 bp in length. The maximum number of the spacer sequence in a genome analyzed was 151, while the least was merely two. A bacteriophage interaction is seen as a critical event in CRISPR-Cas spacer acquisition because it gives selective pressure to stay intact, particularly in clinically relevant pathogens. The amount of phage-targeting spacers was shown to be positively associated with the overall number of spacers in each genome. In this study, totally 366 sites were found to be spacer targeted phage regions and the total number of self-targeting regions were about 156 in the sequence analyzed (Figure 1). Since phage interaction is believed to be a potent evolutionary process for sustaining CRISPR-Cas systems, a sizable portion of spacers (22%) were estimated to target phage DNA. Only 8% of spacers were anticipated to target plasmids. Because

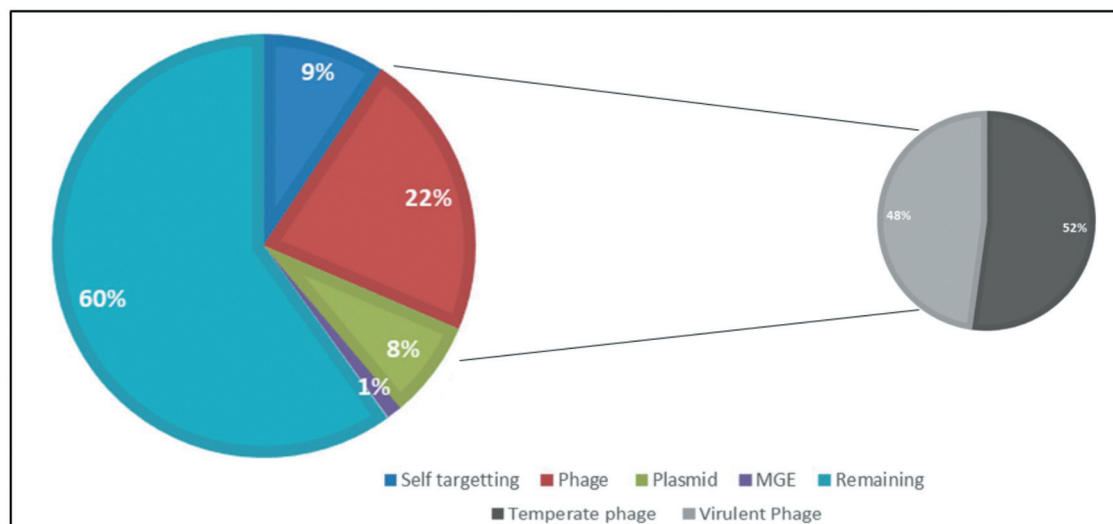


Figure 1. Spacer targeting sequences in CRISPR arrays

Table 2. CRISPR Cas regions present in the *Neisseria spp.*

S. No	Acc. No	CRISPR Types	Region	Repeats	No of Repeats	Repeat Length	No of Spacers	Spacer length
1	CP000381.1	II-C	401433 - 405981	GATTCGGCTGGCGGGGAATGACGG	3	26	2	42
2	CP016672.1	II-C	2099389 - 2103937	GTTGAGTCCCTTTCATTTCCAGTGTACAAT	10	36	9	48
3	FR774048.1	II-C	375710 - 380258	ATTGAGCACTGCGAAATGAGAAAGGGAGCTACAAC	26	36	25	30
4	CP002422.1	II-C	1919555 - 1924101	GTTGAGTCCCTTTCATTTCCAGTGTACAAT	23	36	22	30
5	FM99788.1	II-C	1917073 - 1921621	ATTGAGCACTGCGAAATGAGAAAGGGAGCTACAAC	18	36	17	30
6	CP016671.1	II-C	401 - 4949	GTTGAGTCCCTTTCATTTCCAGTGTACAAC	5	36	4	30
7	CP016654.1	II-C	549773 - 554321	GTTGAGTCCCTTTCATTTCCAGTGTACAAT	26	36	25	30
8	CP016647.1	II-C	2117129 - 2121677	GTTGAGTCCCTTTCATTTCCAGTGTACAAT	26	36	25	30
9	AL157959.1	II-C	609568 - 614116	GTTGAGTCCCTTTCATTTCCAGTGTACAAT	17	36	16	30
10	CP016646.1	II-C	950918 - 955466	GTTGAGTCCCTTTCATTTCCAGTGTACAAT	27	36	26	30
11	CP016660.1	II-C	1326170 - 1330718	ATTGAGCACTGCGAAATGAGAAAGGGAGCTACAAC	16	36	15	30
12	CP007524.1	II-C	612661 - 617209	GTTGAGTCCCTTTCATTTCCAGTGTACAAT	24	36	23	30
13	CP007726.1	I-C	1479046 - 1483607	GTTTCAATACACAGCCGCCCGAAAGGGGCTG	11	31	10	34
14	FN995097.1	II-C	1890078 - 1894625	GTTTCAACACACAGCCGCTAGAGGGGGCTGA	11	32	10	34
15	CP012392.1	II-C	1805076 - 1809623	ATTGTAGCACTGCGAAATGAGAAAGGGAGCTACAAC	10	36	9	30
16	CP031332.1	II-C	318131 - 322675	ATTGTAGCACTGCGAAATGAGAAAGGGAGCTACAAC	19	36	18	30
17	CP020401.2	II-C	1048461 - 1053009	CCGTCAATCCCGGCGAGGGGGAATC	4	36	3	30
18	CP021723.1	II-C	84429 - 88976	GTTGAGTCCCTTTCATTTCCAGTGTACAAT	3	26	2	44
19	CP020420.2	II-C	915140 - 919688	GTTGAGTCCCTTTCATTTCCAGTGTACAAT	30	36	29	30
20	CP021518.1	II-C	84427 - 88974	GTTGAGTCCCTTTCATTTCCAGTGTACAAT	15	36	14	30
21	CP021523.1	II-C	83506 - 88053	GTTGAGTCCCTTTCATTTCCAGTGTACAAT	19	36	18	30
22	CP039887.1	II-C	1775428 - 1779972	CCAGCCGCTTCAGGGGCTGTGTGAAAC	15	36	14	30
23	CP021516.1	I-C	570933 - 581613	ATTGTAGCACTGCGAAATGAGAAAGGGAGCTACAAC	152	32	151	34
24	CP021725.1	II-C	84423 - 88970	GTTGAGTCCCTTTCATTTCCAGTGTACAAT	21	36	20	30
25	CP023429.1	I-C	2060384 - 2070426	GTTGAGTCCCTTTCATTTCCAGTGTACAAT	15	36	14	30
26	CP021521.1	II-C	815633 - 820185	GTTTCAACACACAGCCGCCGTTGGGGCTGA	18	36	17	30
27	CP031255.1	II-C	81087 - 85634	GTTGAGTCCCTTTCATTTCCAGTGTACAAT	14	36	13	30
28	CP021522.1	I-C	426210 - 430763	ATTGTAGCACTGCGAAATGAGAAAGGGAGCTACAGC	24	32	23	34
29	CP045960.1	II-C	1708507 - 1720752	GTTTCAACACACAGCCGCCGAAAGGGGGCTGG	23	36	22	30
30	CP020402.2	II-C	848677 - 853225	GTTGAGTCCCTTTCATTTCCAGTGTACAAT	26	36	25	30
31	CP021520.1	II-C	84193 - 88740	GTTGAGTCCCTTTCATTTCCAGTGTACAAT	15	36	14	30
32	CP039886.1	I-C	515098 - 526750	GTTGAGTCCCTTTCATTTCCAGTGTACAAT	17	36	16	30
33	CP040504.1	I-F	1856374 - 1860948	TTTCTAAAGCTGCCTATTCGGCAGGTAAC	37	36	36	30
34	CP031699.1	II-C	2005639 - 2016144	TTTCTAAGCTGCCTATTCGGCAGGTAAC	18	36	17	30
			1387090 - 1391609	ATTGTAACTACGAGATGAGAGGGAGCTACAAC	7	33	6	34
				TTTCTAAGCTGCCTATTCGGCAGGTAAC	28	36	27	30
				TTTCTAAGCTGCCTATTCGGCAGGTAAC	44	28	43	32
				TTTCTAAGCTGCCTATTCGGCAGGTAAC	18	28	17	32
				ATTGTAACTACGAGATGAGAGGGAGCTACAAC	12	36	11	30

S. No	Acc. No	CRISPR Types	Region	Repeats	No of Repeats	Repeat Length	No of Spacers	Spacer length
35	CP021724.1	II-C	84362 - 88909	GTTGTAGTCCCATTCATTTCCAGTGTACAAT	14	36	13	30
36	CP031334.1	II-C	309325 - 313869	ATTGTAGCACTCGAAATGAGAAATGGAGCTACAAC	43	36	42	30
37	CP012694.1	II-C	2049829 - 2054377	GTTGTAGTCCCTTTTCATTTCCAGTGTACAAT	19	36	18	30
38	CP031253.1	II-C	168076 - 172624	GTTGTAGTCCCTTTTCATTTCCAGTGTACAAT	12	36	11	30
39	CP016883.1	II-C	371884 - 376432	GTTGTAGTCCCTTTTCATTTCCAGTGTACAAT	32	36	31	30
40	CP031324.1	II-C	996535 - 1001079	GTTGTAGTCCCATTCATTTCCAGTGTACAAT	30	36	29	30
41	CP046027.1	I-C	1631803 - 1640082	TCAGCCACTCGGGTGGCTGTGTGTTGAAAC	20	32	19	34
42	CP022527.1	I-C	177305 - 185856	GTTTCAACACTCAGCCGCCGAAAGCCGGCTGC	26	32	25	34
43	CP021517.1	II-C	84425 - 88972	GTTGTAGTCCCATTCATTTCCAGTGTACAAT	15	36	14	30
44	CP022278.1	I-C	1936631 - 1946895	GTTTCAATACACAGCCACCCTGGAGGTTGGCTG	38	33	37	34
		I-C	1193128 - 1202381	GTTTCAACACACAGCCGCCGAAAGCCGGCTGG	172	32	171	35
		III-B	1331696 - 1350397	GTCGGAAGACTTGCCCACTAATCGGGGATTAAGAC	14	36	13	34
45	CP031251.1			GTTTAAATCCCCGATTAGTGGGCAAGTCTCCGAC	19	36	18	34
		I-A	2100402 - 2106823	GTTTAAATCCCCATGTTGGGGAGGTTTTTCAGAG	21	36	20	34
				GTTTAAATCCCCATGTTGGGGAGGTTTTTCAGAG	20	36	19	35
46	CP016682.1	II-C	25073 - 29621	ATTGTAGCACTCGAAATGAGAAAGGGAGCTACAAC	20	36	19	30
47	CP016680.1	II-C	1226815 - 1231363	ATTGTAGCACTCGAAATGAGAAAGGGAGCTACAAC	26	36	25	30
48	CP021519.1	II-C	85186 - 89733	GTTGTAGTCCCATTCATTTCCAGTGTACAAT	15	36	14	30
49	CP031252.1	I-C	223404 - 234018	CAGCCGCTTTAGCCGGCTGTGTGTTGAAAC	25	31	24	35
50	CP020422.2	II-C	1284066 - 1288614	GTTGTAGTCCCTTTTCATTTCCAGTGTACAAT	37	36	36	30
51	CP031328.1	II-C	2209402 - 2213946	ATTGTAGCACTCGAAATGAGAAATGGAGCTACAAC	23	36	22	30
		III-B	1698165 - 1717071	GTCGGAAGACTTGCCCACTAATCGGGGATTAAGAC	20	36	19	34
				GTTTAAATCCCCGATTAGTGGGCAAGTCTCCGAC	18	36	17	34
53	CP065653.1	II-C	1780305 - 1790271	CCAGCCGCTTCGGGGCTGTGTGTTGAAAC	76	32	75	34
54	CP073116.1	II-C	1516025 - 1520573	ATTGTAGCACTCGAAATGAGAAAGGGAGCTACAAC	19	36	18	30
55	CP053939.1	I-C	1877116 - 1882260	ATTGTAGCACTCGAAATGAGAAAGGGAGCTACAAC	10	36	9	30
56	CP065726.1	II-C	483233 - 497654	CCAGCCGCTTCAGGGGCTGTGTGTTGAAAC	16	32	15	34
		III-A	1601771 - 1606315	ATTGTAGCACTCGAAATGAGAAAGGGAGCTACAAC	19	36	18	30
		II-C	1125145 - 1125533	TCTCAATCCCCGTGTGTGTGGGCTTTTGTGTC	6	36	5	34
57	CP059570.1	II-C	2469750 - 2474265	GTTGTAGTCCCTCTCCTCATCTCGTAGTGTACAAT	23	36	22	30
58	CP073119.1	II-C	95952 - 100497	ATTGTAGCACTCGAAATGAGAAAGGGAGCTACAAC	23	36	22	30
59	CP091522.1	I-C	1584845 - 1595472	GTTTCAACACACAGCCGCCGAAAGCCGGCTGG	27	32	26	35
60	CP073115.1	II-C	178250 - 189166	TCAGCCGCTTCGGGGCTGTGTGTTGAAAC	74	32	73	35
		II-C	2248300 - 2252845	ATTGTAGCACTCGAAATGAGAAAGGGAGCTACAAC	7	36	6	30
		III-A	1138380 - 1143001	GTTTAAATCCCCGAAATGGTGGGCTTTGTTTCAAT	50	36	49	33
61	CP091509.1		464699 - 481428	GTTGTAGTTCCTCTCTCATCTCGTAGTGTACAAT	15	36	14	30
		I-C	2469067 - 2482172	GTTTCAACACACAGCCGCCGAAAGGGCTGA	8	32	7	34
				GTTTCAACACACAGCCGCCGAAAGGGCTGG	8	32	7	35
				GTCGGAAGACTTGCCCACTAATCGGGGATTAAGAC	7	36	6	33
				GTCGGAAGACTTGCCCACTAATCGGGGATTAAGAC	6	32	82	34
62	CP059566.1	III-B	863873 - 879969	GTTTAAATCCCCGATTAGTGGGCAAGTCTCCGAC	3	36	2	33
				GTTTAAATCCCCGATTAGTGGGCAAGTCTCCGAC	4	36.2	3	34
		I-C	1179516 - 1192803	CCAGCCGCTTCGGGGCTGTGTGTTGAAAC	83	35.2	5	35

S. No	Acc. No	CRISPR Types	Region	Repeats	No of Repeats	Repeat Length	No of Spacers	Spacer length
63	CP060414.1	II-C	2238654 - 2243142	ATTGTAGCACTGCGAGATGAAAGAGAAAGCTACAAC GTTGTAGCTTCCTCTTCAATCTCGCAGTGTACAAT	22	36	21	30
64	CP059567.1	I-C	1474197 - 1484682	GTTTCAACACACAGCCGCCGAAAGCGGCTGA	3	32	2	33
65	CP091510.1	II-C	2367224 - 2371744	GTTGTAGCTCCCTTTCATATTCGACAGTGTACAAT	17	32	3	35
		I-C	232682 - 2339182	GTTTCAACACACACAGCCGCCGAAAGTGGCTGA	4	36	16	30
66	CP073114.1	II-C	1369084 - 1373627	GTTGTAGCTCCCTTTCATATTCGACAGTGTACAAT GTTTCAACACACAGCCGCCGAAAGCGGCTGA	26	36	25	30
67	CP059565.1	I-C	6517 - 15886	GTTGTAGCTTCCTCTCTCATCTCGTAGTGTACAAT	4	36	3	30
		II-C	863809 - 868414	GTTGTAGCTTCCTCTCTCATCTCGTAGTGTACAAT AGTCGGAAAGACTTACCCCACTAGTCGGGGATAAACT	26	36	25	30
		III-B	1517659 - 1534284	GTTTAAATCCCGATTAGTGGGCAAGTCTCCGAC GTTTAAATCCCGATTCTGTGGGCAAGT	11	36	10	34
68	CP094241.1	I-C	1835421 - 1848345	CAGCCGCCCTTAGCGGGCTGTGTGTTGAAAC	9	28	8	42
69	CP064367.1	II-C	869274 - 873822	ATTGTAGCACTGCGAAATGAGAAAGGGAGCTACAAC GTTTCAACACACAGCCGCCGAAAGCGGCTGG	19	36	18	30
		I-C	920 - 10662	ATTGTAGCACTGCGAAATGAGAAAGGGAGCTACAAC	5	36	4	30
70	CP073118.1	II-C	757607 - 762151	GTTTCAACACACAGCCGCCGAAAGCGGCTGG	23	32	22	34
		III-B	779344 - 797781	GTCGGAAGACTTGGCCCACTAATCGGGGATTAAGAC GTTTAAATCCCGATTAGTGGGCAAGTCTCCGAC	16	36	15	33
71	CP072524.1	I-C	1096743 - 1106398	GTTTCAACACACAGCCGCCGAAAGCGGCTGG	62	32	61	34
		I-C	484640 - 495508	TCAGCCGCCCTCGGGGGCTGTGTGTTGAAAC	12	32	11	34
72	CP062976.1	I-C	870835 - 875393	TCAGCCGCCCTCGGGGGCTGTGTGTTGAAAC	37	36	32	30
		II-C	80955 - 85499	ATTGTAGCACTGCGAAATGAGAAAGGGAGCTACAAC	33	32	36	34
73	AP024489.1	II-C	742194 - 746741	GTTGTAGCTCCCTTTCATATTCGACAGTGTACAAT	10	36	9	30
		II-C	1724281 - 1734277	ATTGTAGCACTGCGAAATGAGAAAGGGAGCTACAAC CCAGCCGCCCTCAGGGGCTGTGTGTTGAAAC	28	36	27	30
74	CP073117.1	I-C	920001 - 931498	CCAGCCGCCCTCAGGGGCTGTGTGTTGAAAC	98	32	97	35
		I-C	188995 - 198248	CCAGCCGCCCTCAGGGGCTGTGTGTTGAAAC	10	32	9	35
75	CP116766.1	I-C	473845 - 478364	GTTTCAACACACAGCCGCCGAAAGCGGCTGA	31	32	30	34
76	LT906434.1	I-C	1953431 - 1957964	GTTTCAACACACAGCCGCCGAAAGCGGCTGC	62	32	61	34
77	LR134287.1	II-C	153056 - 159598	ATTGTAACACTACGAGATGAGAGAGGGAGCTACAAC	12	36	11	30
78	OW969598.1	II-C	106683 - 111227	GTTGTAGCTCCCTTTCATATTCGACAGTGTACAAT	27	36	26	30
79	LR134533.1	I-C	1223399 - 1227947	GTTTCAACACACAGCCGCCGAAAGCGGCTGT	63	32	62	35
80	LS483369.1	II-C	1226810 - 1231355	GTTGTAGCTCCCTTTCATATTCGACAGTGTACAAT	8	36	35	30
81	OX336253.1	II-C	1889746 - 1900991	ATTGTAGCACTGCGAAATGAGAAAGGGAGCTACAAC	7	36	35	30
82	LR134516.1	I-C	918256 - 929848	ATTGTAGCACTACGAGATGAGAGAGGGAGCTACAAC	7	36	35	30
		I-C	1905654 - 1910215	GTTTCAACACACAGCCGCCGAAAGCGGCTGA	4	32	31	35
83	LT571436.1	I-C	2423410 - 2433620	GTTTCAACACACAGCCGCCGAAAGCGGCTGT	79	34	33	34
84	LS483435.1	I-C	1519022 - 1523570	GTTTCAACACACAGCCGCCGAAAGCGGCTGT	11	31	30	34
85	LR134313.1	I-C	81278 - 85826	GTTTCAACACACAGCCGCCGAAAGCGGCTGT	36	31	30	35
86	LR134525.1	II-C	91278 - 85826	GTTGTAGCACTGCGAAATGAGAAAGGGAGCTACAAC	19	36	35	30
87	LR134522.1	II-C	91517 - 96065	GTTGTAGCTCCCTTTCATATTCGACAGTGTACAAT	22	36	35	30
88	LR134526.1	II-C	82689 - 87237	GTTGTAGCTCCCTTTCATATTCGACAGTGTACAAT	39	36	35	30
89	LR134528.1	II-C		GTTGTAGCTCCCTTTCATATTCGACAGTGTACAAT	15	36	35	30

Table 3. Stability of CRISPR direct repeats in *Neisseria spp.*

S. No	CRISPR Type	Repeat Sequence	Frequency (%)	Folding score (kcal/mol)
DR1	I-A	GTCTTAATCCCCATGTGGTGGGGAGGTTTTTCAGAG	47.57 %	-10.66
DR2	I-C	CCAGCCGCCTTCAGGCGGCTGGTGTGTTGAAAC	90.22 %	-19.36
DR3	I-C	GTTTCAATACACAGCCACCCGCGAGGGTGGCTG	69.64 %	-19.22
DR4	I-C	TCAGCCGCCTTCGGGCGGCTGTGTGTTGAAAC	90.70 %	-17.06
DR5	I-C	CAGCCGCCTTTAGGCGGCTGTGTGTTGAAAC	90.00 %	-16.06
DR6	I-F	TTTCTAAGCTGCCTGTGCGGCAGGTAAC	38.57 %	-8.69
DR7	II-C	GTTTCAACACACAGCCGCCTAGAGGCGGCTGA	80.56 %	-16.63
DR8	II-C	ATTGTAGCACTGCGAGATGAAAGAGGAAGCTACAAC	33.55 %	-7.37
DR9	II-C	CCGTCATTCCC GCGCAGGCGGGAATC	79.71 %	-13.84
DR10	II-C	GATTCCC GCTGCGCGGGAATGACGG	38.57 %	-8.69
DR11	II-C	GTTGTAGCTTCCTCTTTCATCTCGCAGTGCTACAAT	64.43 %	-8.07
DR12	III-A	TCTCAATCCC GGTGTGATGGGGCTTTTTTGTGTCC	56.17 %	-9.46
DR13	III-B	AGTCGGAAGACTTACCCCACTAGTCGGGGATAAAACT	47.57 %	-9.96
DR14	III-B	GTCGGAAGACTTGCCCACTAATCGGGGATTAAGAC	84.00 %	-9.31
DR15	III-B	GTCTTAATCCCCGATTGCGGGCAAGTCTTCCGAC	28.48 %	-7.77
DR16	I-C, II-C	GTTTCAACACACAGCCGCCGGAAGGCGGCTG	79.10 %	-16.04
DR17	II-C, III-A, I-C	GTTGTAGCTTCCTCTCTCATCTCGTAGTGCTACAAT	64.83 %	-8.07

of the presence of Anti CRISPR (Acr) genes or the lack of homologous Cas genes, self-targeting spacers were prevalent in genomes anticipated to have inactivated CRISPR-Cas systems. The identified phages were further categorized into temperate and virulent groups. Among these groups, approximately 52% of the phages were classified as temperate, while the remaining 48% were classified as virulent. Notably, phage sequences from *Haemophilus* phage, *Ralstonia* phage, *Enterobacteria* phage, *Burkholderia* phage, and *Pseudomonas* phage were observed at a higher frequency in the dataset. Interestingly, some spacers were found to be identical as *Neisseria* plasmid sequences, despite not being derived from the current host bacteria. Additionally, there were 16 spacer sequences that exhibited matches with plasmid and phage sequences, suggesting potential interactions and exchange of genetic material between these mobile genetic elements. Among the spacers analyzed, approximately 60% did not show any recognizable target in our database searches.

### Stability of CRISPR direct repeats

The structural stability and intramolecular structure of distant direct repeats were performed using RNAfold web server for the dataset (Table 3). One hundred and forty direct repeat sequences of *Neisseria spp.* were grouped into 17 categories based on sequence homology. The tool will design the RNA structure based on the bit score that represents the stability of repeats. In this study, the repeat regions DR2, DR3, DR4, DR5, DR7 and DR16 found to have folding scores between -16 to -19 kcal/mol which indicates stable secondary structure whereas other direct repeat regions found to have fold scores. The difference in the structural stability of CRISPR repeats has a significant consequence in pre-crRNA processing since it helps in forming tracrRNA. The formation of tracrRNA with closed hairpin structure will elevate the genome editing efficiency by 10 folds and

also it will minimize the prescreening of gRNAs towards targeting the gene of interest [14, 15].

### Relation between the CRISPR Cas system and bacterial drug resistance

The AR gene analysis in CRISPR positive *Neisseria spp.* was conducted by performing BLASTN search against the Resfinder and CARD databases. The analysis findings reveal that 30 out of the 89 genomes showed no detected AR genes, constituting approximately 33.7% of the sampled data. In the analyzed *Neisseria* genomes with CRISPR type II-C, a notable finding was the presence of efflux pump resistance genes in the majority of the sequences (71%). These efflux pump genes include *farB*, *mtrF*, *mtrC*, *mtrA*, and *norM*. Among the *Neisseria spp.* possessing both III-B and I-C CRISPR types, the majority of the *spp.* (75%) were found to harbor only the *norM* efflux gene (Table 4). The *norM* gene encode an efflux pump that facilitates the removal of hydrophobic agents, which can include antibiotics, nonionic detergents, certain antibacterial peptides, bile salts, and steroidal hormones. This gene's activity leads to a decrease in susceptibility to fluoroquinolones [16]. However, there was one exception, where a *Neisseria mucosa* genome was identified to harbor additional resistance genes. This particular strain was found to carry genes such as *aph(6)-Id*, *aph(3'')-Ib*, *sul2*, *blaTEM-1*, and *tet(B)*, in addition to the *norM* gene. *blaTEM* genes confer resistance to amoxicillin-clavulanate in clinical settings. However, they maintain susceptibility to inhibition by tazobactam, which subsequently renders them susceptible to the combination of piperacillin and tazobactam [17]. Determinants of tetracycline resistance were more susceptible to tigecycline whereas aminoglycoside resistances are susceptible to amikacin [18, 19].

Statistical analysis was computed to measure the association of CRISPR and the AR genes in the *Neisseria*

Table 4. Correlation of CRISPR Cas system and AR genes

S. No	Acc. No	CRISPR Types			Antibiotic Resistance Genes	Species	Country
1	CP039887.1	II-C	I-C		No AR genes	<i>Neisseria subflava</i>	USA
2	CP023429.1	I-C	II-C		No AR genes	<i>Neisseria weixii</i>	China
3	CP031255.1	II-C	I-C		No AR genes	<i>Neisseria elongata</i>	USA
4	CP040504.1	II-C	I-F		<i>norM</i>	<i>Neisseria</i>	Australia
5	CP031251.1	III-B	I-A	I-C	No AR genes	<i>Neisseria subflava</i>	USA
6	CP020452.2	III-B	I-C		<i>aph(6)-Id, aph(3'')-Ib, sul2, blaTEM-1, tet(B), norM</i>	<i>Neisseria mucosa</i>	USA
7	CP059570.1	III-A	II-C		No AR genes	<i>Neisseria dentiae</i>	UK
8	CP073119.1	I-C	II-C		No AR genes	<i>Neisseria subflava</i>	Singapore
9	CP091509.1	II-C	III-A	I-C	No AR genes	<i>Neisseria dumasiana</i>	USA
10	CP059566.1	III-B	I-C		<i>norM</i>	<i>Neisseria sicca</i>	UK
11	CP091510.1	II-C	I-C		No AR genes	<i>Neisseria arctica</i>	USA
12	CP059565.1	I-C	II-C		No AR genes	<i>Neisseria wadsworthii</i>	USA
13	CP094241.1	III-B	I-C		<i>norM</i>	<i>Neisseria macacae</i>	South Korea
14	CP073118.1	II-C	I-C		No AR genes	<i>Neisseria subflava</i>	Singapore
15	CP072524.1	I-C	III-B		<i>norM</i>	<i>Neisseria sicca</i>	China
16	CP062976.1	II-C	I-C		No AR genes	<i>Neisseria</i>	China
17	CP073117.1	I-C	II-C		No AR genes	<i>Neisseria subflava</i>	Singapore
18	LR134516.1	II-C	I-C		No AR genes	<i>Neisseria animaloris</i>	UK

Table 5. Presence of CRISPR Cas loci in *Neisseria spp.* and its associations with AR genes

Species	Total No of Species	No of CRISPR positive Species	Observed no of Species has both CRISPR and AR genes (O)	Expected no of Species possessing both CRISPR and AR genes (E)	Log frequency-ratios (Log(O/E))
<i>Neisseria animalis</i>	2	2	2	0.36	0.75
<i>Neisseria animaloris</i>	2	1	1	0.32	0.5
<i>Neisseria arctica</i>	1	1	0	0	0
<i>Neisseria bacilliformis</i>	1	0	0	0.14	0
<i>Neisseria brasiliensis</i>	1	1	1	0.16	0.81
<i>Neisseria canis</i>	1	1	1	0.16	0.81
<i>Neisseria chenwenguii</i>	1	1	1	0.16	0.81
<i>Neisseria cinerea</i>	2	2	2	0.36	0.75
<i>Neisseria dentiae</i>	1	1	0	0	0
<i>Neisseria dumasiana</i>	1	1	0	0	0
<i>Neisseria elongata</i>	4	4	3	0.68	0.65
<i>Neisseria flavescens</i>	1	1	1	0.16	0.81
<i>Neisseria gonorrhoeae</i>	169	0	0	50.94	0
<i>Neisseria lactamica</i>	4	2	2	0.36	0.75
<i>Neisseria macacae</i>	1	1	1	0.16	0.81
<i>Neisseria meningitidis</i>	136	44	44	119.94	-0.44
<i>Neisseria mucosa</i>	3	2	2	0.36	0.75
<i>Neisseria muscoli</i>	1	1	1	0.16	0.81
<i>Neisseria perflava</i>	1	0	0	0.14	0
<i>Neisseria polysaccharea</i>	1	0	0	0.14	0
<i>Neisseria shayegani</i>	1	1	1	0.16	0.81
<i>Neisseria sicca</i>	3	2	1	0.32	0.5
<i>Neisseria</i>	8	7	3	0.91	0.52
<i>Neisseria subflava</i>	8	8	7	2.22	0.5
<i>Neisseria wadsworthii</i>	1	1	0	0	0
<i>Neisseria weaveri</i>	2	2	1	0.17	0.76
<i>Neisseria weixii</i>	1	1	0	0	0
<i>Neisseria zalophi</i>	1	0	0	0.14	0
<i>Neisseria zoodegmatis</i>	1	1	1	0.16	0.81

*spp.* (Table 5). A positive log frequency-ratio signifies a positive association, suggesting that AR genes tend to coexist with CRISPR Cas. Conversely, a negative association is observed when the presence of CRISPR Cas tends to exclude AR genes. It was found that the *Neisseria spp.* with several CRISPR arrays often had either no AR genes or only one AR gene in their genomes. The presence of efflux pump genes has been identified in the majority of the *Neisseria spp.* Efflux pumps are specialized transporters in bacterial cells that play a crucial role in AR. It actively eliminate antibiotics from the bacterial cell, lowering their intracellular concentration and decreasing their ability to fight infections. However, when more than one array region was present in the

*Neisseria* genome along with CRISPR type II-C, no similar pattern of harboring efflux pump genes was observed.

## Discussions

Prokaryotes, in response to daunting survival challenges, have evolved CRISPR-Cas systems as their defense mechanisms. Within the gastrointestinal tract, a rich array of natural phages exists, setting the stage for an unending struggle between bacteria and bacteriophages. Bacterial *spp.* equipped with these CRISPR-Cas systems are prime candidates for industrial applications because of their robust resistance to bacteriophages. The interplay between AR and CRISPR-Cas

systems in *Neisseria* pathogens is a critical concern due to the rise of AR strains. *Neisseria* species, like *N. gonorrhoeae* and *N. meningitidis*, have developed resistance to multiple antibiotics, diminishing our ability to treat infections effectively. *N. meningitidis* can lead to various clinical conditions, including meningococemia, pneumonia, septic arthritis, pericarditis, and urethritis. *N. gonorrhoeae* primarily causes sexually transmitted infections, with symptoms such as genital discharge and discomfort during urination [20]. However, CRISPR-Cas systems, which function as a bacterial immune system, offer a unique avenue for addressing this issue. These systems capture and store genetic material from invading elements like plasmids carrying AR genes, and later use this information to target and destroy matching sequences. Consequently, researchers are exploring the use of CRISPR technology to selectively eliminate AR genes within *Neisseria* pathogens, potentially restoring their susceptibility to antibiotics and providing a novel strategy to combat AR strains. This approach not only has the potential to extend the efficacy of existing antibiotics but also represents a significant development in the ongoing battle against AR, a public health crisis of global significance.

A comprehensive investigation into the prevalence and diversity of CRISPR-Cas systems was conducted in a collection of 360 *Neisseria* spp. These bacterial strains were sourced from a variety of hosts, including *Homo sapiens* (humans), *Felis catus* (cats), *Mus musculus* (mice), *Anser albifrons* (white-fronted goose), *Plateau pika* (a small mammal), Rhesus monkeys, marmots, cattle, poultry and guinea pigs. Among these spp. 89 were identified to harbor CRISPR arrays. Notably, 69% of the tested spp. (16 out of 89) were found to harbor the type II-C CRISPR system, while 28% (31 out of 89) exhibited the type I-C system. Type I-C systems employ a complex of multiple Cas proteins, known as the cascading complex, to target and cleave foreign DNA during interference. In contrast, Type II-C systems, exemplified by Cas9, rely on a single effector protein for both target recognition and DNA cleavage, making them simpler and widely used in genome editing applications. Earlier research in Gram-negative bacteria, particularly *Pseudomonas*, revealed a high prevalence of the CRISPR type I-F system [21]. On the other hand, studies involving *Klebsiella* species identified the presence of the typical Type I-E and I-F CRISPR-Cas systems within their genomic makeup [22]. These findings illustrate the diversity and distribution of CRISPR-Cas systems across different bacterial species, highlighting their adaptability in various microbial environments. The results of this particular study appear to diverge from earlier literature, notably the research by (Burstein *et al*, 2016) [23]. Burstein and colleagues reported that Class I CRISPR sys-

tems were predominant among prokaryotes. In contrast, the study suggests that within *Neisseria* spp. Class II Type C CRISPR systems are the most commonly encountered.

In this study, 366 regions within phage genomes that were targeted by CRISPR spacers were found, indicating the potential role of the CRISPR-Cas system in defending against these specific viral regions. Additionally, the analysis revealed 156 regions within the examined sequences where the CRISPR-Cas system could target its own genetic material (self-targeting spacers). This discovery underscores the intricate nature of CRISPR-Cas systems, encompassing both their defensive capabilities and the intriguing phenomenon of self-targeting, which could have ramifications for understanding the immune response and genetic regulation in these organisms. In a comparative analysis conducted by (Parra *et al*, 2023) the examination of *Pseudomonas* genomes revealed the presence of 2050 spacers within their CRISPR arrays [24]. Approximately, 52% of these spacers exhibited similarity to bacteriophage sequences, while 26% matched chromosomal DNA and 22% corresponded to plasmid DNA. Notably, no instances of potential self-targeting spacers were identified within the CRISPR arrays, suggesting the existence of a protective mechanism preventing autoimmunity in *Pseudomonas*. Conversely, a study by (Devi *et al*, 2019), focusing on *Klebsiella*, uncovered a different scenario. Here, 3% of the spacers were found to be self-targeting and less than 9% of the spacer sequences in *Klebsiella* displayed matches to known plasmids (6%) or phages (2.8%) in existing databases, underscoring the limited understanding of the various adversaries that bacteria encounter in their environment [25]. The frequency of self-targeting spacers in the CRISPR array is likely to have correlation with phage targeting regions. The inclusion of a greater number of phage and plasmid sequences to the database was thought to be responsible for the considerable fall in the proportion of self-targeting spacers [26]. These findings emphasize the dynamic interplay between CRISPR systems and the microbial challenges it faces, shedding light on the ongoing evolutionary arms race between bacteria and their viral and genetic adversaries.

A total of 140 direct repeat sequences from *Neisseria* spp. were categorized into 17 groups, primarily based on their sequence homology. The number of repeats and its structural stability in a CRISPR-Cas system serves as an important indicator of its functionality and integrity. A higher number of repeats usually denote that the CRISPR-Cas system is complete and functioning effectively. In such cases, the system is fully capable of defending the organism against foreign genetic elements like viruses and plasmids. Conversely, when the number of repeats is intermediate, it indicates that

the CRISPR–Cas system has experienced recent erosion or degradation. This erosion may have been caused by the loss of functional Cas genes or other factors that compromise the system’s ability to protect against invaders effectively. In instances where the number of repeats is low, only relics of the CRISPR–Cas system are noticed [27]. This suggests that the system might have been severely reduced in its functionality, potentially leaving the organism more susceptible to viral and plasmid infections. The presence of specific secondary structure motifs within CRISPR repeats is essential for the generation and loading of crRNAs in many CRISPR–Cas systems. These repeats exhibit structural diversity, and (Kunin *et al*, 2007) research findings suggested that the system likely relies on an RNA intermediate, as evidenced by compensatory base changes, including G:U base pairs, within the stem regions of structured repeats [18].

Numerous studies have highlighted the genetic exchange in the development of AR in the pathogenic *Neisseria spp* [28, 29]. By examining the genomic and phylogenetic distributions of CRISPR–Cas systems in various bacteria, have sought evidence of how these systems might function in preventing the acquisition of foreign DNA elements. A study by (Wheatley *et al*, 2020) supporting this hypothesis in the case of *Pseudomonas aeruginosa*, a bacterial species known for having both large core genome and accessory genome [30]. In such organisms, the presence of CRISPR–Cas systems may indeed contribute to genome reduction by inhibiting the acquisition of foreign DNA elements. Similarly, previous research on 16 *E. faecalis* genomes indicated that the presence of CRISPR–Cas systems was negatively correlated with AR. To validate and extend this finding, a more comprehensive analysis was conducted, involving 514 *E. faecalis* genomes [31]. The results revealed that approximately two-thirds of these genomes (338 out of 514) lacked CRISPR–Cas systems. Interestingly, these 338 genomes without CRISPR–Cas systems also exhibited multiple AR genes, conferring them resistance to various drug classes. This suggests that the absence of CRISPR–Cas systems may contribute to the prevalence of AR in *E. faecalis spp*. Additionally, a prior study using 672 clinical isolates of *P. aeruginosa* similarly found that bacteria with CRISPR–Cas systems had lower sulfonamide resistance [32]. This convergence of results shows that the presence of CRISPR–Cas systems in pathogens may be associated with a decreased likelihood of carrying AR genes, thus acting as a defense mechanism against AR. In-depth investigations by (Pursey *et al*, 2021) focused on modeling the association between CRISPR–Cas systems and indicators of HGT [33]. The study by (García *et al*, 2018) made an intriguing observation regarding *E. coli* genomes. They found that approximately 30% of these ge-

nomes, specifically 1706 out of 5661 analyzed, contained resistance genes related to antibiotics such as beta-lactam, quinolone, macrolide, and trimethoprim, but surprisingly lacked CRISPR–Cas systems [34]. It was align with another prior research that has shown how CRISPR–Cas systems can impede natural transformation, a key mechanism for HGT, in specific bacterial species, as illustrated in the case of *N. meningitides* [35]. The genome-wide correlation analysis conducted by (Shehreen *et al*, 2019) revealed that the majority of bacterial species showed no strong correlation between the presence of CRISPR–Cas systems and AR genes, their study identified specific clinically important bacterial species where this relationship exhibited either a positive or negative correlation [36]. This indicates that the connection between CRISPR–Cas systems and AR genes is not uniform across all species and emphasizes the need for a tailored, species-specific approach to understand these interactions fully in the context of AR mechanisms. One plausible explanation could be the selective pressure exerted by antibiotic exposure, which might favor the acquisition of AR genes through HGT over the maintenance of CRISPR–Cas systems. It is conceivable that in the evolutionary history of these strains, ancestors lost their CRISPR–Cas systems due to their reduced relevance in the face of antibiotic-driven selection.

## Conclusion

In-silico examination of the CRISPR–Cas system in *Neisseria spp*. which was identified across genomes of varied geographical location was considered for the analysis. The CRISPR Cas arrays were discovered in 89 *Neisseria* genomes, 69% of which contained the type II-C CRISPR system and 28% had the type I-C system. In this investigation, 366 regions were identified to be spacer targeted phage regions, with about 156 self-targeting regions out of 1661 distinct spacers. The structural stability of the direct repeat regions was also studied. The direct repeat regions found to have fold score between – 16 to -19 kcal/mol, it indicates stable secondary structure. AR genes were absent in 30 of the 89 *Neisseria spp*. A striking observation was the existence of efflux pump resistance genes in the vast majority of the sequences examined harboring CRISPR type II-C. It was found that *spp*. with several CRISPR arrays frequently have no AR genes or only one AR gene in their genomes. The presence of the CRISPR–Cas system was linked to a decrease in the number of AR genes. The finding raises interesting questions about the potential mechanisms underlying the absence or presence of CRISPR Cas system in relation with AR genes. Therefore, gaining a deeper understanding of the complex relationship between CRISPR–Cas systems

and AR in *Neisseria* spp requires further investigation to identify additional factors that contribute to the emergence and dissemination of AR genes.

## Conflict of Interest:

The authors certify that there is no conflict of interest with any financial organization regarding the material discussed in the manuscript.

## Funding:

No funding was received for this work.

## Data availability:

All data's are enclosed in the manuscript.

## Authors' contributions:

Santhiya K – execution, data analysis, interpretation and manuscript drafting; Ananthasubramanian M – given substantial contributions to the study conception and design; manuscript editing. All authors read and approved the final version of the manuscript.

## References

- Kirkcaldy RD, Weston E, Segurado AC, Hughes G. Epidemiology of gonorrhoea: a global perspective. *Sex Health*. 2019 Sep;16(5):401-411. doi: 10.1071/SH19061. PMID: 31505159; PMCID: PMC7064409.
- Mahapure K, Singh A. A Review of Recent Advances in Our Understanding of *Neisseria* gonorrhoeae. *Cureus*. 2023 Aug 14;15(8):e43464. doi: 10.7759/cureus.43464. PMID: 37711920; PMCID: PMC10498933.
- Arber W. Horizontal Gene Transfer among Bacteria and Its Role in Biological Evolution. *Life (Basel)*. 2014 May 16;4(2):217-24. doi: 10.3390/life4020217. PMID: 25370194; PMCID: PMC4187160.
- Karah N, Samuelsen Ø, Zarrilli R, Sahl JW, et al. CRISPR-cas subtype I-Fb in *Acinetobacter baumannii*: evolution and utilization for strain subtyping. *PLoS One*. 2015 Feb 23;10(2):e0118205. doi: 10.1371/journal.pone.0118205. PMID: 25706932; PMCID: PMC4338279.
- Yang Y, Xu J, Ge S, Lai L. CRISPR/Cas: Advances, Limitations, and Applications for Precision Cancer Research. *Front Med (Lausanne)*. 2021 Mar 3;8:649896. doi: 10.3389/fmed.2021.649896. PMID: 33748164; PMCID: PMC7965951.
- Arroyo-Olarte RD, Bravo Rodríguez R, Morales-Ríos E. Genome Editing in Bacteria: CRISPR-Cas and Beyond. *Microorganisms*. 2021 Apr 15;9(4):844. doi: 10.3390/microorganisms9040844. PMID: 33920749; PMCID: PMC8071187.
- Couvin D, Bernheim A, Toffano-Nioche C, Touchon M, et al. CRISPRCasFinder, an update of CRISPRFinder, includes a portable version, enhanced performance and integrates search for Cas proteins. *Nucleic Acids Res*. 2018 Jul 2;46(W1):W246-W251. doi: 10.1093/nar/gky425. PMID: 29790974; PMCID: PMC6030898.
- Zhang F, Zhao S, Ren C, Zhu Y, et al. CRISPRminer is a knowledge base for exploring CRISPR-Cas systems in microbe and phage interactions. *Commun Biol*. 2018 Oct 31;1:180. doi: 10.1038/s42003-018-0184-6. PMID: 30393777; PMCID: PMC6208339.
- Jia B, Raphenya AR, Alcock B, Waglechner N, et al. CARD 2017: expansion and model-centric curation of the comprehensive antibiotic resistance database. *Nucleic Acids Res*. 2017 Jan 4;45(D1):D566-D573. doi: 10.1093/nar/gkw1004. Epub 2016 Oct 26. PMID: 27789705; PMCID: PMC5210516.
- Florensa AF, Kaas RS, Clausen PTL, Aytan-Aktug D, et al. ResFinder - an open online resource for identification of antimicrobial resistance genes in next-generation sequencing data and prediction of phenotypes from genotypes. *MicrobGenom*. 2022 Jan;8(1):000748. doi: 10.1099/mgen.0.000748. PMID: 35072601; PMCID: PMC8914360.
- Zuker M, Stiegler P. Optimal computer folding of large RNA sequences using thermodynamics and auxiliary information. *Nucleic Acids Res*. 1981 Jan 10;9(1):133-48. doi: 10.1093/nar/9.1.133. PMID: 6163133; PMCID: PMC326673.
- Hofacker IL. Vienna RNA secondary structure server. *Nucleic Acids Res*. 2003 Jul 1;31(13):3429-31. doi: 10.1093/nar/gkg599. PMID: 12824340; PMCID: PMC169005.
- Jiang F, Doudna JA. The structural biology of CRISPR-Cas systems. *Curr Opin Struct Biol*. 2015 Feb;30:100-111. doi: 10.1016/j.sbi.2015.02.002. Epub 2015 Feb 24. PMID: 25723899; PMCID: PMC4417044.
- Kunin V, Sorek R, Hugenholtz P. Evolutionary conservation of sequence and secondary structures in CRISPR repeats. *Genome Biol*. 2007;8(4):R61. doi: 10.1186/gb-2007-8-4-r61. PMID: 17442114; PMCID: PMC1896005.
- Doench JG, Fusi N, Sullender M, Hegde M, et al. Optimized sgRNA design to maximize activity and minimize off-target effects of CRISPR-Cas9. *Nat Biotechnol*. 2016 Feb;34(2):184-191. doi: 10.1038/nbt.3437. Epub 2016 Jan 18. PMID: 26780180; PMCID: PMC4744125.

16. Rouquette-Loughlin C, Dunham SA, Kuhn M, Balthazar JT, et al. The NorM efflux pump of *Neisseria gonorrhoeae* and *Neisseria meningitidis* recognizes antimicrobial cationic compounds. *J Bacteriol.* 2003 Feb;185(3):1101-6. doi: 10.1128/JB.185.3.1101-1106.2003. PMID: 12533487; PMCID: PMC142806.
17. Tew LS, She LY, Chew CH. Isolation, Antimicrobial Susceptibility Profile and Detection of *Sul1*, *bla*<sub>TEM</sub>, and *bla*<sub>SHV</sub> in Amoxicillin-Clavulanate-Resistant Bacteria Isolated From Retail Sausages in Kampar, Malaysia. *Jundishapur J Microbiol.* 2016 Sep 14;9(10):e37897. doi: 10.5812/jjm.37897. PMID: 27942365; PMCID: PMC5136445.
18. Fluit AC, Florijn A, Verhoef J, Milatovic D. Presence of tetracycline resistance determinants and susceptibility to tigecycline and minocycline. *Antimicrob Agents Chemother.* 2005 Apr;49(4):1636-8. doi: 10.1128/AAC.49.4.1636-1638.2005. PMID: 15793159; PMCID: PMC1068614.
19. Atassi G, Medernach R, Scheetz M, Nozick S, et al. Genomics of Aminoglycoside Resistance in *Pseudomonas aeruginosa* Bloodstream Infections at a United States Academic Hospital. *Microbiol Spectr.* 2023 Jun 15;11(3):e0508722. doi: 10.1128/spectrum.05087-22. Epub 2023 May 16. PMID: 37191517; PMCID: PMC10269721.
20. Humbert MV, Christodoulides M. Atypical, Yet Not Infrequent, Infections with *Neisseria* Species. *Pathogens.* 2019 Dec 20;9(1):10. doi: 10.3390/pathogens9010010. PMID: 31861867; PMCID: PMC7168603.
21. Yadav G, Singh R. In silico analysis reveals the co-existence of CRISPR-Cas type I-F1 and type I-F2 systems and its association with restricted phage invasion in *Acinetobacter baumannii*. *Front Microbiol.* 2022 Aug 17;13:909886. doi: 10.3389/fmicb.2022.909886. PMID: 36060733; PMCID: PMC9428484.
22. Shen J, Lv L, Wang X, Xiu Z, et al. Comparative analysis of CRISPR-Cas systems in *Klebsiella* genomes. *J Basic Microbiol.* 2017 Apr;57(4):325-336. doi: 10.1002/jobm.201600589. Epub 2017 Feb 3. PMID: 28156004.
23. Burstein D, Sun CL, Brown CT, Sharon I, et al. Major bacterial lineages are essentially devoid of CRISPR-Cas viral defence systems. *Nat Commun.* 2016 Feb 3;7:10613. doi: 10.1038/ncomms10613. PMID: 26837824; PMCID: PMC4742961.
24. Parra-Sánchez Á, Antequera-Zambrano L, Martínez-Navarrete G, Zorrilla-Muñoz V, et al. Comparative Analysis of CRISPR-Cas Systems in *Pseudomonas* Genomes. *Genes (Basel).* 2023 Jun 25;14(7):1337. doi: 10.3390/genes14071337. PMID: 37510242; PMCID: PMC10379622.
25. Devi V, Chhibber S. In silico Analysis of CRISPR-Cas System in *Klebsiella* Species. *J Appl Bioinforma-Comput Biol.* 2019 Jan 22; 8:1. doi: 10.4172/2329-9533.1000163
26. Stern A, Keren L, Wurtzel O, Amitai G, et al. Self-targeting by CRISPR: gene regulation or autoimmunity? *Trends Genet.* 2010 Aug;26(8):335-40. doi: 10.1016/j.tig.2010.05.008. Epub 2010 Jul 1. PMID: 20598393; PMCID: PMC2910793.
27. Zhu Y, Huang Z. Recent advances in structural studies of the CRISPR-Cas-mediated genome editing tools. *Nat Sci Rev.* 2019 May;6(3):438-451. doi: 10.1093/nsr/nwy150. Epub 2018 Nov 29. PMID: 34691893; PMCID: PMC8291651.
28. Vanbaelen T, Van Dijke C, Laumen J, Gonzalez N, et al. Global epidemiology of antimicrobial resistance in commensal *Neisseria* species: A systematic review. *Int J Med Microbiol.* 2022 Apr;312(3):151551. doi: 10.1016/j.ijmm.2022.151551. Epub 2022 Feb 22. PMID: 35231823.
29. Kenyon C, Buyze J, Wi T. Antimicrobial Consumption and Susceptibility of *Neisseria gonorrhoeae*: A Global Ecological Analysis. *Front Med (Lausanne).* 2018 Nov 27;5:329. doi: 10.3389/fmed.2018.00329. PMID: 30538989; PMCID: PMC6277557.
30. Wheatley RM, MacLean RC. CRISPR-Cas systems restrict horizontal gene transfer in *Pseudomonas aeruginosa*. *ISME J.* 2021 May;15(5):1420-1433. doi: 10.1038/s41396-020-00860-3. Epub 2020 Dec 21. PMID: 33349652; PMCID: PMC8105352.
31. Palmer KL, Gilmore MS. Multidrug-resistant enterococci lack CRISPR-cas. *mBio.* 2010 Oct 12;1(4):e00227-10. doi: 10.1128/mBio.00227-10. PMID: 21060735; PMCID: PMC2975353.
32. van Belkum A, Soriaga LB, LaFave MC, Akella S, et al. Phylogenetic Distribution of CRISPR-Cas Systems in Antibiotic-Resistant *Pseudomonas aeruginosa*. *mBio.* 2015 Nov 24;6(6):e01796-15. doi: 10.1128/mBio.01796-15. PMID: 26604259; PMCID: PMC4669384.
33. Pursey E, Dimitriu T, Paganelli FL, Westra ER, et al. CRISPR-Cas is associated with fewer antibiotic resistance genes in bacterial pathogens. *Philos Trans R Soc Lond B Biol Sci.* 2022 Jan 17;377(1842):20200464. doi: 10.1098/rstb.2020.0464. Epub 2021 Nov 29. PMID: 34839714; PMCID: PMC8628084.
34. García-Martínez J, Maldonado RD, Guzmán NM, Mojica FJM. The CRISPR conundrum: evolve and maybe die, or survive and risk stagnation. *Microb Cell.* 2018

- 
- May 16;5(6):262-268. doi: 10.15698/mic2018.06.634. PMID: 29850463; PMCID: PMC5972030.
35. Zhang Y, Heidrich N, Ampattu BJ, Gunderson CW, et al. Processing-independent CRISPR RNAs limit natural transformation in *Neisseria meningitidis*. *Mol Cell*. 2013 May 23;50(4):488-503. doi: 10.1016/j.molcel.2013.05.001. PMID: 23706818; PMCID: PMC3694421.
36. Shehreen S, Chyou TY, Fineran PC, Brown CM. Genome-wide correlation analysis suggests different roles of CRISPR-Cas systems in the acquisition of antibiotic resistance genes in diverse species. *Philos Trans R Soc Lond B Biol Sci*. 2019 May 13;374(1772):20180384. doi: 10.1098/rstb.2018.0384. PMID: 30905286; PMCID: PMC6452267.



Received for publication, September, 19, 2023  
Accepted, October, 09, 2023

*Original article*

## **In vitro propagation of *Lobelia chinensis* Lour. under different LED lights**

**XIN-LEI BAI, HOSAKATTE NIRANJANA MURTHY\*, SO YOUNG PARK\***

<sup>1</sup> Department of Horticultural Science, Chungbuk National University, Cheongju 28644, Republic of Korea

### **Abstract**

The current study was performed to verify the effect of light quality especially of light-emitting diodes (LEDs) on the *in vitro* regeneration of *Lobelia chinensis*. Nodal explants were cultured on MS medium supplemented with 30 g L<sup>-1</sup> sucrose and treated with red (R), blue (B), white (W) combination red/blue (1:1; RB), and red/blue/green (1:1:1; RGB) LED sources. After 4 weeks of culture regeneration capabilities, growth characteristics, and bioactive compounds were evaluated. RB treatments were found suitable for shoot regeneration, shoot growth, and root regeneration from shoots. Photosynthetic pigments, total phenolics, flavonoid content, and DPPH, ABTS, and FRAP antioxidant activities were highest with plants regenerated under RB LED. HPLC analysis of plants revealed the highest accumulation of catechin and myricetin in the plants regenerated under RB light sources.

### **Keywords**

Antioxidant activities, *In vitro* regeneration, Light quality, Light emitting diodes

---

✉ \*Corresponding author: Hosakatte Niranjana Murthy. e-mail: hnmurthy60@gmail.com;  
So Young Park. e-mail: soyark7@cbnu.ac.kr

## Introduction

*Lobelia chinensis* Lour. is an important medicinal plant that is used in traditional Chinese medicine and it possesses varied pharmacological activities such as anticancer, anti-inflammatory, antioxidant, antipyretic, detumescent, diuretic, and, immunomodulatory effects [1]. The major phytochemicals are phenolics, flavonoids, alkaloids, and terpenes [1]. There is a huge demand for this plant for its utilization in traditional Chinese and oriental medicine. The natural resource of this plant has dwindled and there are also instances of adulterants in *L. chinensis* herbal products [2]. Therefore, in the current study, we applied plant tissue culture methods for the production of *L. chinensis* biomass and utilization of biomass for pharmaceutical and cosmeceutical uses.

Light is one of the prominent environmental factors that affect the plant's growth, development, and physiological processes. Light intensity, quality, and photoperiod all are reported to influence the growth and physiological characteristics of the plants. In research and commercial laboratories, light emitting diodes (LED) are taking the place of conventional light sources like fluorescent, metal halide, high-pressure solid, and incandescent lights due to their distinctive qualities such as long life, low energy consumption, small mass and volume, low radiant heat output, and their capacity to emit a narrow spectrum of light [3].

The influence of monochromatic LED light sources such as red, blue, and green and their combination have been experimented on varied plants [3]. However, there hasn't been enough focus on the application of wavelength-specific LEDs to influence morphogenesis, micropropagation, and the accumulation of bioactive compounds in regenerated plants. Additionally, because plant responses to certain environments are extremely genotype-dependent, each species, variety, growth stage, and tissue type must be evaluated separately [3]. To the best of our knowledge, there have been no studies on the micropropagation of *L. chinensis* and the effect of light quality on *in vitro* morphogenesis, and growth of plantlets. In the current study, we assessed the micropropagation potential, growth of plantlets, and accumulation of antioxidants and bioactive compounds in regenerated plants of *L. chinensis* grown *in vitro* under different LED treatments.

## Materials and Methods

### 1. Plant material

*Lobelia chinensis* Lour. stem segments containing one or two nodes and alternate leaves without roots (1.5 cm in length) were collected from stock plants of *Lobelia chinensis* which were maintained in the greenhouse at Chungbuk

National University, Korea. The explants were surface disinfected with 1% (w/v) bavistin and then washed for five minutes in 10% (v/v) Tween-20. Following surface sterilization with 0.1% (w/v) aqueous mercuric chloride (HgCl<sub>2</sub>) for a period of 2-3 minutes, the explants were placed in 95% alcohol for 20–30 seconds. The explants were then cultured on MS medium [4] supplemented with 30 g L<sup>-1</sup> sucrose. Prior to autoclaving 2.4 g L<sup>-1</sup> gelrite was added and the pH of the medium was set at 5.7 with 1N HCl or NaOH and then autoclaved for 15 minutes at 15 psi and 121°C. All of the chemicals were of an analytical grade (Duschefa, Harlem, The Netherlands). 15 mL of medium was distributed to 60 mm x 15 mm Petri dishes. Explants were cultivated horizontally on the medium surface, dishes were sealed with parafilm, and cultures were incubated in a tissue culture room at a temperature of 25°C, with a 16 light/8 dark photoperiod that provided 40 μmol m<sup>-2</sup> s<sup>-1</sup> of irradiance, cool fluorescent lamps, and 60% relative humidity. Explants were subcultured once in four weeks.

### 2. Light Quality

To investigate the effect of light quality on the regeneration of plants, we used light sources (GF-320s; Good Felling Co. Ltd., Seong-nam, Korea). The cultures were placed under four different light sources: red (R), blue (B), red/blue1 (RB), and red1/green1/blue1 (RGB), and white (W) LED was used as control. The cultures were maintained under 60 μmol m<sup>-2</sup> s<sup>-1</sup> and as spectral energy sources, the emission of blue LED was 440 nm, red was at 650 nm, and green was at 550 nm. The red or blue LED was provided with a 60 stick/400 tip (GFLE-102R) respectively, tip size: 3 mm, stick width: 100 mm, stick length: 290 mm, tip interval: 9.9 mm; red + blue LED was provided with a red 30 stick/400 tips and blue 30 stick/400 tip; red + blue + green LED provided with a red 20 stick/400 tip, blue 20 stick/400 tips, and a green 20 stick/400 tips used to arrange the panel. The light intensity and spectral parameters were adjusted using an LI-250A light meter with a Q50604 (LI-COR, USA).

### 3. Data collection

All the cultures were maintained for four weeks and data on the number of shoots per explant, shoot length (cm), leaf area (mm<sup>2</sup>), number of roots (per plant), root length (cm), and fresh weight (mg/explant) were documented.

### 4. Estimation of chlorophyll and carotenoid content

Chlorophyll a, chlorophyll b, total chlorophyll, and carotenoid of *in vitro* regenerated plants were assessed by using 200 mg fresh weight of tissue samples from the third leaf from the top of plantlets and were subjected to extraction using 80% acetone. The absorbance was measured using a

spectrophotometer (Libra S22, Biochrome Ltd., Cambridge, UK) at the following wavelengths maxima (Amax): Chlorophyll a at 663 nm, chlorophyll b at 645 nm, and total carotenoids at 470 nm.

## 5. Preparation of plant extract

The dried samples were reflexed (LS-2050-S10, LS-TECH, Korea) with 30 mL 80% ethanol at 80 °C for 1 h and passed through filter paper (Advantec 110 mm, Toyo Roshi Kaisha Ltd., Japan). The final volume of the solution was set at 30 mL using 80% ethanol.

## 6. Estimation of total phenolic content

Total phenolic content (TPC) was estimated by using the Folin Ciocalteu reagent method [5]. Briefly, a known amount of sample was taken and made up to 3 mL with distilled water, and 0.1 mL of 2 N Folin Ciocalteu reagent was added, followed by incubation for 6 minutes, and then 0.5 mL of 20% Na<sub>2</sub>CO<sub>3</sub> was added to each tube. Tubes were kept in warm water for 30 minutes and the absorbance was read at 760 nm using a UV-visible spectrophotometer. Gallic acid was used as the standard compound.

## 7. Estimation of total flavonoid content

The flavonoid content of extracts was analyzed as per the method of HARBORNE [5]. To brief, 0.1 mL of extract was taken and made up the volume to 3 mL by using distilled water followed by the addition of 0.15 mL of 10% AlCl<sub>3</sub> and 2 mL of 1 M NaOH after 5 min of incubation at room temperature. Solutions were vortexed and absorbance was measured at 510 nm. Catechin was used as standard.

## 8. Analysis of antioxidant activities

### 8.1. 2,2-Diphenyl 1-picrylhydrazyl (DPPH) radical scavenging assay

Extract (0.1 mL) was added with 1.9 mL of 0.1 mM DPPH solution prepared in ethanol. The tubes were vortexed and incubated in the dark for 15 min. The discoloration of the DPPH solution was measured at 517 nm against ethanol as blank using a UV-visible spectrophotometer. Gallic acid was used as standard and the activity of the extracts was expressed as mg gallic acid equivalent (GAE)/g extract [6].

### 8.2. 2,2'-azino-bis (3-ethybenzothiazoline-6-sulphonic acid (ABTS) assay

The ABTS solution was prepared by mixing 7 mM of ABTS and 2.45 mM potassium persulfate in a ratio of 1:1 and stored in the dark for 24 h. At the time of analysis, the ABTS solution was diluted with phosphate buffer (pH 7.3) to obtain the value of 0.70 at 732 nm. Fifty microliters of the extract were added to 950 microliters of diluted ABTS solution and the mixture was allowed to stay in the dark for 10

min then absorbance was measured at 732 nm using UV-visible spectrophotometry. Antioxidant activity was expressed in percentage i.e., ABTS radical scavenging activity = absorbance of control solution-absorbance of sample solution/absorbance of control solution x 100 [6].

## 8.3. Ferric reducing antioxidant power (FRAP) assay

FRAP reagent was prepared by mixing 300 mM acetate buffer of pH 3.6, 10 mM 2,4,6-tripyridyl-s-triazine (TPTZ) in 40 mM HCl, and 20 mM FeCl<sub>2</sub>.6H<sub>2</sub>O in the ratio 10:1:1. 0.2 mL of extract was added with 3 mL of FRAP reagent, tubes were vortexed and incubated for 6 min at room temperature, and absorbance was measured at 593 nm using a UV-visible spectrophotometer. Ascorbic acid was used as standard and activity is expressed as mg ascorbic acid equivalent (AAE)/g extract [6].

## 9. Quantification of phenolic compounds using high-performance liquid chromatography (HPLC)

Extraction and analysis of phenolic compounds were carried out by the procedure of BURIN et al. [7]. The powdered sample (0.1 g) was mixed with 10 mL of 80% ethanol and the extract was obtained by ultrasonication as explained above. The extract was concentrated using nitrogen gas dissolved in 0.5 mL 80% ethanol and used for analysis. The extract was filtered through a membrane filter (0.45 µm) and used for analysis. HPLC equipment (2690 Separation Module, Waters Chromatography, Milford, USA) included a photodiode array detector (PDA), and compound separation was performed using a Fortis C18 column (5 µm, 150 x 4.6 mm). The mobile phase consists of acetic acid and water (1:99 v/v) (solvent A) and acetic acid and acetonitrile (1:99 v/v) (solvent B) and was filtered using Whatman Glass microfiber filters before use. The flow rate was 1.0 mL.min<sup>-1</sup> and the column temperature was 25°C. The peaks were detected at 280 nm and compounds were identified and quantified based on the retention time of standards and peak areas.

## 10. Statistical analysis

All experiments were conducted in a completely randomized design. Five replicate cultures were maintained for each treatment and mean values of replicates were presented as results. Three different readings were taken with spectrophotometric analysis. HPLC analysis was carried out with three replicate samples. The experimental data were subjected to analysis of variance (ANOVA) followed by Duncan's multiple range test (DMR) at  $p \leq 0.05$ . All data analysis was carried out using IBM SPSS version 22.0.

**Table 1.** Effect of light quality on regeneration of plants of *Lobelia chinensis* after 4 weeks of culture

Light quality	No. of shoots/ node	Shoot length (cm)	Leaf area (mm <sup>2</sup> )	No. of roots/plant	Root length (cm)	FW (mg/plant)
W	4.1b	2.3bc	14.5c	18.0ab	1.9c	590.0c
R	4.1b	3.1a	23.5b	17.1b	2.0bc	788.0ab
B	4.8ab	2.0c	36.2a	10.9c	2.0bc	755.0ab
RB	5.8a	2.4bc	35.5a	19.9a	2.3ab	862.0a
RGB	5.2ab	2.5b	30.6a	15.1b	2.4a	658.0bc

Nodal segments were cultured on Murashige and Skoog (MS) medium supplemented with 30 g L<sup>-1</sup> sucrose.

W: White; RGB: Red1: Green1: Blue1; RB: Red1: Blue1; R: Red; B: Blue. Data represent mean values (n=10).

Mean different letters differ significantly from each other per DMRT ( $p \leq 0.05$ ).

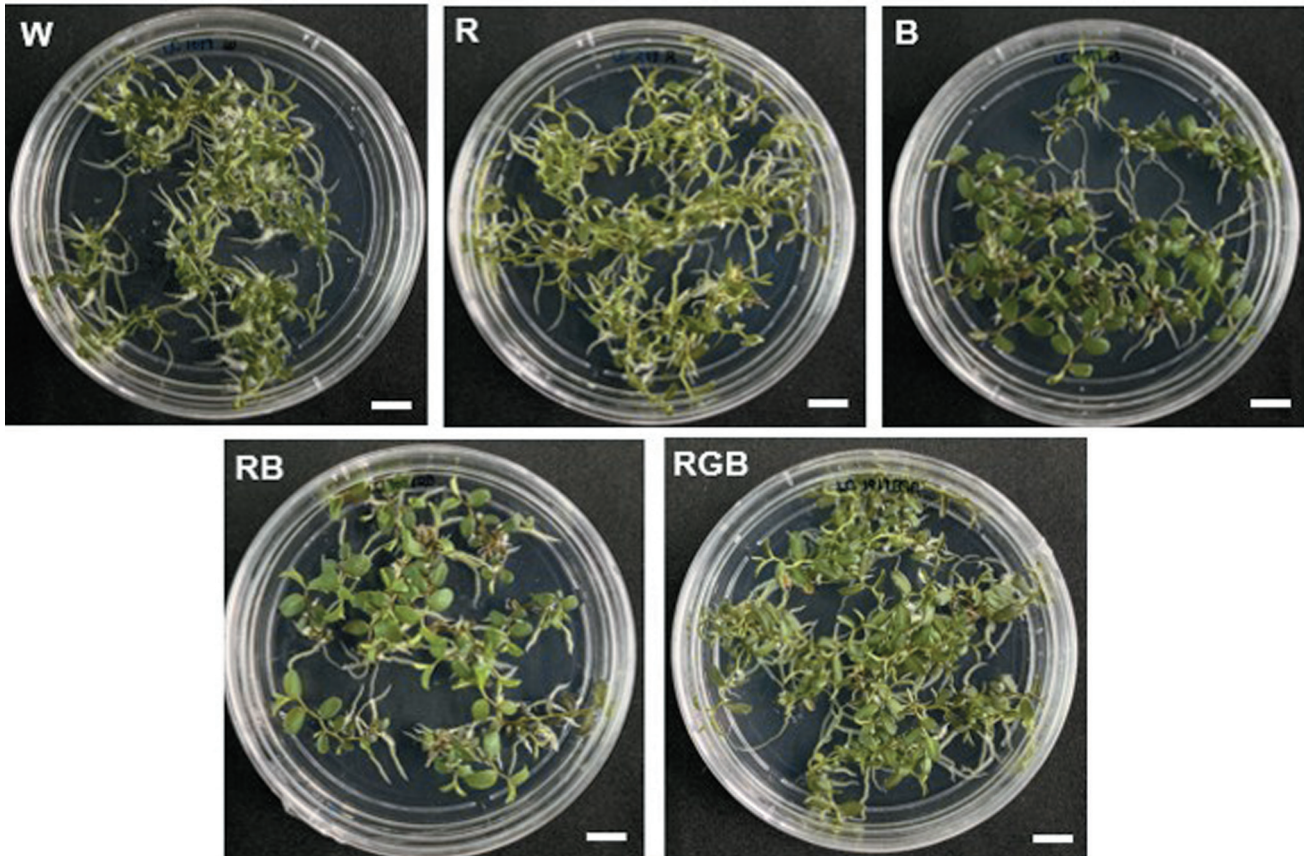


Figure 1. Effect of different LED treatments on *in vitro* regeneration and growth of *Lobelia chinensis* plants. W: white, R: red, B: blue, RB: red1: blue 1, RGB: red1: blue1: green 1. Bar = 1 cm.

## Results

### Regeneration of plants with different LED light sources and growth characteristics

Shoot regeneration of *L. chinensis*, the growth of shoots, and the rooting of shoots were significantly influenced by the types of LED light conditions to which the culture was exposed (Table 1 and Figure 1). The number of shoots regenerated from nodal explants was 4.1 and 4.8 per node explant with the cultured exposed to R and B LED, whereas the optimum shoots of 5.8 per explant were recorded with RB LED treatments. Similarly, a maximum of 19.1 roots was regenerated per shoot with RB treatments. The fresh weight of plantlets was also the highest (862.0 mg/plant) with cul-

tures exposed under RB LEDs. Leaf area was highest with *L. chinensis* plants which are regenerated under B LEDs (Table 1 and Figure 2).

### Analysis of metabolites accumulation and antioxidant activities

Analysis of photosynthetic pigments from *L. chinensis* leaves showed that plants regenerated under B LED possessed 19.8 mg g<sup>-1</sup> fresh weight (FW) of chlorophyll a, 6.6 mg g<sup>-1</sup> FW of chlorophyll b, 26.4 mg g<sup>-1</sup> FW of total chlorophyll, and 5.3 mg g<sup>-1</sup> FW of carotenoids. The plants that were grown in R, RB, RGB, and W LED sources also possessed similar levels of chlorophyll and carotenoid contents (Figure 3).

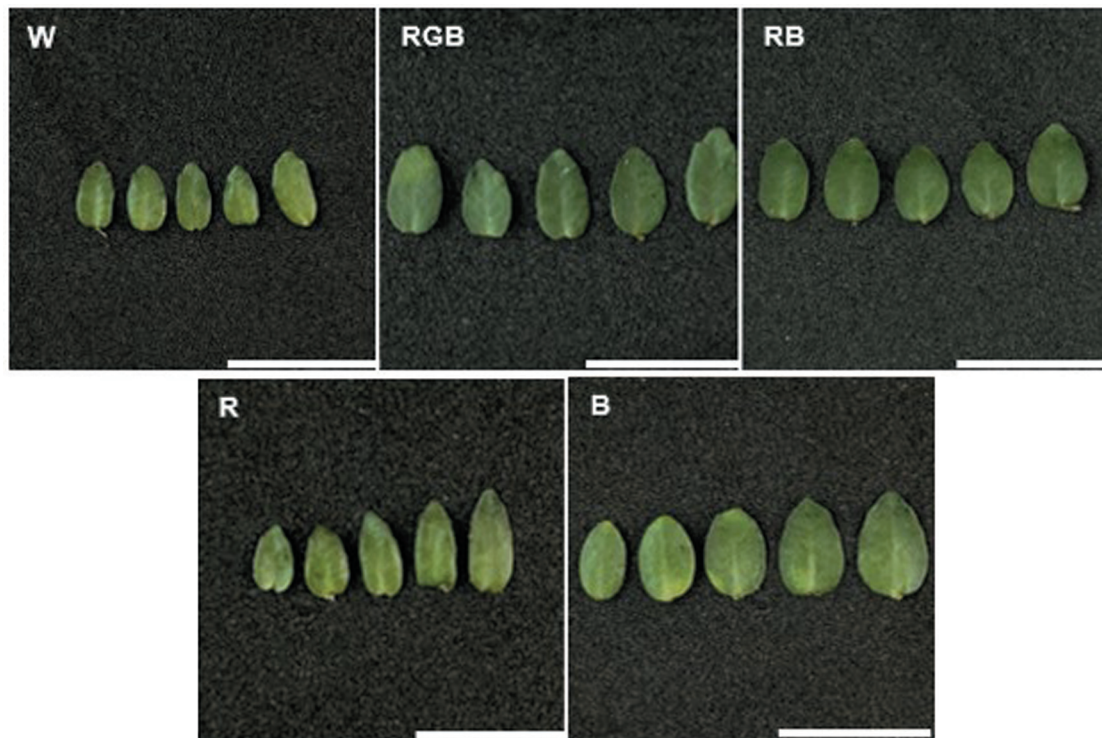


Figure 2. Effect of different LED treatments on leaf architecture of *Lobelia chinensis* plants. W: white, R: red, B: blue, RB: red1: blue 1, RGB: red1: blue1: green 1. Bar = 1 cm.

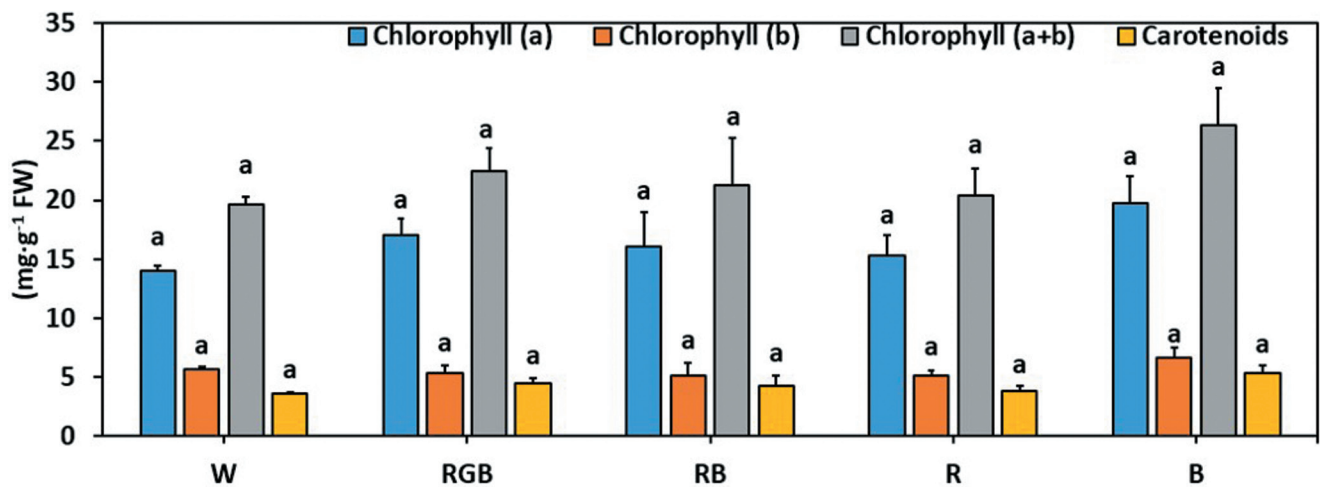


Figure 3. Effect of different LED treatments on chlorophyll a, chlorophyll b, total chlorophyll, and carotenoid contents of *Lobelia chinensis* plants. W: white, R: red, B: blue, RB: red1: blue 1, RGB: red1: blue1: green 1. Data are means  $\pm$  standard deviation ( $n = 5$ ). Different alphabetical letters indicate significant differences at  $p < 0.05$  according to Duncan's test.

The total phenolic and flavonoid content of the plants grown under different LEDs was investigated and results are presented in Figure 4. We found that the total phenolic contents were highest in the plants that were grown under RB mixed light treatments (23.75 mg GAE g<sup>-1</sup> DW) followed by R LED (20.10 75 mg GAE g<sup>-1</sup> DW) and RGB (17.53 75 mg GAE g<sup>-1</sup> DW) treatments. The total flavonoid content was highest in plants cultivated under RB LED (3.96 mg CE g<sup>-1</sup> DW) followed by RGB treatment (2.76 mg CE g<sup>-1</sup> DW).

We have recorded the potent antioxidant activity of plant extracts that were cultivated under RB LEDs as depicted by ABTS, DPPH, and FRAP assays (Figure 5). The antioxidant assay showed the highest scavenging ABTS (99.17%), and DPPH (31.24%) radicles by the plant extracts grown under RB treatments. Similarly, plants grown under RB LED exhibited the highest FRAP activity (19.95 mg/g) compared to the plants grown under other light sources.

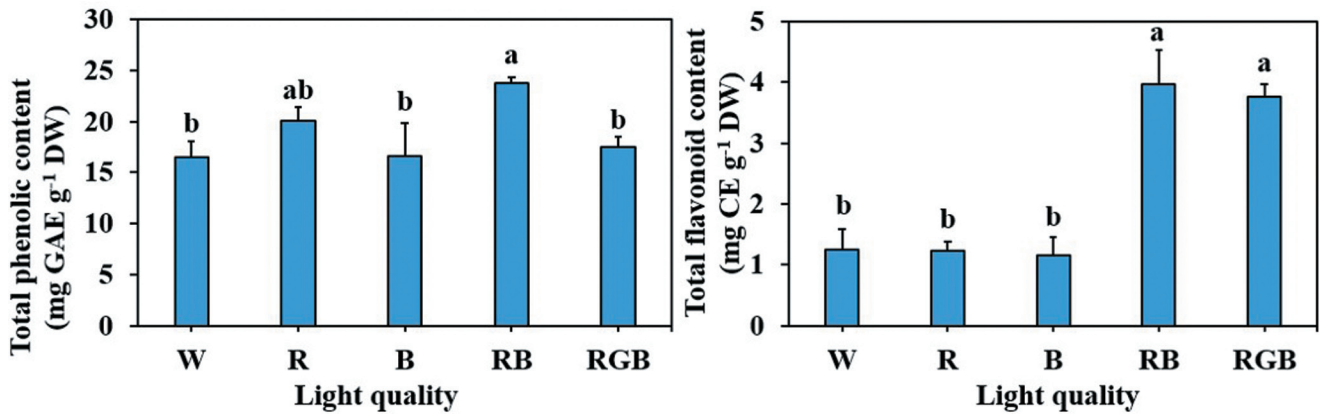


Figure 4. Effect of different LED treatments on the accumulation of total phenolics and flavonoids in *Lobelia chinensis* plants. W: white, R: red, B: blue, RB: red1: blue 1, RGB: red1: blue1: green 1. Data are means  $\pm$  standard deviation ( $n = 5$ ). Different alphabetical letters indicate significant differences at  $p < 0.05$  according to Duncan's test.

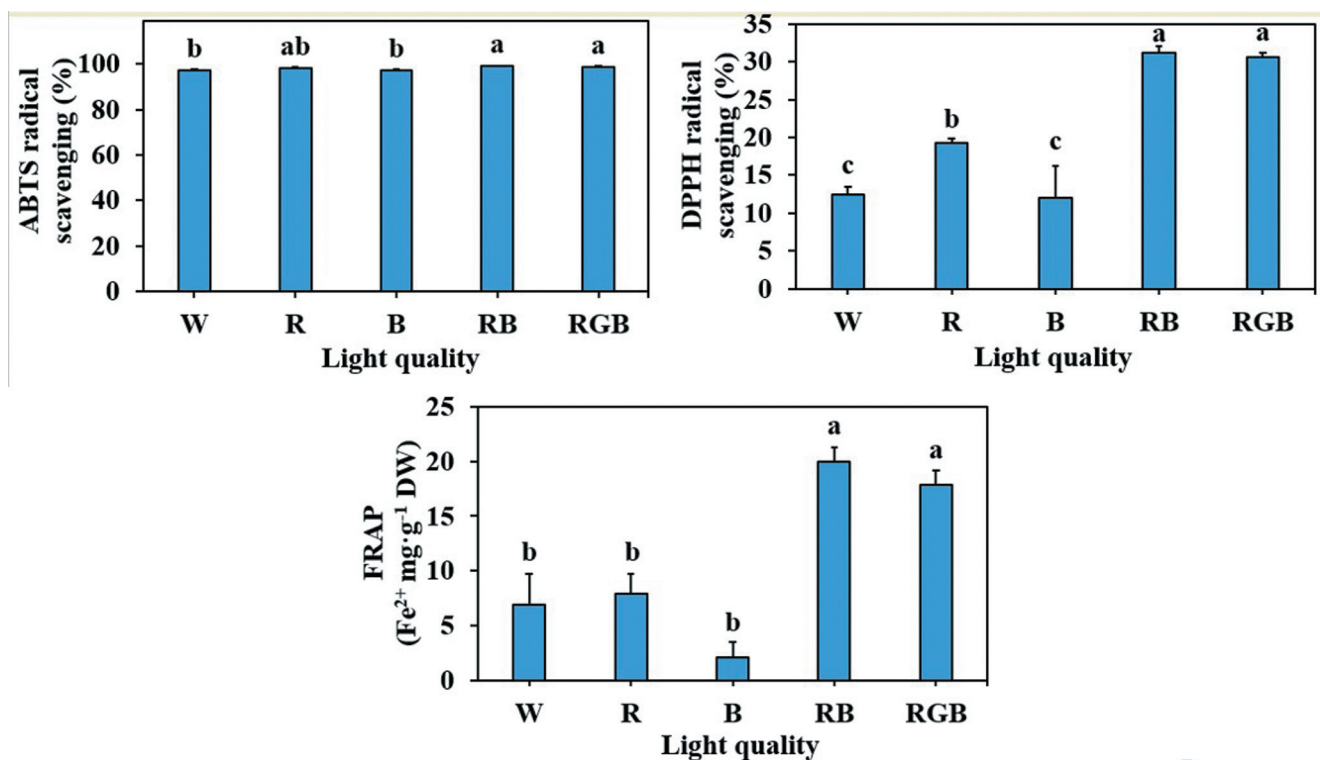


Figure 5. ABTS, DPPH, and FRAP antioxidant assay data of *Lobelia chinensis* plants regenerated under different LED treatments. W: white, R: red, B: blue, RB: red1: blue 1, RGB: red1: blue1: green 1. Data are means  $\pm$  standard deviation ( $n = 5$ ). Different alphabetical letters indicate significant differences at  $p < 0.05$  according to Duncan's test.

### Analysis of phenolic compounds using HPLC

We evaluated the phenolic compounds present in the which were regenerated under different LED treatments through HPLC analysis and the results are presented in Figure 6. The phenolic compounds such as protocatechuic acid, catechin hydrate, phloretic acid, rutin, ferulic acid, salicylic acid, naringin, myricetin, luteolin, quercetin, apigenin, kaempferol, and biochanin were detected in the extracts of plants grown under different LEDs. Only myricetin and catechin were in higher concentrations and again plants

that were regenerated under RB LED had  $4.30 \mu\text{g}^{-1} \text{g DW}$  and  $6.55 \mu\text{g}^{-1} \text{g DW}$  respectively (Figure 6).

### Discussion

In the current study, the *in vitro* regeneration potential of *L. chinensis* and growth characteristics were optimum with the plants regenerated under RB light when compared to monochromatic R or B or RGB combination (Table 1 and Figures 1 and 2). It was reported that the different spectral qualities of light stimulated plant morphogenesis *in vitro*,

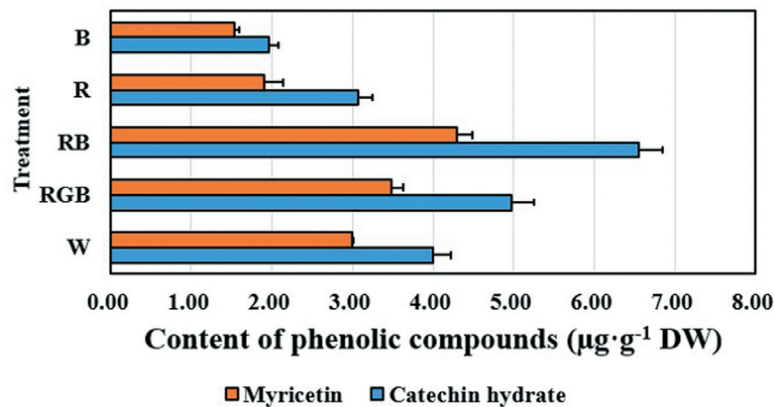


Figure 6. Amount of myricetin and catechin hydrate obtained from *Lobelia chinensis* plants grown under different LED treatments. W: white, R: red, B: blue, RB: red:blue, RGB: red:blue:green. Data are means  $\pm$  standard deviation (n = 5).

and also demonstrated varied physiological and morphological responses [3]. Previous studies have revealed enhanced shoot multiplication *in vitro* and shoot growth in *Gerbera jamesonii* cv. Dura [8] under RB treatments compared to monochromatic R or B blue light sources. However, better shoot regeneration was reported under R LED treatments in *Stevia reboudiana* [9]. These results demonstrate that the morphogenetic response differs in different species and this might be due to variation in endogenous growth regulator levels on exposure to varied light treatments. The results of our experiments showed that RB treatment resulted in the highest induction of roots from shoots (Table 1). These results are concurrent with *Gerbera jamesonii* cv. Shy Pink [10]—wherein RB light sources induced the highest root induction.

Our results demonstrated that blue light is responsible for better leaf growth and the highest leaf area was recorded with plants grown under blue light sources (Table 1). Similar to the current results B LEDs favored the growth of leaves regenerated *in vitro* in *Gerbera jamesonii* cv. Shy Pink [10]. The results of our study have demonstrated the highest biomass accumulation (862.0 mg/plant) was with the plants regenerated under RB LEDs. Earlier reports have shown that the biomass of plants cultivated under different light sources varied considerably. For example, while fluorescent light treatments were good enough for biomass accumulation in *Gerbera jamesonii* cv. Dura plants [8]. The results of the study revealed that optimum chlorophyll and carotenoid contents were with the plants regenerated under B LED light (Figure 3). It was reported that the positive effect of chlorophyll synthesis in *Rehmannia glutinosa* [11] plants grown under R light, while in *Lectuca sativa* plants blue light influenced the accumulation of carotenoids [12].

*L. chinensis* plants that were regenerated under RB LED possessed the highest amount of phenolics, and flavonoids

(Figure 4), and extracts from these plants showed higher levels of antioxidant activities (Figure 5). TAULAVUORI et al. [13] suggested that both B and R light may be needed to regulate the accumulation of phenolics in *Ocimum basilicum*. Therefore, we believe that both B and R light may be needed for the regulation biosynthesis of phenolics and flavonoids in *L. chinensis*.

HPLC analysis of plants regenerated under RB LED showed the presence of varied phenolic compounds including protocatechuic acid, catechin hydrate, phloretic acid, rutin, ferulic acid, salicylic acid, naringin, myricetin, luteolin, quercetin, apigenin, kaempferol, and biochanin, whereas concentrations of myricetin and catechin were highest among them (Figure 6). Myricetin and catechin are the major flavonoids found in several species and are known for varied biological activities [14,15]. Therefore, the *L. chinensis* plant biomass produced *in vitro* could be used for varied therapeutic uses.

## Conclusion

In this study, we investigated the effect of light quality on *in vitro* regeneration, growth, and accumulation of bioactive compounds in *Lobelia chinensis*. The results showed that RB LED treatment is superior for plant regeneration as the plants regenerated under this light displayed enhanced vegetative growth and also possessed higher concentrations of phenolics and flavonoids. These findings suggest the efficacy of LED light sources in plant tissue culture laboratories in place of traditional fluorescent lamps.

## Funding

This work was partially supported by the Industrial Strategic Technology Development Program (Grant number P0018148) funded by the Ministry of Trade, Industry & Energy (MOTIE, Korea)

## Conflicts of Interest

The authors declare no conflict of interest.

## References

- Chen MW, Chen WR, Zhang JM, Long XY, Wang YT. *Lobelia chinensis*: chemical constituents and anticancer activity perspective. *Chin J Nat Med*. 2014 Feb 12(2):103-7. doi: 10.1016/S1875-5364(14)60016-9. PMID: 24636059.
- Sun W, Yan S, Li J, Xiong C, Shi Y, Wu L, Xiang L, Deng B, Ma W, Chen S. Study of Commercially Available *Lobelia chinensis* Products Using Bar-HRM Technology. *Front Plant Sci*. 2017 Mar 8:351. doi: 10.3389/fpls.2017.00351. PMID: 28360920; PMCID: PMC5352710.
- Dutta Gupta S, Jatothu B. Fundamentals and applications of light emitting diodes (LEDs) *in vitro* plant growth and morphogenesis. *Plant Biotechnol Rep*. 2013 Mar 7: 211-220. doi.org/10.1007/s11816-013-0277-0.
- Murashige T, Skoog F. A revised medium for growth and bioassays with tobacco tissue cultures. *Physiol Plant*. 1962 July 15(3):473-497. doi.org/10.1111/j.1399-3054.1962.tb08052.x.
- Harborne AJ. *Phytochemical methods: A guide to modern techniques of plant analysis*. 1994. Springer, Dordrecht, The Netherlands. <https://doi.org/10.1007/978-94-009-5570-7>.
- Munteanu IG, Apetrei C. Analytical Methods Used in Determining Antioxidant Activity: A Review. *Int J Mol Sci*. 2021 Mar 25;22(7):3380. doi: 10.3390/ijms22073380. PMID: 33806141; PMCID: PMC8037236.
- Burin VM, Arcari SG, Costa LL, Bordignon-Luiz MT. Determination of some phenolic compounds in red wine by RP-HPLC: method development and validation. *J Chromatogr Sci*. 2011 Sep 49(8):647-51. doi: 10.1093/chrsi/49.8.647. PMID: 21859541.
- Pawlowska B, Zupnik M, Szewczyk-Taranek B, Cioc M. Impact of LED light sources on morphogenesis and levels of photosynthetic pigments in *Gerbera jamesonii* grown *in vitro*. *Hortic Environ Biotechnol*. 2018 Jan 21; 59(1): 115-123. doi.org/10.1007/s13580-018-0012-4.
- Ramirez-Mosqueda MA, Inglesias-Andreu LG, Bautista-Aguilar JR. The effect of light quality on growth and development of *in vitro* plantlet of *Stevia rebaudina* Bertoni. *Sugar Tech*. 2017 May-June 19(3):331-336. doi.org/ 10.1007/s12355-016-0459-5.
- Lim MJ, Murthy HN, Song HY, Lee SY, Park SY. Influence of white, red, blue, and combination of LED lights on *in vitro* multiplication of shoots, rooting, and acclimatization of *Gerbera jamesonii* cv. 'Shy Pink' plants. *Agronomy* 2023 Aug 13(9): 2216. doi.org/10.3390/agronomy13092216.
- Manivannan A, Soundararajan P, Halimah N, Blue LED light enhances growth, phytochemical contents, and antioxidative enzyme activities of *Rehmannia glutinosa*, cultured *in vitro*. *Hortic Environ Biotechnol*. 2015 Mar 56(1): 105-113. doi.org/10.1007/s13580-015-0114-1.
- Johkan M, Shoji K, Goto F, Hashida SN, Yoshihara T. Blue light emitting diode light irradiation of seedlings improves seedling quality and growth after transplanting in red leaf lettuce. *HortScience* 2010, 45(12): 1809-1814. doi.org/10.21273/HORTSCI.45.12.1809.
- Taulavuori K, Hyoky V, Oksanen J, Taulavuori E, Julkunen-Tiitto R. Species-specific differences in synthesis of flavonoids and phenolic acids under increasing periods of enhanced blue light. *Environ Exp Bot*. 2016 Jan 121(1): 145-150. doi.org/10.1016/j.envexpbot.2015.04.002.
- Ganeshpurkar A, Saluja A. The pharmacological potential of catechin. *Ind J Biochem Biophys*. 2020 Oct 57 (5): 505-511.
- Semwal DK, Semwal RB, Combrinck S, Viljoen A. Myricetin: A Dietary Molecule with Diverse Biological Activities. *Nutrients*. 2016 Feb 16;8(2):90. doi: 10.3390/nu8020090. PMID: 26891321; PMCID: PMC4772053.



Received for publication, September, 22, 2023  
Accepted, October, 10, 2023

## Review

# Lifestyle features as co-factors in head and neck cancer development

**MARIAN CONSTANTIN<sup>1,2</sup>, ROXANA ELENA CRISTIAN<sup>3</sup>, IOANA CRUNTEANU<sup>4</sup>,  
SORIN TUDORACHE<sup>4\*</sup>, CORNELIU OVIDIU VRANCIANU<sup>2,5,6</sup>**

<sup>1</sup> Institute of Biology of Romanian Academy, 296 Splaiul Independentei, 060031 Bucharest, Romania

<sup>2</sup> The Research Institute of the University of Bucharest, ICUB, Bucharest, Romania

<sup>3</sup> Department of Biochemistry and Molecular Biology, Faculty of Biology, University of Bucharest, 050095 Bucharest, Romania

<sup>4</sup> Faculty of Medicine, Titu Maiorescu University, Bucharest, Romania

<sup>5</sup> Microbiology Immunology Department, Faculty of Biology, University of Bucharest, 050095 Bucharest, Romania

<sup>6</sup> National Institute of Research and Development for Biological Sciences, 296 Splaiul Independentei, District 6, 060031 Bucharest, Romania

## Abstract

Ranked sixth most prevalent worldwide, head and neck cancers (HNCs) affect an increasing number of people. Several factors contribute to their occurrence, including genetic and epigenetic aberrations and lifestyle factors, including heavy smoking, alcohol consumption, chewing betel quid (Areca nuts), poor oral hygiene, consumption of pro-inflammatory foods, inhalation of chemical compounds, asbestos dust, and infections with HPV (human papillomavirus) and EBV (Epstein-Barr virus). Often diagnosed in advanced stages, they have a mortality rate of about 50% at 5 years and pose a serious threat to human health.

## Keywords

lifestyle factors, genetic aberration, pro-inflammatory food, chemical compounds

---

✉ \*Corresponding author: Sorin Tudorache, Faculty of Medicine, Titu Maiorescu University, Bucharest, Romania;  
email: soryntudorache@yahoo.com

## Introduction

The head and neck region comprises the organs of the upper airways, the cranial cavity, the eyes, the ears, their appendages, the endocrine glands, the cervical spine, the cranial and cervical musculature, the blood vessels, including large blood vessels, the internal and external carotid arteries, the jugular veins and intracranial venous sinuses, the nerves and the integument covering them. Head and neck cancers (HNCs) refer to cancers occurring in the upper aerodigestive tract (nasal cavity; oral cavity with the lips, oral floor, hard palate, palatine veil, tongue, gums, and salivary glands; pharynx, with the nasopharyngeal, oropharyngeal and laryngopharyngeal/hypopharyngeal sectors, with the tonsils and the Eustachian tube communicating with the middle ear; larynx, with the vocal cords, glottis, and epiglottis). More than 90% of HNCs originate in the squamous cells lining the mucosa of the upper aerodigestive tract and are the sixth most common cancer, with more than half a million new cases annually [1] (in 2020, the number of new cases is estimated to be more than 900,000 [2, 3]).

The development of HNCs occurs in several stages, starting with the mutation of a single gene (usually *TP53*, Tumor Protein 53/Tumor Suppressor P53), continuing with the accumulation of somatic alterations in oncogenes (e.g., in the RAS–RAF–MEK–ERK and PIK3–AKT–mTOR signaling pathways), in tumor suppressor genes (e.g., *p16/INK4A/CDKN2A1*, Cyclin Dependent Kinase Inhibitor 2A) and in cell cycle regulatory genes (e.g., *CCND1*, Cyclin D1) and is favored by various lifestyle features, including heavy smoking (active and passive) and alcohol consumption, implicated in the etiology of about 72% of cases, chewing betel quid (Areca nuts), poor oral hygiene, consumption of pro-inflammatory foods (fried, smoked or roasted meat), inhalation of chemical compounds, asbestos dust, genetic factors [4-6], and HPV (human papillomavirus) and EBV (Epstein-Barr virus) infections, which are involved in the etiology of about 25% of cases (Fig. 1) [7, 8].

Although people with HNCs benefit from cytoreductive surgery, radiotherapy, and chemotherapy treatment when needed, and although metastasis is low (around 10%) due to diagnosis at advanced stages and high risk of recurrence, mortality at five years after diagnosis is high (around 50%), and is higher for primary laryngopharyngeal/hypopharyngeal tumors. Even after the cure, people with HNCs have a high lifetime risk of death, especially if they are smokers [6]. This paper aims to review the main unhealthy lifestyle factors (tobacco smoking, al-

cohol consumption, chewing Areca nuts (betel quid), and some eating habits) that can lead to HNCs.

## Tobacco smoking

Tobacco (*Nicotiana tabacum* L.) is consumed as cigarettes or as chewing tobacco and snuff (generically referred to as smokeless tobacco, with the habit of smoking associated or not with alcohol consumption being present in about 90% of HNCs and ranking first in their etiology [9]. For regular smokers, the average risk of HNCs is ten times higher for men and five times higher for women than for non-smokers; for heavy smokers, it is up to 20 times higher than for non-smokers. Smoking dark tobacco also increases the risk of HNCs by 2.5 times compared to light smoking tobacco and 35 times compared to not smoking at all. Smoking cessation significantly reduces this risk without eliminating it, so that five years after quitting, the risk of oral and pharyngeal cancers falls by half [9, 10]. Cigarette smoke contains about  $10^{10}$  particles/cm<sup>3</sup>. About 95% of smoke aerosols are gases (mostly nitrogen, oxygen, monoxide, and carbon dioxide, but also other volatile compounds) and less than 5% particles [11]. 3044 compounds have been isolated from cigarette smoke, of which 69 have carcinogenic and genotoxic effects. These could be potentially responsible for inducing some of the chromosomal and gene abnormalities identified in smokers: (a) chromosomal aberrations; (b) sister chromatid exchanges; (c) micronuclei in peripheral lymphocyte nuclei; (d) carcinogen-nitrogen-base adducts in bronchial and laryngeal epithelial cells (absent in non-smokers) or in placental cells in smoking mothers, where they occur with a markedly higher frequency than placental cells of non-smoking mothers (16/17, in smokers compared to 3/16 in non-smokers) [12], and thus, significantly increasing the risk of upper aerodigestive and lung cancers, depending on the intensity and duration of the smoking habit [10]. The formation of adducts (complexes formed by a nitrogenous base and the carcinogen) is essential for carcinogenesis, as it determines the occurrence of point mutations, one of the leading causes of HNCs. The carcinogen is introduced from the external environment, as such, or can be derived by metabolism from a procarcinogen (e.g., benzo[a]pyrene, very common in anthropogenic environments), and, having an affinity for the nitrogenous bases in DNA, interacts with them, causing, in case of errors in the corrective mechanisms, the formation of point mutations (Fig. 1), including those in *TP53* gene [13]. The IARC classifies eleven compounds in cigarette smoke as having a very high carcinogenic risk to humans: 2-naphthylamine, 4-aminodiphenyl, benzene, vinyl chloride, ethylene oxide, arsenic, beryllium, nickel salts, chromium VI salts, cadmium salts and 210 polonium com-

pounds [12]. Since 3044 compounds, some with carcinogenic effects, have been isolated from tobacco, other forms of tobacco consumption intended for chewing and snuffing, wet and dry (so-called smokeless tobacco), are also risk factors for HNCs, with less relevance than smoking, mainly due to the antioxidants present in tobacco [14-18].

Carbon monoxide from cigarette smoke gets into the blood and, combined with hemoglobin in red blood cells, which has 200–280 times more affinity for carbon monoxide than oxygen, forms carboxyhemoglobin. This is more stable than carbohemoglobin (produced by combining carbon dioxide with hemoglobin) or oxyhemoglobin (produced by oxygenating hemoglobin) [19]. Increased carboxyhemoglobin concentration reduces the ability to discharge oxygen from the blood and its availability in tumors, and HNCs are known for the ease with which they enter hypoxia [20].

At the same time, nicotine induces vasoconstriction, exacerbating the hypoxic state [21]. Further, it increases glucose uptake, glycolysis, and acidification of the tumor microenvironment, promoting HIF1A synthesis and initiating the angiogenesis pathway mediated by VEGFs [20] (Fig. 1).

## Alcohol consumption

Frequent consumption of alcohol is a significant risk factor for the development of neoplasia in the upper aerodigestive region, especially in the oral, oropharyngeal, laryngopharyngeal and laryngeal regions, especially in association with smoking or consumption of other tobacco products [22-24]. Regardless of the association with tobacco, alcohol: (1) solubilizes some carcinogens and permeabilizes the plasma membranes of the epithelial cells, favoring the penetration of the former into the cytoplasm and nucleus; (2) can produce changes in the salivary glands, with increased saliva viscosity and insufficient moistening of the oral and oropharyngeal mucous membranes, which become sensitive to the action of some carcinogens; (3) exhibits toxic action on the epithelia; (4) reduces esophageal motility; (5) stimulates gastro-esophageal reflux, leading to local metaplasia; (6) activates cytochrome P450, which metabolizes it to acetaldehyde, which converts some procarcinogens (e.g. nitrosamines, aflatoxins, vinyl chloride, polycyclic hydrocarbons, etc.) into carcinogens, and which metabolizes retinoic acid, a light-signaling neuromodulator necessary for growth and for the regulation of gap junction-mediated coupling of retinal neurons, reducing its concentration and generating metabolites that interfere with cell cycle development and cellular hyper-regeneration; (7) promotes tumor processes, by impairing the cell-mediated immune surveillance and cytotoxic function of NK cells and by reducing tissue folate concentrations [24]. The first metabolite of alcohol,

acetaldehyde, has carcinogenic effects by (1) affecting DNA synthesis; (2) interacting with some proteins, including enzymes involved in DNA repair and methylation, disrupting their functionality; (3) interacting directly with DNA, forming stable adducts and contributing to point mutations. Since alcohol metabolism to acetaldehyde can occur under the action of microorganisms in the oral cavity, the two compounds show conjugate effects in oral tumorigenesis. Based on these effects, in 2012, IARC included alcohol and acetaldehyde in the category of carcinogens for the human body, indicating that the impact of alcohol on the risk of HNCs depends more on the amount of alcohol consumed and not necessarily on its concentration in each drink [23-25]. The risk of HNCs decreases by 15% five years after cessation of consumption, and at least 20 years after cessation, the risk of HNCs may become close to or similar to that of people who do not consume alcohol at all [24].

Both alcohol and smoking are essential factors in the tumorigenesis of HNCs, so together, these habits manifest amplified synergistic effects, with alcohol solubilizing carcinogens from cigarette smoke and contributing to the permeabilization of cell membranes for carcinogens [26, 27]. Together, smoking and alcohol consumption account for approximately 72% of HNCs [1] (Fig. 1).

## Chewing Areca nuts (betel quid)

Areca nuts (betel nuts) are the fruits of the Areca palm (*Areca catechu* L.) and, wrapped in betel leaves (*Piper betle* L.), together with limestone dust, obtained by grinding the shells of marine invertebrates or limestone from quarries, catechu, a resinous extract from the matrix of *Senegalia catechu* (L.f.) P.J.H.Hurter & Mabb trees or *Senegalia polyacantha* (Willd.) Seigler & Ebinger subsp. *polyacantha*, and, commonly outside Papua New Guinea, tobacco powder, are called betel quid and chewed by some ethnic groups in Southeast Asia (Bangladesh, Myanmar, China, Cambodia, India, Indonesia, Laos, Malaysia, Nepal, Pakistan, Papua New Guinea, the Philippines, Singapore, Sri Lanka, Taiwan, Thailand, and Vietnam), but also by some minority communities in Fiji, Kenya, Mauritius, South Africa, Uganda, and Tanzania, for their psychotropic effects, due to the alkaloids in Areca nuts (arecoline, arecaidine, guvacine, guvacoline, and arecolidine) [15, 22, 28, 29]. Worldwide, the number of betel quid consumers is 600 million [30, 31]. In ripe Areca nuts, alkaloids constitute a minor fraction (0.15–0.67%), and of these, arecoline is predominant (0.12–0.24%), with the remainder consisting of saccharides (17.8–25.7%), polyphenols/tannins (11.1–17.8%), fats (1.3–17%), fiber (11.4–15.4%), fat (9.5–15.1%), protein (6.2–7.5%) ash (1.1–1.5%) and moisture (38.9–56.7%) [32]. Arecoline has a structure

close to nicotine's [30]. In rats, the metabolization of areca nuts alkaloids in the presence of nitrites results in four nitrosamines (N-nitrosoguvacoline, 3-(methylnitrosamino)propionitrile, 3-(methylnitrosamino)propionaldehyde and N-nitrosoguvacine), two of which (N-nitrosoguvacoline and N-nitrosoguvacine), which have been identified in the saliva of betel quid chewers [33, 34]. Metabolites of alkaloids in Areca

nuts are cytotoxic, genotoxic, and carcinogenic through ROS production, DNA damaging, and promoting of inflammation and hypoxia [35, 36], producing oral precancerous lesions and representing essential risk factors in the etiology of oral cancers in people who chew them, particularly in Papua New Guinea. In people who also add tobacco powder to betel quid, smoke, or consume alcohol, their effects are amplified [37].

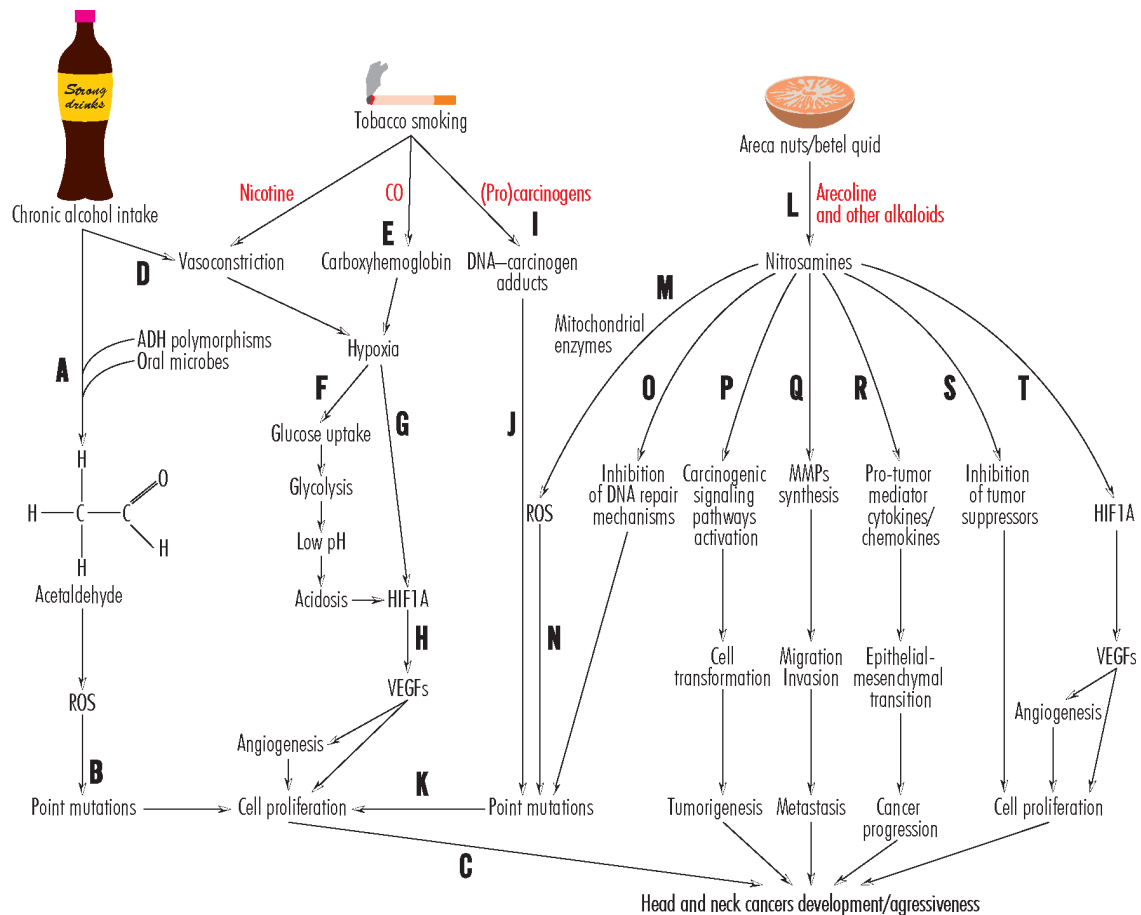


**Figure 1.** Overview of the mode in which carcinogens derived from alcohol, cigarette smoke and Areca nuts/betel quid lead to HNCs. In the case of alcohol consumption, oral microorganisms, in the presence of ADH polymorphisms, produce acetaldehyde (A), which, *via* ROS produced, can generate point mutations (B), cell proliferation and HNC (C). On the other hand, through vasoconstriction (D), alcohol consumption and nicotine derived from cigarette smoke favor the onset or progression of hypoxia. The most intense hypoxic effect, however, is caused by carbon monoxide (CO), resulting from the incomplete combustion of organic matter in the cigarette (E). It combines with hemoglobin from carboxyhemoglobin or oxyhemoglobin to form carboxyhemoglobin, a stable complex that can only be broken down by large amounts of oxygen in the blood, reaching through strong ventilation. Hypoxia contributes to the establishment of acidosis (F) and induces HIF1A synthesis (G), which in turn induces the synthesis of VEGFs (H). These lead to angiogenesis and tumour vascularization, and cell proliferation, sustaining the aggressiveness of HNCs (C). Finally, procarcinogens from cigarette smoke are metabolized into carcinogens (I), such as benzo[a]pyrene, which, by complexing guanine in DNA, renders it unavailable for cytosine and causes it to pair with adenine, inducing insertion of a point mutation (J). When these mutations occur in certain genes, they can lead to cell proliferation (K) and HNCs (C). Regular consumption of Areca nuts in the form of betel quid introduces the alkaloids the nuts contain into the body. Arecoline is the most abundant alkaloid in Areca nuts and, in the oral cavity, it can be converted to nitrosamines (L). These can be metabolized by microbial enzymes (M), with the production of reactive oxygen species, which can give point mutations (N). Nitrosamines contribute to the inhibition of error repair mechanisms in DNA, favoring the perpetuation of point mutations (O). Nitrosamines also activate the signaling pathways that maintain carcinogenesis (P), induce synthesis of MMPs (Q), cytokines or chemokines mediating the tumour process (R), inhibit tumour suppressors (S) and promote HIF1A production (T), all of which favor the development and aggressiveness of HNCs.

Carcinogenic and pro-tumor effects of Areca nut extract or arecoline are due: (1) formation of reactive oxygen species by mitochondrial enzymes, species that interact with DNA, proteins and lipids, and produce significant cellular damage [35]; (2) activation of carcinogenic signaling pathways, including RAS–RAF–MEK–ERK [31]; (3) activation of signaling pathways involved in G1/S or G2/M cell arrest [38]; (4) stimulation of synthesis of pro-tumor mediator cytokines/chemokines (IL6, IL8 [39] and receptors EGFR [31]); (5) triggering genetic defects, including hyperdiploid chromosomal changes associated with impaired p53 function and inhibition of DNA repair mechanisms (in keratinocytes and oral epithelial cells) (Shih et al., 2020); (6) inhibition of tumor suppressors, through activation of PI3/AKT, MEK/ERK, AMPK/mTOR, or HIF1A signaling pathways [31]; (7) stimulation of hypoxia-inducible factor 1 (HIF1) production, which contributes to malignant transformation [40]; (8) promotion of cell motility by promoting synthesis of matrix metalloproteinases (MMPs), including MMP, MMP2 [35], MMP8 [41], and MMP9 [42], and suppression of TIMP functions [31], and epithelial–mesenchymal transition [35, 43] (Fig. 1). MMP1 [16, 44] and MMP9 [42] are found at high levels in saliva and tumor tissues of betel quid chewers; MMP1 is proposed to be used as a marker for oral cancer [16, 44].

## Several eating habits

It is well known that a balanced diet, including all nutrients from vegetables, dairy, low-fat cheeses, pulses, boiled lean white meat, cooked fish, etc., promotes a healthy lifestyle and reduces the risk of many diseases, including cancers. On the other hand, the predominant consumption of pro-inflammatory diets, fried foods, fatty and processed meats and sweets, and the reduced consumption of fresh fruit and vegetables are risk factors for developing diseases, including laryngeal cancer [45, 46]. Dried and salted meats, including fish, concentrate N-nitrosodimethylamine and N-nitrosoethylamine, which, combined with alcohol consumption, amplify carcinogenic genomic DNA alkylation several-fold in tissues of the oral cavity, pharynx, and larynx [47, 48]. Similarly, the consumption of meat and fried potatoes or eggs, especially when this habit is frequent and is associated with smoking and the consumption of alcohol, seems to favor the development of laryngeal cancers, particularly supraglottic cancers, with odds ratios for the highest level of consumption compared to the lowest of 3.06 for fish or shellfish meat, 1.86 for potatoes, 1.85 for eggs or omelet and 1.63 for beef or veal [49–51]. Some studies [51] indicate a positive correlation between oral cancers and red or processed meat consumption but not be-

tween these and oropharyngeal and laryngeal cancers, just as no correlation can be made between fish meat consumption and HNCs. For fried, roasted, or smoked foods of animal origin, thermal preparation favors, under conditions of dehydration, the pyrolysis of polypeptides to amino acids and the interaction between amino acids and creatine, forming polycyclic aromatic hydrocarbons, including benzopyrenes and heterocyclic aromatic amines, which, under the action of cytochrome P4501A2 (CYP1A2) and N-acetyltransferase (NAT2), are activated to mutagens and carcinogens for the upper aerodigestive sphere [51, 52], and smoking meat enriches it in compounds derived from burning wood or coal, including aldehydes, phenolic compounds, volatile hydrocarbons, and some volatile metal compounds. Another compound that results during frying, including that of potatoes, is acrylamide, recognized by the IARC in 1994 as a potential human carcinogen [50, 53]. The formation of these compounds appears to be influenced by the food preparation method, with fat frying generating the highest concentrations of acrylamide and polycyclic aromatic hydrocarbons and air frying lower amounts, but not by the method of thawing frozen products [54].

## Other factors

Exposure to solar radiation, some occupations, including those in paper and paper products, metal, leather, food and textile industries, where workers are exposed to asbestos, formaldehyde, coal dust, wood dust, grease, oils, including cutting oils, naphthalene, exhaust fumes, other types of pollution, certain sexual practices that predispose to viral infections, such as sexual promiscuity, same-sex sexual relations or early sexual debut, membership of socially disadvantaged groups, etc., are additional risk factors in the etiology of head and neck cancers [6, 8, 55–58].

## Conclusions

HNCs are favored by some lifestyle peculiarities, including heavy smoking (active and passive), alcohol consumption, betel quid (Areca nut) chewing, poor oral hygiene with an imbalance of the local microbial community, -inflammatory diet (e.g., consumption of fried, smoked, or roasted meat), inhalation of chemical compounds, asbestos dust, genetic factors, and HPV and EBV infections. Due to diagnosis at advanced stages, most HNCs often have poor prognoses, low overall response rates, survival of several months without tumor progression, and overall survival of five years or less. Under these circumstances, strategies to prevent HNCs are compulsory and aim at (1) developing efficient algorithms for the early detection of neoplasms in high-risk individuals and reducing contact

with risk factors, including limiting smoking and alcohol consumption, Areca nuts chewing and pro-inflammatory foods consumption; (2) identification of individuals at high risk of developing HNCs, reduction of exposure to airborne pollutants and modification of dietary habits to reduce exposure to orally introduced carcinogens), and (3) halting or slowing the cancer progression, this requiring strict adherence to therapeutic management in these individuals. The data shown here underline the necessity of preventive strategies, including improved algorithms for reducing contact with risk factors and the early detection of HNC in high-risk individuals, as well as for halting or slowing the HCN progression by strict adherence to therapeutic protocols.

## Conflict of interest

The authors declare that they have no conflicts of interest.

## Funding

This study was supported by the Romanian Executive Agency for Funding Higher Education, Research, Development, and Innovation, UEFISCDI (<https://uefiscdi.gov.ro/>) research project FDI 0690/2023, the “Analysis of the potential for sustainable use of vegetation specific to the Danube-Danube Delta-Black Sea system” project, awarded by the European Regional Development Fund through the Competitiveness Operational Program 2014–2020, contract no. 108630, Project No. RO1567-IBB05/2023 awarded by the Institute of Biology Bucharest of the Romanian Academy, and “The core program within the National Research Development and Innovation Plan, 2022–2027”, carried out with the support of the Ministry of Research, Innovation and Digitalization (MCID), project no. 23020101, Contract no. 7N from 3 January 2023.

## References

- Gormley M, Creaney G, Schache A, Ingarfield K, Conway DI. Reviewing the epidemiology of head and neck cancer: definitions, trends and risk factors. *Br Dent J.* (2022) 233(9):780-786. doi: 10.1038/s41415-022-5166-x.
- International Statistical Classification of Diseases and Related Health Problems 10th Revision, Version:2019 [Accessed on December 30, 2022]. Available from: <https://icd.who.int/browse10/2019/en#/C00-C14>.
- Miserocchi G, Spadazzi C, Calpona S, De Rosa F, Usai A, De Vita A, Liverani C, Cocchi C, Vanni S, Calabrese C, Bassi M, De Luca G, Meccariello G, Ibrahim T, Schiavone M, Mercatali L. Precision Medicine in Head and Neck Cancers: Genomic and Preclinical Approaches. *J Pers Med.* (2022) 12(6):854. doi: 10.3390/jpm12060854.
- Trizna Z, Schantz SP. Hereditary and environmental factors associated with risk and progression of head and neck cancer. *Otolaryngol Clin North Am.* (1992) 25(5):1089-103.
- Foulkes WD, Brunet JS, Sieh W, Black MJ, Shenouda G, Narod SA. Familial risks of squamous cell carcinoma of the head and neck: retrospective case-control study. *BMJ.* (1996) 313(7059):716-21. doi: 10.1136/bmj.313.7059.716.
- Argiris A, Karamouzis MV, Raben D, Ferris RL. Head and neck cancer. *Lancet.* 2008 May 17;371(9625):1695-709. doi: 10.1016/S0140-6736(08)60728-X.
- Constantin M. Epidemiology, diagnosis, symptoms and TNM classification of head and neck cancers. *Rom Biotechnol Lett.* (2022) 27(5):3699-3712 doi: 10.25083/rbl/27.5/3699.3712.
- Mehanna H, Paleri V, West CM, Nutting C. Head and neck cancer--Part 1: Epidemiology, presentation, and prevention. *BMJ.* (2010) 341:c4684. doi: 10.1136/bmj.c4684.
- Dhull AK, Atri R, Dhankhar R, Chauhan AK, Kaushal V. Major Risk Factors in Head and Neck Cancer: A Retrospective Analysis of 12-Year Experiences. *World J Oncol.* (2018) 9(3):80-84. doi: 10.14740/wjon1104w.
- Andersson ER, Sandberg R, Lendahl U. Notch signaling: simplicity in design, versatility in function. *Development.* (2011) 138(17):3593-612. doi: 10.1242/dev.063610.
- Hecht SS. Tobacco smoke carcinogens and lung cancer. *J Natl Cancer Inst.* (1999) 91(14):1194-210. doi: 10.1093/jnci/91.14.1194.
- IARC Working Group on the Evaluation of Carcinogenic Risks to Humans, IARC Monographs on the Evaluation of Carcinogenic Risks to Humans, 83, Tobacco Smoke and Involuntary Smoking, 2004.
- Gibbons DL, Byers LA, Kurie JM. Smoking, p53 mutation, and lung cancer. *Mol Cancer Res.* (2014) 12(1):3-13. doi: 10.1158/1541-7786.MCR-13-0539.
- Wyss AB, Hashibe M, Lee YA, Chuang SC, Muscat J, Chen C, Schwartz SM, Smith E, Zhang ZF, Morgenstern H, Wei Q, Li G, Kelsey KT, McClean M, Winn DM, Schantz S, Yu GP, Gillison ML, Zevallos JP, Boffetta P, Olshan AF. Smokeless Tobacco Use and the Risk of Head and Neck Cancer: Pooled Analysis of US Studies in the INHANCE Consortium. *Am J Epidemiol.* (2016) 184(10):703-716. doi: 10.1093/aje/kww075.
- Asthana S, Labani S, Kailash U, Sinha DN, Mehrotra R. Association of Smokeless Tobacco Use and Oral Cancer: A Systematic Global Review and Meta-Analysis.

- ysis. *Nicotine Tob Res.* (2019) 21(9):1162-1171. doi: 10.1093/ntr/nty074.
16. Chang CP, Siwakoti B, Sapkota A, Gautam DK, Lee YA, Monroe M, Hashibe M. Tobacco smoking, chewing habits, alcohol drinking and the risk of head and neck cancer in Nepal. *Int J Cancer.* ((2020) 147(3):866-875. doi: 10.1002/ijc.32823.
17. Hajat C, Stein E, Ramstrom L, Shantikumar S, Polosa R. The health impact of smokeless tobacco products: a systematic review. *Harm Reduct J.* (2021) 18(1):123. doi: 10.1186/s12954-021-00557-6.
18. Ilic I, Ilic M. Chewing Tobacco and Mortality of Lip and Oral Cavity Cancer. *Biology and Life Sciences Forum.* (2022) 18(1):5. doi: 10.3390/Foods2022-12998.
19. Schimmel J, George N, Schwarz J, Yousif S, Suner S, Hack JB. Carboxyhemoglobin Levels Induced by Cigarette Smoking Outdoors in Smokers. *J Med Toxicol.* (2018) 14(1):68-73. doi: 10.1007/s13181-017-0645-1.
20. Lee JJW, Kunaratnam V, Kim CJH, Pienkowski M, Hueniken K, Sahoaler A, Lam ACL, Davies JC, Brown CM, De Almeida JR, Huang SH, Waldron JN, Spreafico A, Hung RJ, Xu W, Goldstein DP, Liu G. Cigarette smoking cessation, duration of smoking abstinence, and head and neck squamous cell carcinoma prognosis. *Cancer.* (2023) 129(6):867-877. doi: 10.1002/encr.34620.
21. Whitehead AK, Erwin AP, Yue X. Nicotine and vascular dysfunction. *Acta Physiol (Oxf).* (2021) 231(4):e13631. doi: 10.1111/apha.13631.
22. Johnson DE, Burtness B, Leemans CR, Lui VWY, Bauman JE, Grandis JR. Head and neck squamous cell carcinoma. *Nat Rev Dis Primers.* (2020) 6(1):92. doi: 10.1038/s41572-020-00224-3.
23. Koo HY, Han K, Shin DW, Yoo JE, Cho MH, Jeon KH, Kim D, Hong S, Jun JK. Alcohol Drinking Pattern and Risk of Head and Neck Cancer: A Nationwide Cohort Study. *Int J Environ Res Public Health.* (2021) 18(21):11204. doi: 10.3390/ijerph182111204.
24. Ferraguti G, Terracina S, Petrella C, Greco A, Minni A, Lucarelli M, Agostinelli E, Ralli M, de Vincentiis M, Raponi G, Polimeni A, Ceccanti M, Caronti B, Di Certo MG, Barbato C, Mattia A, Tarani L, Fiore M. Alcohol and Head and Neck Cancer: Updates on the Role of Oxidative Stress, Genetic, Epigenetics, Oral Microbiota, Antioxidants, and Alkylating Agents. *Antioxidants (Basel).* (2022) 11(1):145. doi: 10.3390/antiox11010145.
25. IARC Working Group on the Evaluation of Carcinogenic Risks to Humans. *Personal Habits and Indoor Combustions.* Lyon (FR): International Agency for Research on Cancer (2012). (IARC Monographs on the Evaluation of Carcinogenic Risks to Humans, No. 100E.) CONSUMPTION OF ALCOHOLIC BEVERAGES. Available from: <https://www.ncbi.nlm.nih.gov/books/NBK304390/>.
26. Howren MB, Christensen AJ, Pagedar NA. Problem alcohol and tobacco use in head and neck cancer patients at diagnosis: associations with health-related quality of life. *Support Care Cancer.* (2022) 30(10):8111-8118. doi: 10.1007/s00520-022-07248-3.
27. Rades D, Zwaan I, Janssen S, Yu NY, Schild SE, Idel C, Pries R, Hakim SG, Soror T. Evaluation of the Impact of Smoking and Alcohol Consumption on Toxicity and Outcomes of Chemoradiation for Head and Neck Cancer. *Anticancer Res.* (2023) 43(2):823-830. doi: 10.21873/anticancer.16224.
28. IARC Working Group on the Evaluation of Carcinogenic Risks to Humans, IARC Monographs on the Evaluation of Carcinogenic Risks to Humans, 89, *Smokeless Tobacco and Some Tobacco-specific N-Nitrosamines* (2007).
29. Hu Y, Zhong R, Li H, Zou Y. Effects of Betel Quid, Smoking and Alcohol on Oral Cancer Risk: A Case-Control Study in Hunan Province, China. *Subst Use Misuse.* (2020) 55(9):1501-1508. doi: 10.1080/10826084.2020.1750031.
30. Chen L, Pan J. Dual cyclin-dependent kinase 4/6 inhibition by PD-0332991 induces apoptosis and senescence in oesophageal squamous cell carcinoma cells. *Br J Pharmacol.* (2017) 174(15):2427-2443. doi: 10.1111/bph.13836.
31. Senevirathna K, Pradeep R, Jayasinghe YA, Jayawickrama SM, Illeperuma R, Warnakulasuriya S, Jayasinghe RD. Carcinogenic Effects of Areca Nut and Its Metabolites: A Review of the Experimental Evidence. *Clin Pract.* (2023) 13(2):326-346. doi: 10.3390/clin-pract13020030.
32. Mathew P, Austin RD, Varghese SS, Kumar MAD. Role of areca nut and its commercial products in oral submucous fibrosis-a review. *J Adv Med Dent Scie Res.* (2014) 2(3):192-200.
33. Giri S, Idle JR, Chen C, Zabriskie TM, Krausz KW, Gonzalez FJ. A metabolomic approach to the metabolism of the areca nut alkaloids arecoline and arecaine in the mouse. *Chem Res Toxicol.* (2006) 19(6):818-27. doi: 10.1021/tx0600402.
34. Myers AL. Metabolism of the areca alkaloids - toxic and psychoactive constituents of the areca (betel) nut. *Drug Metab Rev.* (2022) 54(4):343-360. doi: 10.1080/03602532.2022.2075010.

35. Li S, Hong X, Wei Z, Xie M, Li W, Liu G, Guo H, Yang J, Wei W, Zhang S. Ubiquitination of the HPV Oncoprotein E6 Is Critical for E6/E6AP-Mediated p53 Degradation. *Front Microbiol.* (2019) 10:2483. doi: 10.3389/fmicb.2019.02483.
36. Thakur N, Mehrotra R. Carcinogenic Alkaloids Present in Areca Nut. In: Patel, V.B., Preedy, V.R. (eds) *Handbook of Substance Misuse and Addictions*. Springer, Cham. (2022). doi: 10.1007/978-3-030-67928-6\_84-1.
37. Moss WJ. The Seeds of Ignorance - Consequences of a Booming Betel-Nut Economy. *N Engl J Med.* (2022) 387(12):1059-1061. doi: 10.1056/NEJMp2203571.
38. Tseng SK, Chang MC, Su CY, Chi LY, Chang JZ, Tseng WY, Yeung SY, Hsu ML, Jeng JH. Arecoline induced cell cycle arrest, apoptosis, and cytotoxicity to human endothelial cells. *Clin Oral Investig.* (2012) 16(4):1267-73. doi: 10.1007/s00784-011-0604-1.
39. Sun J, Tang Q, Zhang J, Chen G, Peng J, Chen L. Possible Immunotherapeutic Strategies Based on Carcinogen-Dependent Subgroup Classification for Oral Cancer. *Front Mol Biosci.* (2021) 8:717038. doi: 10.3389/fmolb.2021.717038.
40. Pereira KM, Chaves FN, Viana TS, Carvalho FS, Costa FW, Alves AP, Sousa FB. Oxygen metabolism in oral cancer: HIF and GLUTs (Review). *Oncol Lett.* (2013) 6(2):311-316. doi: 10.3892/ol.2013.1371.
41. Kazmi A, Abbas Z, Saleem Z, Haider S, Farooqui WA, Ahmed S. Relation of salivary MMP-8 with oral submucous fibrosis and oral squamous cell carcinoma: a cross sectional analytical study. *BMJ Open.* (2022) 12(12):e060738. doi: 10.1136/bmjopen-2021-060738.
42. Chang CC, Lee WT, Hsiao JR, Ou CY, Huang CC, Tsai ST, Chen KC, Huang JS, Wong TY, Lai YH, Wu YH, Hsueh WT, Wu SY, Yen CJ, Chang JY, Lin CL, Weng YL, Yang HC, Chen YS, Chang JS. Oral hygiene and the overall survival of head and neck cancer patients. *Cancer Med.* (2019) 8(4):1854-1864. doi: 10.1002/cam4.2059.
43. Joseph JP, Harishankar MK, Pillai AA, Devi A. Hypoxia induced EMT: A review on the mechanism of tumor progression and metastasis in OSCC. *Oral Oncol.* (2018) 80:23-32. doi: 10.1016/j.oraloncology.2018.03.004.
44. Chu LJ, Chang YT, Chien CY, Chung HC, Wu SF, Chen CJ, Liu YC, Liao WC, Chen CH, Chiang WF, Chang KP, Wang JS, Yu JS. Clinical Validation of a Saliva-Based Matrix Metalloproteinase-1 Rapid Strip Test for Detection of Oral Cavity Cancer. *Biomed J.* (2023) S2319-4170(23)00031-8. doi: 10.1016/j.bj.2023.04.002.
45. Mazul AL, Shivappa N, Hébert JR, Steck SE, Rodriguez-Ormaza N, Weissler M, Olshan AF, Zevalos JP. Proinflammatory diet is associated with increased risk of squamous cell head and neck cancer. *Int J Cancer.* (2018) 143(7):1604-1610. doi: 10.1002/ijc.31555.
46. Bozzetti F, Cotogni P. Nutritional Issues in Head and Neck Cancer Patients. *Healthcare (Basel).* (2020) 8(2):102. doi: 10.3390/healthcare8020102.
47. Irani S. New Insights into Oral Cancer-Risk Factors and Prevention: A Review of Literature. *Int J Prev Med.* (2020) 11:202. doi: 10.4103/ijpvm.IJPVM\_403\_18.
48. Dalmartello M, Decarli A, Ferraroni M, Bravi F, Serraino D, Garavello W, Negri E, Vermunt J, La Vecchia C. Dietary patterns and oral and pharyngeal cancer using latent class analysis. *Int J Cancer.* (2020) 147(3):719-727. doi: 10.1002/ijc.32769.
49. Perloy A, Maasland DHE, van den Brandt PA, Kremer B, Schouten LJ. Intake of meat and fish and risk of head-neck cancer subtypes in the Netherlands Cohort Study. *Cancer Causes Control.* (2017) 28(6):647-656. doi: 10.1007/s10552-017-0892-0.
50. Sandmael JA, Sand K, Bye A, Solheim TS, Oldervoll L, Helvik AS. Nutritional experiences in head and neck cancer patients. *Eur J Cancer Care (Engl).* (2019) 28(6):e13168. doi: 10.1111/ecc.13168.
51. Martinovic D, Tokic D, Puizina Mladinic E, Usljebrka M, Kadic S, Lesin A, Vilovic M, Lupi-Ferandin S, Ercegovic S, Kumric M, Bukic J, Bozic J. Nutritional Management of Patients with Head and Neck Cancer-A Comprehensive Review. *Nutrients.* (2023) 15(8):1864. doi: 10.3390/nu15081864.
52. Sahin S, Ulusoy HI, Alemdar S, Erdogan S, Agaoglu S. The Presence of Polycyclic Aromatic Hydrocarbons (PAHs) in Grilled Beef, Chicken and Fish by Considering Dietary Exposure and Risk Assessment. *Food Sci Anim Resour.* (2020) 40(5):675-688. doi: 10.5851/kosfa.2020.e43.
53. Lee JS, Han JW, Jung M, Lee KW, Chung MS. Effects of Thawing and Frying Methods on the Formation of Acrylamide and Polycyclic Aromatic Hydrocarbons in Chicken Meat. *Foods.* (2020) 9(5):573. doi: 10.3390/foods9050573.
54. Başaran B, Çuvalcı B, Kaban G. Dietary Acrylamide Exposure and Cancer Risk: A Systematic Approach to Human Epidemiological Studies. *Foods.* (2023) 12(2):346. doi: 10.3390/foods12020346.
55. Flanders WD, Rothman KJ. Occupational risk for laryngeal cancer. *Am J Public Health.* (1982) 72(4):369-72. doi: 10.2105/ajph.72.4.369.
56. Muscat JE, Wynder EL. Diesel exhaust, diesel fumes, and laryngeal cancer. *Otolaryngol Head Neck Surg.* (1995) 112(3):437-40. doi: 10.1016/s0194-5998(95)70280-6.

57. Menvielle G, Luce D, Goldberg P, Leclerc A. Smoking, alcohol drinking, occupational exposures and social inequalities in hypopharyngeal and laryngeal cancer. *Int J Epidemiol.* (2004) 33(4):799-806. doi: 10.1093/ije/dyh090.
58. Galbiatti AL, Padovani-Junior JA, Maniglia JV, Rodrigues CD, Pavarino EC, Goloni-Bertollo EM. Head and neck cancer: causes, prevention and treatment. *Braz J Otorhinolaryngol.* (2013) 79(2):239-47. doi: 10.5935/1808-8694.20130041.



Received for publication, October, 25, 2023  
Accepted, November, 02, 2023

*Original Article*

## **The potential of the radiation technologies to improve the quality of dietary supplements**

**MARIA ADRIANA ACASANDREI<sup>1,\*</sup>, SILVANA VASILCA<sup>1</sup>, ERHAN IONUZ<sup>1</sup>,  
ANDREEA SERBAN<sup>1</sup>, FLORIN ADRIAN ALBOTA<sup>1</sup>, MIOARA ALEXANDRU<sup>1,\*</sup>,  
LAURA TRANDAFIR<sup>1</sup>, FLORINA LUCICA ZORILA<sup>1</sup>, MIHAI CONSTANTIN<sup>1</sup>,  
MIHALIS CUTRUBINIS<sup>1</sup>, SILVIU STEFANESCU<sup>2</sup>, LUCICA SIMA<sup>2</sup>,  
IOAN VALENTIN MOISE<sup>1</sup>**

<sup>1</sup> Horia Hulubei National Institute for Physics and Nuclear Engineering, 30 Reactorului Street, 077125, Magurele, Ilfov, Romania

<sup>2</sup> Health Laboratory S.R.L., Bucharest, Romania

### **Abstract**

The use of dietary supplements has much increased over recent decades, principally due to the need to correct dietary deficiencies but also for their supportive role in certain medical treatments. While they are regulated as food, with certain specific regulations and requirements that distinguish them from conventional foods, the manufacturers can choose to adhere to higher standards, that allows them a future upgrade as pharmaceuticals or medical devices. This paper presents the results of exploratory studies for the introduction of gamma irradiation as a method of control of the microbial contamination for egg lyophilizates currently marketed as dietary supplements. Characterization studies were performed with the goal of upgrading the products for the pharmaceutical market. The irradiation treatment improved their microbiological quality by the exerted microbicidal effect and it can be used as long as the other properties (physico-chemical and/or therapeutic) are not affected.

### **Keywords**

avian immunoglobulin, dietary supplements, pharmaceuticals, gamma irradiation, amino acids, microbiological contamination.

---

✉ \*Corresponding author: Maria Adriana Acasandrei, e-mail: macasan@nipne.ro; Phone number: +(4021)4046134  
Mioara Alexandru, e-mail: mioara.alexandru@nipne.ro; Phone number: +(4021)4042369

## Introduction

Dietary supplements are an important aspect of modern life. Their use has much increased over recent decades, because of their large availability, the need to try to reduce dietary deficiencies but also for their supportive role in medical treatment in certain situations [1].

Egg lyophilizates are used as dietary supplements due to their valuable nutritional profile. They are rich in several essential nutrients, making them a good source of vitamins, minerals, and protein. A particular case is when egg lyophilizates are enriched with immunoglobulins.

Egg yolk immunoglobulins (IgY) have been identified for more than a hundred years, having as their first biological effect the protection of chicks from infection. IgY represents the main antibody produced by plasma cells in the body of the domestic chicken (*Gallus domesticus*). It corresponds to the immunoglobulin IgG produced by mammals.

By inoculating chickens with different bacterial antigens, specific antibacterial IgY can be obtained, which are passively transferred from the hen's serum to the yolk. The process of obtaining IgY from egg yolk is relatively simple and inexpensive.

IgY is a relatively stable protein that can be stored at 2-4 °C. In lyophilized form, IgY activity remains constant for months at temperatures of -20 °C or even for a month at 37 °C. IgY, due to its multiple advantages, compared to IgG derived from mammals, can be used in several fields such as alternative therapies, prophylaxis and acute passive immunization. The effects of passive immunization by oral administration of specific IgY have been demonstrated in several clinical trials [2].

The therapeutic use of the egg lyophilizates with enriched IgY content need proper characterization of the biochemical compounds and, taking into account their intended use, the compliance with microbiological quality requirements.

For products of animal origin, ensuring batch to batch uniformity and microbiological quality is challenging. Lyophilization is known to reduce bioburden, but is not accepted as a sterilization method in the absence of precise quantification of a parameter related to bioburden reduction. Pharmaceutical GMP [3] guidelines call for the use, whenever possible, of a terminal sterilization method. Since thermal or gas (EO) sterilization are not appropriate for the egg lyophilizates, gamma irradiation was taken into consideration.

Radiation sterilization is widely accepted in the production of medical devices (almost 50% of sterile single-use medical devices are sterilized by radiation) and is gaining momentum in the pharmaceutical field. There are specific GMP guidelines for the use of radiation for sterilization of the medicinal prod-

ucts [4]. In case of dietary supplements there is no requirement for sterilization (oral use) but the competitive advantage obtained by introducing gamma irradiation is given by an increase in confidence in the microbial stability of the products for several years (increasing the period of validity/marketing). Furthermore, by proving the sterility of the egg lyophilizates the way is opened for their use as intermediate products in the aseptic manufacturing process.

The current study involves testing selected physical and chemical properties of egg lyophilizates before and after irradiation, as well as microbial characterization. Based on literature data concerning the behavior of egg products to irradiation [5, 6] the analytical methods taken into consideration are HPLC [7,8], for determining the amino acid profile and thermal analysis [9÷14], for determining the water content. The microbiological tests include determination of the total microbial load before and after irradiation and detection of specific microorganisms.

## Materials and methods

Five types of samples (lyophilized powder or liquid extract) from products named as “Imunzyze Wellness” (Wellness), “Imunzyze Complete” (Complete), “Imunzyze Defence” (Defence), “Imunzyze Health” (Health) and “Imunzyze Healthcare” (oral spray, 5 mL bottle) (Healthcare), all manufactured by Health Laboratory SRL, were physically, chemically and microbiologically characterized, before and after irradiation.

### Protein hydrolysis

In order to identify the amino acid profile (AA), a digestion of the samples was carried out in order to hydrolyze the proteins from the freeze-dried samples, to break the peptide bonds and increase the concentration of free amino acids. The Ultrawave Single Reaction Chamber Microwave Digestion System equipment from Milestone (Italy) was used to hydrolyze the samples as follows: 50 mg of each sample were subjected to acid hydrolysis in the vapor phase assisted by microwaves - 6.5 mL hydrochloric acid 6 N, at a temperature of 160°C, for 40 min, at a power of 1000W and an initial pressure of 40 bars in an inert nitrogen atmosphere (N<sub>2</sub>, purity 5.0 or 99.999%). After digestion, the samples were diluted to 15 mL, from which approximately 2 mL were taken in Eppendorf tubes and centrifuged at 9000 RPM. Then 0.1 mL was taken from the supernatant and diluted to 2 mL with deionized water in glass vials for HPLC sample injection. In the HPLC injection method, a volume of approximately 1 µL was taken, which was subsequently subjected to a pre-column derivatization method, using o-phthalaldehyde for the derivatiza-

tion of primary amino acids and fluorenylmethoxycarbonyl chloride for the secondary ones.

### Chromatographic system

The experiments were carried out using liquid chromatography - HPLC (High-performance liquid chromatography), using an Agilent (USA), type 1260 INFINITY II system, with the following configuration: degasser (G1379A); quaternary pump (G7111B); sample thermostat (G7129A), column thermostat (G7116A); UV-Vis detector (DAD) (G7115A). The chromatographic separation was performed on an AdvancedBio AAA column, having 4.6 x 100 mm and particle size of 2.7  $\mu\text{m}$ , thermostated at 40°C. The mobile phase consists of a mixture of aqueous solution of 10 mM  $\text{Na}_2\text{HPO}_4$  and 10 mM  $\text{Na}_2\text{B}_4\text{O}_7$ , brought to pH 8 (solvent 1) and methanol/acetonitrile/water (solvent 2). Gradient elution was applied, using the following profile: at 0 min - 2% solvent 2, for 0.5 min, from min 0 to 14 - linear increase to 55% solvent 2, followed by another linear increase until min 14.2, 100% solvent 2, from min 14.2 to 16.5 - jump back to 2% solvent 2, with a re-equilibration period of 2 minutes. The used flow was 1.5 mL/min, and the UV-Vis spectra were simultaneously recorded in the range 190-400 nm, with a frequency of 0.03 min and a resolution of 2 nm. Four wavelengths were monitored simultaneously to generate the chromatograms (210, 241, 260 and 330 nm).

### Water content tests by thermal analysis (TG)

In the determinations made by thermal analysis, a TG/DSC simultaneous thermal analysis equipment type STA 409 PC Luxx, produced by Netzsch Geratebau GmbH, with the following configuration was used:

- purged and thermostated Sartorius microbalance, maximum mass of 18000 mg, mass resolution of 0.002 mg;
- TG/DSC (sample crucible and reference crucible) sample holder with type S thermocouple (Pt/Rh,  $\pm 3\text{K}$ ); - for DSC, the comparative heat flow is measured between the crucible (cell), the test sample and the reference crucible, by applying a constant heating rate; in practice, the calorimetric technique with differential thermal flux (heat-flux DSC), described above, is used;
- alumina furnace: temperature range 20 - 1500°C, heating speed 0.1 - 50 K/min, temperature control by thermocouple type S;
- dynamic inert atmosphere ( $\text{N}_2$ ), gas with a minimum purity of 99.999%, flow rate 100ml/min: microbalance purge 50 ml/min, furnace purge 50 ml/min from the level of the thermal radiation shield; - aluminum DSC crucibles with perforated lid (25  $\mu\text{L}$ );

Mass of the test specimen: The test specimen consisted of 10 mg of lyophilized powder transferred into a 25  $\mu\text{L}$  alu-

minum crucible, with a perforated lid, manually closed and weighed on an analytical balance (5 decimals per gram).

Temperature program: heating rate of 10 K/min from room temperature (RT) to 590°C, followed by a 10 min isothermal segment.

The temperature ( $^{\circ}\text{C}$ ) and enthalpy (J/g) calibration curves used in the test were drawn through 3 experimental points using high-purity metals (In, Bi and Zn) as reference materials, in the same experimental configuration and the same operating parameters as in the method described above for the test specimen. The processing of the experimental data and the generation of the calibration curves used in the analysis was carried out according to the specifications of the instrument manufacturer.

The sampling was carried out by Health Laboratory Ltd., according to its internal procedures. The sampling of test specimens was carried out with disposable plastic spatulas, transferring a lyophilized product powder into 25  $\mu\text{L}$  aluminum crucibles, with a perforated lid, reproducibly closed with a manual press. For each sample, two samples- the reference (as received from the Ltd company) and the irradiated (decontaminated) sample were tested.

Conditioning method of the tested specimen: before and after irradiation, these were kept in a refrigerator at 8  $^{\circ}\text{C}$ . During the irradiation, the samples stayed at the temperature of the irradiation chamber, which is located around 30  $^{\circ}\text{C}$ . The samples removed from the refrigerator were reweighed on the analytical balance and transferred directly to the TG/DSC sample holder at room temperature, after which the oven was closed and the temperature program started as soon as possible, in order to minimize the unrecorded time of unbound water.

### Microbiological characterization

The microbiological characterization of lyophilized samples included determination of total aerobic microbial count, total fungi and detection of some pathogens (*Escherichia coli*, *Salmonella* sp., *Staphylococcus aureus*), before and after irradiation of the samples.

Culture media and diluents: Tryptic Soy Agar (TSA) for Total Aerobic Microbial Count, Sabouraud Chloramphenicol Agar (SABcfa) for fungi (Yeasts and Mold), Buffered sodium chloride-peptone with 0,1% (w/v) Tween 80 (APS 0,1 % Tw) as diluent.

Reference test strains used for suitability of the microbial contamination test method: *Staphylococcus aureus* ATCC 6538, *Bacillus subtilis* ATCC 6633, *Pseudomonas aeruginosa* ATCC 9027, *Candida albicans* ATCC 10231, *Aspergillus niger* ATCC 16404.

The detection of *Escherichia coli*, Presence/g, *Salmonella* sp., Presence / 10 g, *Staphylococcus aureus*, Presence/g were done by culturing on enrichment non-selective culture media (Tryptic soya broth, TSB) and subculturing on selective media (MacConkey broth, Mckb, MacConkey agar – Mcka, Rappaport-Vassiliadis (RV) enrichment broth, Xylose Lysine Deoxycholate Agar, Mannitol salt agar).

The determination of microbial contamination was carried out in accordance with the requirements of the reference document European Pharmacopoeia, 10th edition, chapter 2.6.12 Microbiological examination of non-sterile products, respectively chapter 2.6.13 Microbiological examination of non-sterile products. Test for specified microorganisms [15–17].

### Gamma irradiation

Gamma irradiation of the test samples was performed at the Gamma Chamber GC-5000 Research Irradiator of the IRASM Technological Irradiation Center from NIPNE. The target dose was 3 kGy. The dose was chosen to achieve the product quality control requirements for industrial scale treatment with ionizing radiation, based on preliminary tests (organoleptic and biochemical) performed by Health Laboratory Ltd. (not reported here).

## Results and discussion

### Amino acids profiling

For the quantification of amino acids from these samples, standard solutions of amino acids were prepared in 0.1 N hydrochloric acid at five different concentrations and kept at a temperature of 4°C. To check linearity and reproducibility, concentrations between 210 and 0.6 ppm were prepared by repeated dilutions on the day of analysis.

In Figure 1, an example of linearity domain is represented, having lysine in concentrations ranging from 0.1827

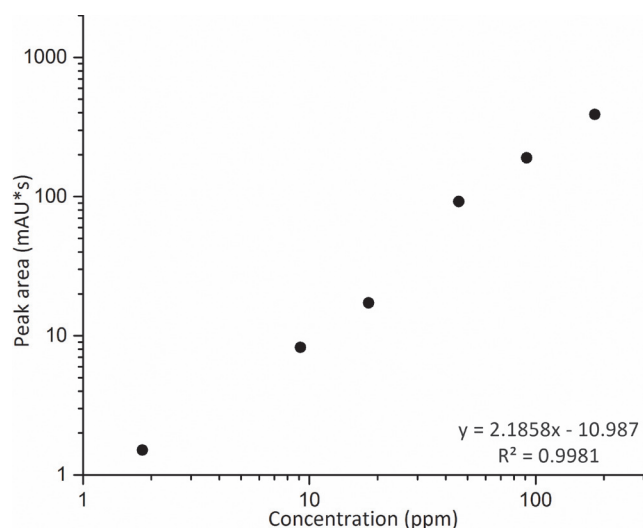


Figure 1. Lysine's calibration curve.

to  $0.1827 \cdot 10^{-2}$  mg/mL. Furthermore, in all the 17 analyzed amino acids, the correlation coefficient ( $R^2$ ) has values higher than 0.997.

### Amino acids from freeze-dried samples

In order to optimize the sample mass for achieving a proper digestion and thus protein hydrolysis, one of the four solid matrices was chosen, "Imunzye Health", five different masses were taken into consideration (5, 10, 50, 100 and 200 mg), subjected to the digestion process and analyzed. For the masses of 5 mg and 10 mg, the amino acids could not be quantified (below LoQ – limit of quantification), however, in Figure 2 it can be seen that each identified amino acid (for the samples of 50, 100 and 200 mg) - represented as a percentage of the total mixture - the fact that the digestion process is stable, apart from the amino acids serine, threonine and proline, in which case more tests are needed in a subsequent method validation. Thus, the mass of 50 mg was selected as the ideal mass to be taken into analysis due to the fact that it allows a good identification and quantification of the analytes. When it comes to the digestion method, the consumption of reagents is reduced 7 times in comparison with the ones found in the literature, while the number of simultaneously processed samples is the maximum for this class of digesters (use of 15 mL ampoules with 15-positions rack).

The amino acid profiles from the four types of non-irradiated lyophilized samples are represented comparatively in Figure 3(a), by their chromatograms at a wavelength of 330 nm. The presence of the same 16 essential and non-essential amino acids can be observed, where certain peaks are coming from the solvent, although with small variations in intensities and in the peak area. It should be mentioned that certain minor variations in concentration may also come from

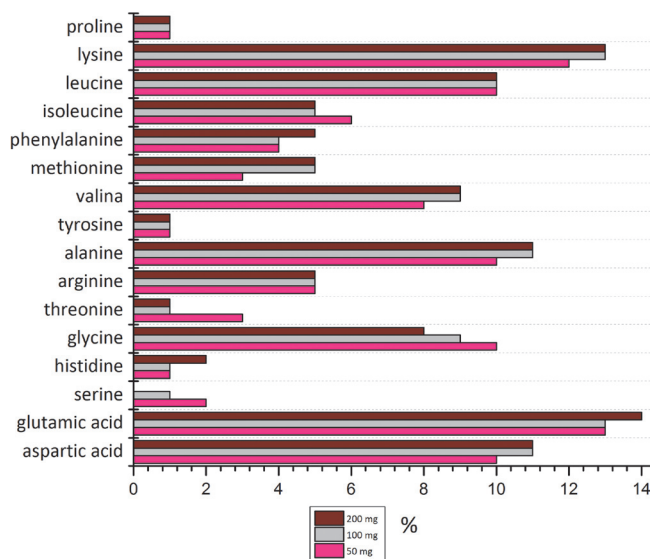


Figure 2. The composition of the samples having 50, 100 and 200 mg from "Imunzye Health" represented as percentage.

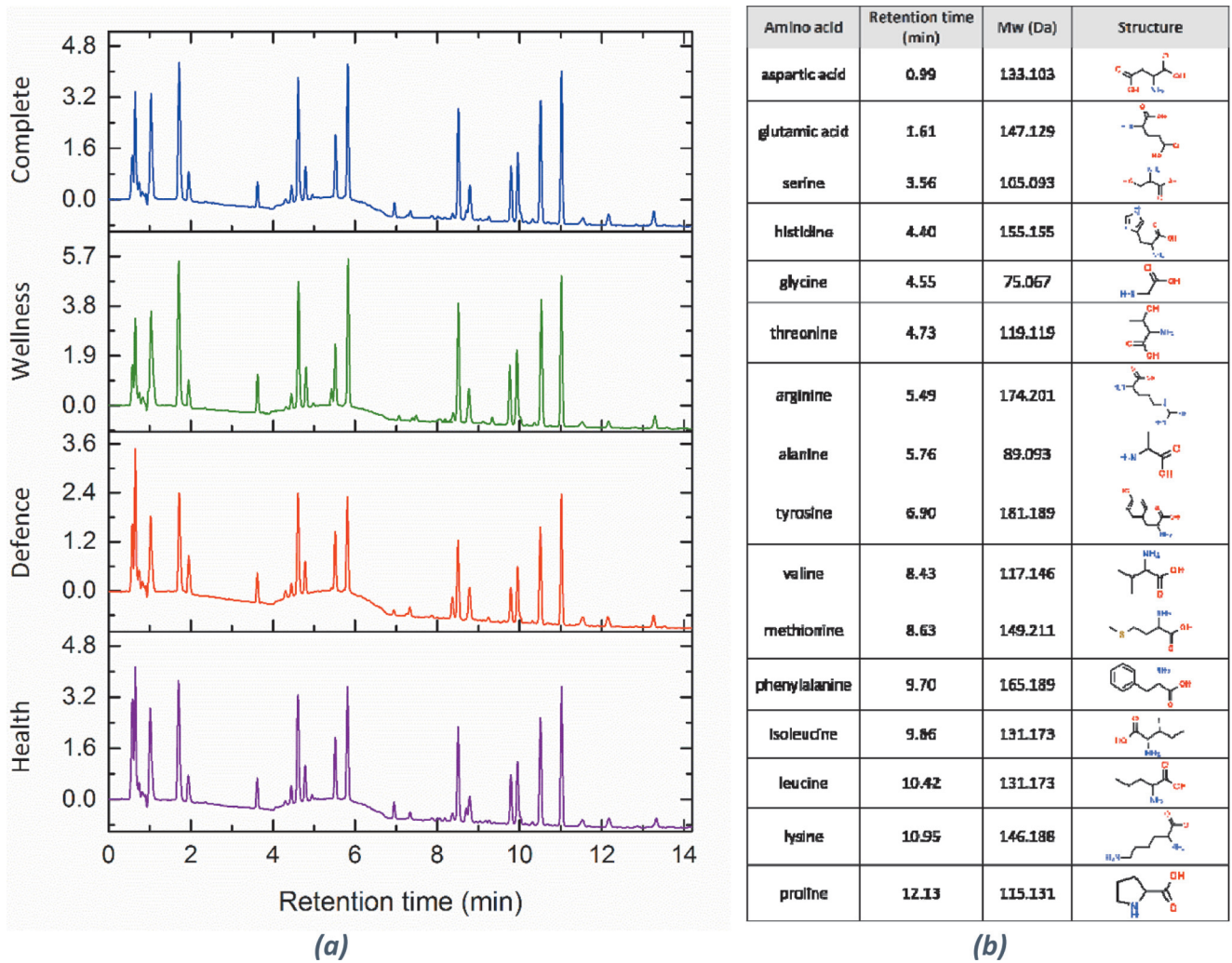


Figure 3. Comparative chromatograms for the four types of lyophilized samples (a), the studied amino acids and their retention times (b).

the inhomogeneity of the samples. The identification of the analytes was carried out on the basis of standard solutions of amino acids, retention time and in certain cases, on the basis of the UV-Vis spectrum, which can be quite similar for most amino acids. The structure of the analyzed or identified compounds, their molecular masses, as well as their retention time is presented in Figure 3(b). On the other hand, 1 g was also sampled from the IH-s spray and analyzed, but there were no quantifiable amino acids.

Figure 4 shows of the four types of freeze-dried, non-irradiated samples, represented as a percentage of the total amino acid content. Their variability can be noticed in each sample, observing discrete variations (probably falling within the standard deviation of the method) between matrices for the same analyte. AA ratios are similar to those reported in literature [18].

Regarding the differences before and after irradiation, in Table 1 the most important percentage decreases in concentration are marked in green in the case of histidine, arginine, tyrosine, methionine and phenylalanine, while the significant

increases in the concentrations of glycine, alanine, valine and lysine are marked in orange. The assumption that these

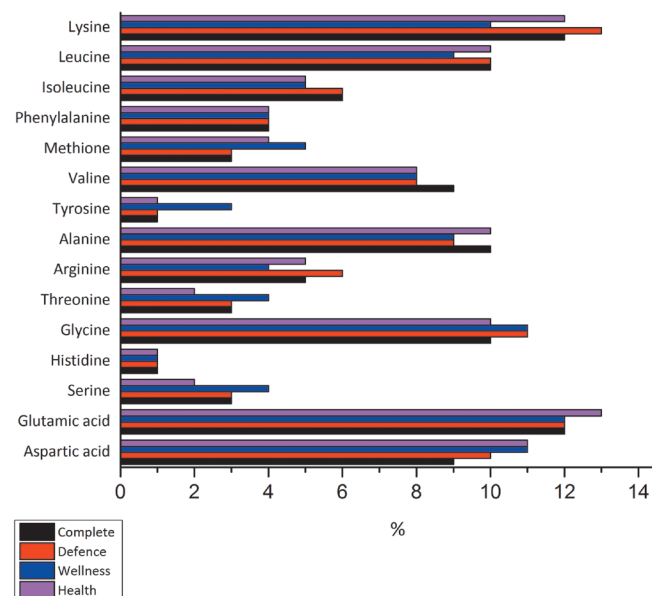


Figure 4. The percentage of amino acids in the freeze-dried samples: Complete, Defence, Wellness and Health.

Table 1. The difference between the amino acids profiles before and after irradiation.

	Complete	Complete*	Defence	Defence*	Wellness	Wellness*	Health	Health*
aspartic acid	8%	9%	8%	10%	9%	11%	9%	11%
glutamic acid	12%	12%	11%	12%	13%	12%	12%	13%
serine	3%	3%	4%	3%	3%	4%	4%	2%
histidine	6%	1%	7%	1%	5%	1%	6%	1%
glycine	4%	10%	4%	11%	4%	11%	4%	10%
threonine	4%	3%	5%	3%	4%	4%	4%	2%
arginine	8%	5%	8%	6%	7%	4%	8%	5%
alanine	6%	10%	5%	9%	6%	9%	6%	10%
tyrosine	4%	1%	6%	1%	4%	3%	5%	1%
valine	7%	9%	6%	8%	7%	8%	7%	8%
methionine	5%	3%	5%	3%	5%	5%	4%	4%
phenylalanine	7%	4%	6%	4%	7%	4%	7%	4%
isoleucine	7%	6%	7%	6%	7%	5%	7%	5%
leucine	9%	10%	9%	10%	9%	9%	9%	10%
lysine	10%	12%	10%	13%	9%	10%	10%	12%
Total	100%	100%	100%	100%	100%	100%	100%	100%

\* Irradiated samples

variations in the content of amino acids after irradiation are due to the transamination reaction with amino transfer is not very viable because lysine - one of the amino acids that does not participate in this type of biochemical reaction - also undergoes concentration variations. Regarding the metabolism of amino acids, transamination reactions are reversible, their reversibility being dependent on the concentration of reactants and reaction products, in which an amino group is removed from an amino acid and transferred to keto-acid acceptors, such as pyruvic acid, from eggs, in order to generate a version of amino acids derived from the keto-acid and a keto-acid generated from the original amino acid.

The variation in the content of amino acids in the irradiated lyophilized samples could be determined by the cleavage of the backbone, thus being transformed into other amino acids, where the newly formed radical is able either to recombine, to be digested into smaller fragments, otherwise it was not separated and identified using this chromatographic method. Thus, in the case of histidine, the imidazole side chain in the structure could have suffered a breakage induced by gamma irradiation, leaving only the  $\alpha$ -amino group and the carboxylic group, thus transforming into glycine, therefore explaining the increase in the concentration of the latter and the decrease of histidine's concentration.

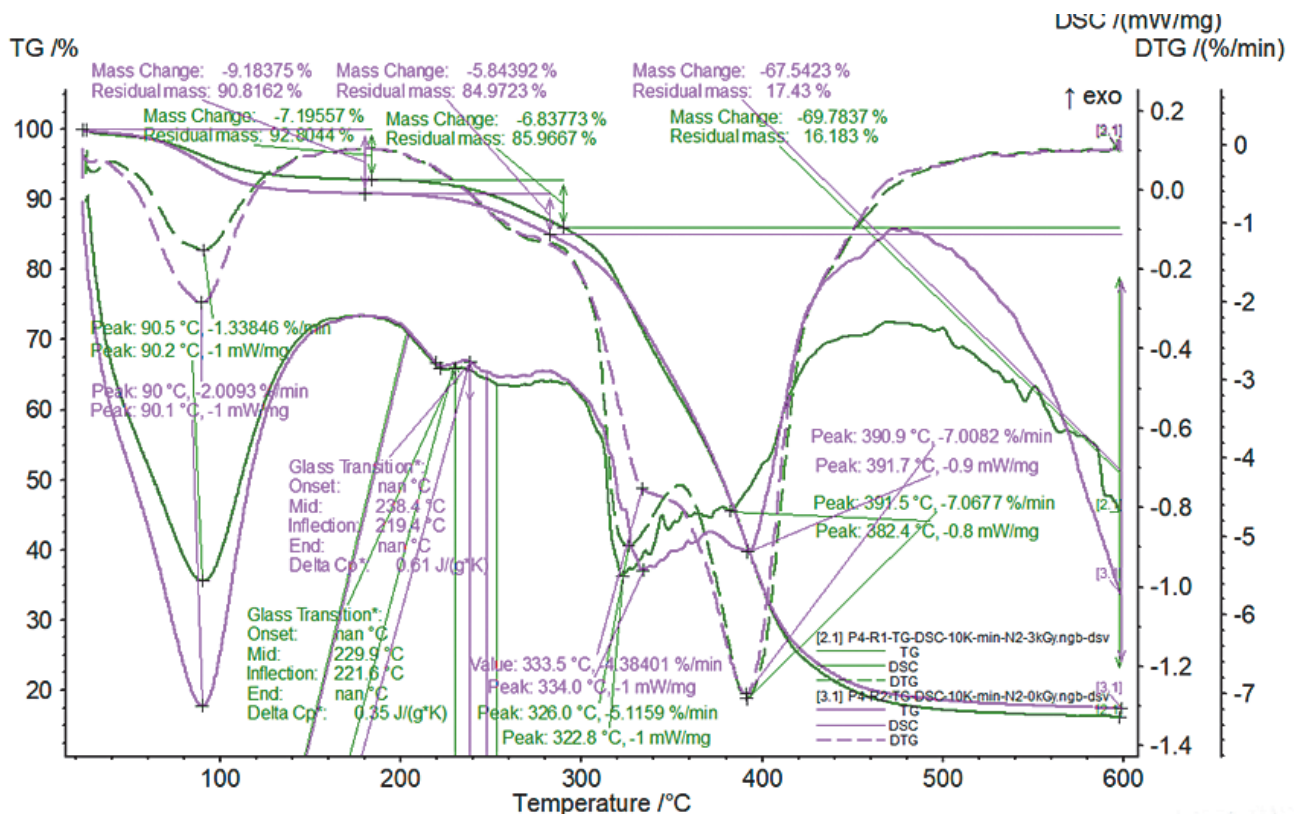


Figure 5. TG/DSC curves in nitrogen, 10K/min, for IMUNYZE HEALTH (P4), batch no.: 1/2023.

Table 2. Water loss and glass transition (ovalbumin) by thermogravimetry (TG).

Sample	First step (% mass)	Water loss		Kinetics (%/ min)	Kinetics (mW/ mg)	Ovalbumin Glass	
		Temp (DTG)	Temp (DSC)			Temp (MID DSC)	Delta Cp (DSC) J/(g*K)
P1(0kGy)	12	89	91	2.3	1.4	232	1.0
P1*(3kGy)	13	81	87	2.5	1.6	231	0.8
stdev	2	3	1	0.5	0.1	1	0.1
P2(0kGy)	6	87	90	1.3	1.0	234	1.1
P2*(3kGy)	9	81	84	1.9	1.4	231	0.9
stdev	1	10	6	0.1	0.1	1	0.1
P3(0kGy)	10	87	90	2.1	1.3	230	0.8
P3*(3kGy)	10	89	91	2.2	1.3	231	0.6
stdev	1	7	6	0.2	0.1	1	0.2
P4(0kGy)	9	87	89	2.0	1.0	229	0.4
P4*(3kGy)	8	83	86	1.6	1.0	229	0.4
stdev	1	11	8	0.2	0.1	1	0.1

\* Irradiated samples

Similarly, the guanidino group from arginine could also suffer a breakage of the covalent bond generated by ionizing radiation, leading to an increase in the concentration of alanine, while the increase in the concentration of valine can be determined either by breaking the phenolic functionality from tyrosine, of the S-methyl thioether side chain from methionine or the phenyl group from phenylalanine.

#### Water content tests by thermal analysis (TG)

In order to define suitable processing, storage conditions, shelf life and use of a product, it is required to determine the product's water content and the mechanism of water–solid interactions. Therefore, in our study there were performed thermal analysis, the TG/DSC curves in nitrogen, 10K/min, for IMUNYZE HEALTH (P4, batch no.: 1/2023) being presented in Figure (5) and the results for all the tested samples summarized in Table 2.

The composition in unbound (absorbed) and bound water was determined to be between 6 - 13% for the analyzed samples - Step 1 TGA - maximum speed DTG/DSC between 81 and 91°C. It does not change significantly before and after irradiation, taking into account the variability of the samples. Also, the maximum peak position does not change significantly.

Beside the water loss peak, on the DSC thermograms can be observed the decomposition peak and a glass transi-

Table 3. Microbiological test results for non-irradiated and irradiated samples.

No	Samples	Non irradiated CFU / g		Irradiated CFU / g	
		TAMC	TYMC	TAMC	TYMC
1.	Health	2.4 x 10 <sup>4</sup>	35	10	< 10
2.	Complete	85	102	< 10	< 10
3.	Wellness	< 10	< 10	< 10	< 10
4.	Defence	1.7 x 10 <sup>4</sup>	60	20	< 10

**TAMC** – Total aerobic microbial count

**TYMC** – Total yeasts and mould count

tion which was attributed to Ovalbumin. From the DTG and DSC peaks it appears that the treatment by gamma irradiation at 3 kGy does not significantly affect the structure of the protein, identified as Ovalbumin, having a glass transition temperature of approximately 230-231°C.

#### Microbiological characterization

The results of the microbiological tests are summarized in table 3.

After analyzing the results obtained for the irradiated products, it is observed that the microbiological parameters are within the maximum limits allowed for pharmaceutical products (for example, the microbial load ID and IH decreased by 2 log<sub>10</sub>, to a total number of aerobic microorganisms TAMC < 10<sup>2</sup> CFU / g). For the other samples, the bioburden after irradiation was below the detection limit. The pathogenic microorganisms were not detected either before or after irradiation. In this context, the treatment with ionizing radiation improves the microbiological quality of products.

#### Conclusions

An HPLC-DAD chromatographic method was developed for the qualitative and quantitative analysis of the amino acid profile in protein powders/spray, based on lyophilized egg, as well as for evaluating the variation of their concentrations following the treatment using ionizing radiation. The method is fast, sensitive and selective; however, only the amino acids from the studied reference materials were reported. For more advanced fundamental research related to the changes in the molecular structure of the amino acids from the investigated products, it would be necessary to develop an LC-MS technique.

The digestion process was stable, the investigated samples show the same amino acid profile, with slightly differ-

ent distributions depending on the matrix. Certain analytes such as histidine, glycine, arginine, alanine, tyrosine, valine, methionine, phenylalanine and lysine, show significant differences (>1%) after gamma irradiation, both increasing and decreasing the concentration. However, to validate that these changes are produced by the treatment with ionizing radiation, more in-depth radiation qualification studies must be carried out, with an extended range of target doses and a statistically significant number of replicates included in the analysis. To optimize the qualitative analysis, but especially the quantitative one, additional experiments are needed, as well as the validation of the method.

For the matrix tested by simultaneous TG-DSC thermal analysis, no significant differences could be identified in both the TGA and DSC signals between the irradiated (target dose of 3 kGy) and non-irradiated samples.

The treatment with gamma radiation at low doses ( $\leq 3$  kGy) improves the microbiological quality of these products through the microbicidal effect exerted and can be used as long as the other properties (physico-chemical and/or therapeutic) are not affected.

The sterility can be achieved by the increase of the irradiation dose, while the properties of interest for the intended use can be maintained by using other physical means (for example: high dose rate, irradiation in modified - non-oxidative atmosphere, or at ultra-low temperatures – dry ice).

## Acknowledgments

This work was supported by the project POC-G, ID: P\_40\_276 (SMIS 107514) “GAMMA-PLUS” - Enhancing competitiveness through innovation and improving manufacturing processes with gamma irradiation technology - subsidiary project no 61/2023 funded by European Regional Development Fund (FEDR), Minister of European Funds in Romania (MFE) and co-funded by Health Laboratory Ltd. Core and IOSIN Programs are supporting IRASM gamma irradiators and laboratories of NIPNE.

## References

1. Tihauan BM, Marinas IC, Barboi G, Dolete G, Onisei T, Serbancea F, Mateescu C, Răscol M. Evaluation of cytotoxicity, nutritional and antioxidative status of lyophilized plant extracts used in dietary supplements. *Rom Biotechnol Lett.* 2021;26(2):2396-2405, doi: 10.25083/rbl/26.2/2396.2405.
2. Wang H, Zhong Q, Lin J. Egg Yolk Antibody for Passive Immunization: Status, Challenges, and Prospects. *Agric. Food Chem.* 2023;71(13):5053–5061.
3. Guideline on the sterilisation of the medicinal product, active substance, excipient and primary container, EMA/CHMP/CVMP/QWP/850374/2015, European Medicines Agency, Committee for Medicinal Products for Human use (CHMP), Committee for Medicinal Products for Veterinary use (CVMP) ([https://www.ema.europa.eu/en/documents/scientific-guideline/guideline-sterilisation-medicinal-product-active-substance-excipient-primary-container\\_en.pdf](https://www.ema.europa.eu/en/documents/scientific-guideline/guideline-sterilisation-medicinal-product-active-substance-excipient-primary-container_en.pdf)).
4. Good manufacturing practice- Annex 12. Use of ionizing radiation in the manufacture of medicinal products, *EudraLex - Volume 4 - Good Manufacturing Practice (GMP) guidelines*, European Medicines Agency, ([https://health.ec.europa.eu/system/files/2016-11/anx12\\_en\\_0.pdf](https://health.ec.europa.eu/system/files/2016-11/anx12_en_0.pdf)).
5. Katusin-Razem B, Mihaljevici B, Razem D, Radiation-Induced Oxidative Chemical Changes in Dehydrated Egg Products, *J. Agric. Food Chem.* 1992;40:662-668.
6. Al-Bachir M, Improvement of Microbiological Quality of Hen Egg Powder Using Gamma Irradiation, *Int. J. Food Stud.* January 2020;9:SI75-SI83.
7. Campmajó G, Cayero L, Saurina J, Núñez O. Classification of Hen Eggs by HPLC-UV Fingerprinting and Chemometric Methods, *Foods.* 2019;8:310.
8. Woo KL. Determination of amino acids in foods by reversed-phase HPLC with new precolumn derivatives, butylthiocarbamyl, and benzylthiocarbamyl derivatives compared to the phenylthiocarbamyl derivative and ion exchange chromatography. *Mol Biotechnol.* 2003;24:69–88.
9. European Pharmacopoeia, 2.2. Physical and physico-chemical methods, 2.2.34. Thermal analysis.
10. Ehrenstein GW, Riedel G, Trawiel P. Thermal Analysis of Plastics. Theory and practice, ISBN 1-56990-362-X, Hanser Gardner Publications. 2004.
11. International Organization for Standardization. Plastics. Differential scanning calorimetry (DSC), Part 1: General principles (ISO Standard No. 11357). 2023. Retrieved from <https://www.iso.org/standard/70024.html>.
12. International Organization for Standardization. Plastics. Thermogravimetry (TG) of polymers, Part 1: General principles (ISO Standard No. 11358). 2022. Retrieved from <https://www.iso.org/standard/79999.html>.
13. Monkos K. The glass transition temperature and temperature dependence of activation energy of viscous flow of ovalbumin, *Curr. Top. Dev. Biol.* 2016;39:13-25.
14. Ferreira M, Hofer C, Raemy A. A calorimetric study of egg white proteins. *Journal of Thermal Analysis and Calorimetry.* 1997;48(3):683-690.
15. European Pharmacopoeia 10<sup>th</sup> Edition Chapter 2.6.12 – Microbiological Examination of Non-Sterile Products,

- 
- Chapter 2.6.13 - Microbiological Examination of Non-Sterile Products - Test for Specified Microorganisms.
16. European Pharmacopoeia 10<sup>th</sup> Edition, Chapter 5.1.4 – Microbiological quality of non-sterile pharmaceutical preparations and substances for pharmaceutical use.
  17. Good Manufacturing Practice (GMP) guidelines, European Medicines Agency, Annex 1 Manufacture of Sterile Medicinal Products.
  18. Lunven P, Marcq C, Carnovale E, Fratoni A. Amino acid composition of hen's egg. *British Journal of Nutrition*. 1973;30(2):189-194. doi:10.1079/BJN19730024.